Pleistocene and Holocene Climate Reconstruction at Two Moose Lake, Central Yukon, using Stable Isotopes and ^{14}C-DOC radiocarbon from Ice wedges, Pore ice and Buried sediments

Submitted by: Michael Grinter

Thesis presented to the Faculty of Graduate and Postdoctoral Studies in partial fulfilment of the requirements for the degree of Master of Science in Earth Sciences

Supervisors:
Dr. Ian D. Clark (Department of Earth Sciences)
Dr. Denis Lacelle (Department of Geography, Co-supervisor)

Department of Earth Sciences
Faculty of Science
University of Ottawa

Thesis Committee:
Bernard Lauriol, University of Ottawa
David Fisher, University of Ottawa

Acknowledgements

First and foremost, I'd like to express my extreme gratitude towards my two supervisors, Dr. Ian Clark and Dr. Denis Lacelle. Had it not been for their support, guidance and funding this thesis would not be possible. Their patience during this long process was commendable, and I truly appreciate you guys not losing faith in me. Denis, because of your class on Polar Regions, I became hooked on the Canadian Arctic, making it a goal of mine to one day visit. Thanks to you (and Ian) I was able to achieve this dream. I'll never forgot the experiences we had in the field (maybe not so much the morning wake-up calls by rocks being thrown at my tent....). Ian, your enthusiasm in the field of geology and willingness to share your knowledge with students is what convinced me to do a Masters. You support throughout this process helped in motivating me to keep going, if not for me, for you.

Thank you to the staff in the G.G. Hatch Isotope lab, Paul Middlestead, Wendy Albi, and Patricia Wickham for all their knowledge and expertise. Thank you to Jean Bjornson for your help with grain size analysis and knowledge of the Yukon. I would also like to thank the staff of the AEL AMS laboratory, Sarah Agnosta, Carley Crann and Gilles St-Jean, who, despite being beyond swamped with the start-up of the lab, were able to spare valuable time to help with radiocarbon analysis. Thank you to Anthony Lapp and Marielle Fontaine for your support and help in the field. You guys made my time there one to remember, and I could not have asked for better company. I should also thank Bernard Lauriol for his help as well. Bernard, your passion for the Arctic speaks volumes, and I appreciated your willingness to get dirty in the trenches with me. Had it not been for your keen eye, I would not have had the chance to study the outcrop at Two Moose Lake.

Lastly, I would like to thank my friends, family and girlfriend Gab for their constant support, encouragement and patience. Had it not been for you guys constantly bugging me as to when I will finally be done with school, I may never have finished. And I did it!

This thesis was funded by Natural Sciences and Engineering Research Council of Canada (NSERC) discovery grants to Dr. Denis Lacelle and Dr. Ian Clark, and by multiple Northern Scientific Training Program (NSTP) grants to Michael Grinter.

Abstract

The objective of this thesis was to reconstruct the Sedimentary, Cryostratigraphic and Paleoclimatic history of Two Moose Lake, central Yukon using a new analytical technique for dating ice wedges using Dissolved Organic Carbon (DOC). During two field seasons in August 2013 and April 2014, 442 samples were collected from a newly exposed headwall of a thaw slump with 7 ice wedges and over 4m of sediment. Using cryostratigraphy, granulometry, stable isotopes and 18 ^{14}C-DOC ages, 4 stratigraphic units were delineated: 1) a sediment-rich ice layer inferred to be of glacial origin (>32ka BP); 2) a silt-rich layer deposited during the Holocene Thermal Maximum (~10 to 8.2ka BP); 3) a silt with organics layer deposited from ~8ka to 6.4ka BP, and 4) a paleo-active layer and modern active layer. ^{14}C-DOC dating indicated two periods of ice wedge activity at Two Moose Lake, the first during the late Pleistocene (31,608 to 12,990 yr cal BP) and from the mid-Holocene to present (6,328 to 892 yr cal BP). The presence of late-Pleistocene aged ice wedges at Two Moose Lake supports the common belief of an unglaciated central Yukon during the most recent McConnell glaciation from 29.6 to 13ka BP. Values for δ^{18}O from the Holocene- and Pleistocene-aged ice wedges were 2-3‰ and 5-9‰ depleted compared those of modern precipitation from Mayo (-22.32‰). Medium-resolution (2-4cm) sampling along with multiple ^{14}C-DOC samples along a transect allowed for the creation of a continuous δ^{18}O and temperature age profile to be developed from multiple ice wedges, showing a strong consistency between overlapping ages. The reconstruction of the paleoclimate of Two Moose lake is consistent with known events from southern Yukon including the Boutellier Inderstadial, a cold unglaciated central Yukon during the McConnell Glaciation, warming during the Holocene Thermal Maximum (HTM) followed by an extreme cooling event at 8.2ka BP, a cooling event at 4.2ka BP, and the subsequent warming to present temperatures.

Table of Contents

List of Figures

List of Tables

1. Introduction

1.1. Permafrost and Ground Ice

1.1.1. Permafrost & Active Layer

Permafrost, according to the International Permafrost Association (2016) is defined as ground (soil or rock and included ice or organic material) that remains at or below 0°C for at least two consecutive years. Permafrost zones can be separated into 5 zones based on the percentage occurrence of permafrost as well as the type: 1) Subsea Permafrost; 2) Isolated Patches (0-10%); 3) Sporadic Discontinuous (10-50%); 4) Extensive Discontinuous (50-90%); and 5) Continuous (90-100%). In continuous zones, permafrost exists everywhere beneath the land surface and the depth of it can vary from around 100m at the southern limit, to upwards of 1000 meters at the northern limit (French and Slaymaker, 1997). The boundaries between the continuous and discountinuous zones coincides with a mean annual air temperature of ~-8°C, corresponding to permafrost temperatures of ~-5°C. In zones of discontinuous permafrost, the distribution of permafrost is complex and often patchy, closely related to the land surface (slope, gradient, orientation, vegetation and snow cover) and proximity to bodies of water. While permafrost may be below 0°C, it may not necessarily be frozen since the freezing point of water within the ground may be depressed to <0°C. As a result, it may be useful to distinguish between temperature (thermal) and state (frozen or unfrozen) conditions of the permafrost. Therefore, in circumstances where ice within permafrost is being studied, it is useful to define the permafrost as 'cryotic'. The majority of permafrost existing today formed during cold glacial periods, and has persisted through warmer (than present) interglacial periods including during the Holocene.

Often synonymous with permafrost is the Active layer, the near-surface layer that thaws and freezes annually. The thickness of the active layer is highly variable, with depths ranging from less than 30cm in peaty terrain and recently laid deposits to over 5m in bedrock exposed at the surface (Burn, 1998). Active layer thickness is also controlled by other factors such as ambient air temperature, slope orientation and angle, vegetation type , snow cover, soil and/or rock type and water content (French and Shur, 2010). Furthermore, the depth of the active layer, or annual thaw, can be highly variable not only annually, but on decadal and millennial time scale. A recent advance in the study of permafrost has been the understanding of the transient

layer or transition zone (Shur et al., 2005), a zone that lies between the active layer and underlying permafrost (Figure 1). Numerous studies have shown the properties between the uppermost boundary of permafrost differ from those of the underlying permafrost, whereby the uppermost part is subject to episodic thaw at points in time and joining the active layer, while at other points it remains frozen and part of the permafrost.

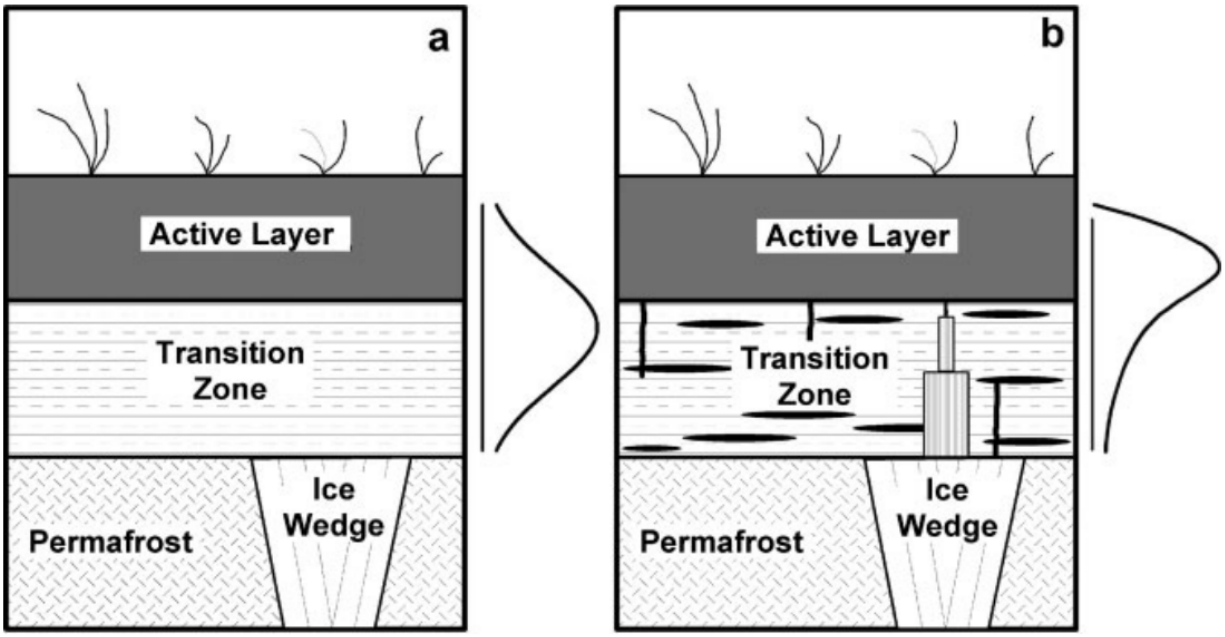

Figure 1. Schematic diagram of a conceptual diagram showing the Active Layer, Transient layer/Transition zone and Permafrost. The center of the curve on the right shows mean annual active layer (relative probability of annual thaw dpeht) for a) immediately following a deep thaw and b) ice enrichment of the transition zone after several centuries. Source: Shur et al., 2005.

This zone has an important impact on the formation of the upper permafrost, soil and cryogenic structures and protection of permafrost during climatic variations (Shur et al., 2005). This transient layer has also been shown to be ice-rich, with a greater ice content than the permafrost below (Pollard and French,1980; Burn et al., 1986; Shur et al., 2005; French and Shur, 2010), indicating the long-term position of the contact between the active layer and permafrost. Ice in this layer appears in various forms including segregation lenses, ice veins and recent/contemporary ice wedges. (Lewkowicz, 1994). Coincidently, the lower limit of the transient layer/transition zone occurs in line with the tops of ice wedges, and thus an indication of the long-term permafrost table. Furthermore, ice within layer/zone is important in maintaining permafrost stability, acting as a buffer between the active layer and permafrost through its ability to absorb latent-heat effects due to its ice-rich nature (Shur et al., 2005).

Observation of changes in active layer thickness, transient layer/transition zone and permafrost depth (ice lenses, istopes, etc.) are extremely important in the understanding and change in climates over a period of time.

1.1.2. Buried Ice

One of the most prominent features within permafrost is the presence of buried ice. Often these bodies of ice are not exposed at the surface, however, ice-rich permafrost below can contain up to 70-90% ice by volume (Pollard and French, 1980; Burn et al., 1986; French and Pollard, 1986; Murton and French, 1994; Burn, 1997; Lacelle et al., 2004; Lacelle et al., 2007, Lacelle et al., 2009; Lachniet et al., 2012). Buried ice will often lay hidden and undiscovered below the ground until exposure through geomorphic modifications (ie. slumps) and thawing of permafrost in response to climate change (Lacelle et al., 2010). The proportion of ice and sediment can be highly variable, and can sometimes be useful to distinguish by cryofacies type (Table 1). Examples of these bodies of ice include massive ice, buried remnant glacier, injection ice, pooled ice, ice lenses and most predominantly, ice wedges (Pollard and French, 1980).

Table 1. Cryofacies types identified by Murton and French (1994) from fieldwork in the Tuktoyaktuk coastlands, Northwest Territories.

Cryofacies type	Volumetric ice content (%)	Cryofacies	Code
Pure ice	100	Pure ice	I
Sediment-poor ice	> 75	Sand-poor ice	SPI
		Aggregate-poor ice	API
Sediment-rich ice	> 50 to ≤75	Sand-rich ice	SRI
		Aggregate-rich ice	ARI
Ice-rich sediment	> 25 to ≤50	Ice-rich sand	IRS
		Ice-rich mud	IRM
		Ice-rich diamicton	IRD
Ice-poor sediment	≤ 25	Ice-poor mud	IPM
		Ice-poor sand	IPS
		Ice-poor gravel	IPG
		Ice-poor diamicton	IPD
		Ice-poor peat	IPP

1.1.3. Ice Wedges

Ice wedges have played an important role since the 1960's to reconstruct Quaternary and late Pleistocene paleotemperatures and climates (Murton, 2013). Ice wedges, often identified by their polygonal-framework and networks on the surface (Figure 2), are one of the most prevalent forms of buried-massive ice in periglacial regions. Once exposed, ice wedges are easily identifiable by their V-shape, truncated top, and vertically irregular stratified ice. In the western Canadian arctic, ice wedges occupy ca. 20% of the ground surface and ice wedge ice may account for up to 80% of ground ice near the surface (Pollard and French, 1980). Typically, ice wedges form in a broad range of stable, aggrading or sloped surfaces, and are often dictated by the trace of a river or shoreline such as in the case of the Mackenzie delta in Yukon, Canada (Plug and Werner, 2008).

Figure 2. Ice wedge polygon framework and networks on the west side of Two Moose Lake, Yukon. The sampling location for this study is indicated by the square (red). Source: Google Earth.

Ice wedges belong to a group of vein- and wedge-shaped structures that are often foliated and can be composed of various proportions of ice, sediment and organic matter depending on conditions during its formation (Murton, 2013). The various amounts of minerals, organic matter

and air inclusions can affect the colouring of the ice wedges, ranging from a clear white to yellowish colour. Various theories exist explaining the process for the formation of an ice wedge. In North American literature, the accepted process for the formation of an ice wedge is from an initial cooling-derived fracture/fissure (frost crack) in perennially frozen ground (and overlaying active layer) caused by tensile stress induced by falling winter temperatures (Allard and Kasper, 1998; Mackay, 2000; Plug and Werner, 2002; Christiansen, 2005). In order for thermal-contraction cracking to occur several conditions are believed to be required (Lachenbruch, 1966; Harry and Godzik, 1988; Allard and Kasper, 1998; Mackay, 2000; Christiansen, 2005; French, 2007; Plug and Werner, 2008, Murton, 2013) including:

1. Long period of cooling with MAAT below -4°C to -6°C
2. Ground/permafrost temperatures between -10°C and -20°C
3. Rapid decrease in temperature to between -25°C to -40°C
4. Ground cooling rate between 0.1°C and -0.6°C/day

Cracking in the arctic typically occurs between mid-January and mid-March when air temperatures are at their coldest (Mackay, 2000). In a study by Fortier and Allard (2005), frost cracks were shown to open after a drop in air temperature of ca. 7.9°C over an average period of 18 hours, with a mean thermal gradient -10.9°C/m in the active layer at the time of cracking. In addition to temperature dependent factors, other site-specific factors such as snow cover, vegetation, creep of frozen ground and particle size influence cracking and cracking frequency (Mackay, 2000).

Following the creation of a frost crack, there are several methods of infilling/wedge growth that can occur, beginning with the creation of an ice vein. Prior to spring melt, fractures may be partially filled by condensation of water vapour, hoarfrost accretion or snow infiltration (Shumski, 1964; Mackay, 1992; French and Guglielmin, 2000). The more commonly accepted method of infilling involves the infiltration of frost cracks by snow meltwater in the spring and the subsequent re-freezing to form an ice vein (Mackay, 1975; Mackay, 1992; Lauriol et al., 1995; Plug and Werner, 2002; Murton, 2013). As this process of thermal-contraction cracking followed by infilling continues, cracking occurs within the ice vein, slowly growing in to V-shaped wedges (Figure 3). Due to the previous year's cracking creating zones of weakness (Mackay, 1975) and ice in fracture cavities generally being weaker than frozen ground (Plug and

Werner, 2002), fractures usually will follow the same path of weakened areas, generally in the middle of the ice wedge along recurring fracture paths as seen in ice wedges on Garry Island in the Arctic Coastal Plain (Mackay, 1992; Mackay, 2000) and at the Illisarvik experimental drained lake site, western Arctic coast in Canada (Mackay and Burn, 2002). However, Mackay (1992) indicated cracking can occur anywhere within the width of the ice. The width of thermal-contraction cracks can vary, but typically can average between 1 to 2cm in width initially, but often decrease to 0.5-1 mm thickness over growth (Mackay, 2000). During these studies, Mackay (2000) noted that many thermal-contraction cracks originated near the permafrost table, propagating both upwards towards the ground surface and downwards through the ice wedge. French and Shur (2010) also noted the formation of folia between each cracking event by loess, silt and macroscopic organic debris blown into the crack during the winter.

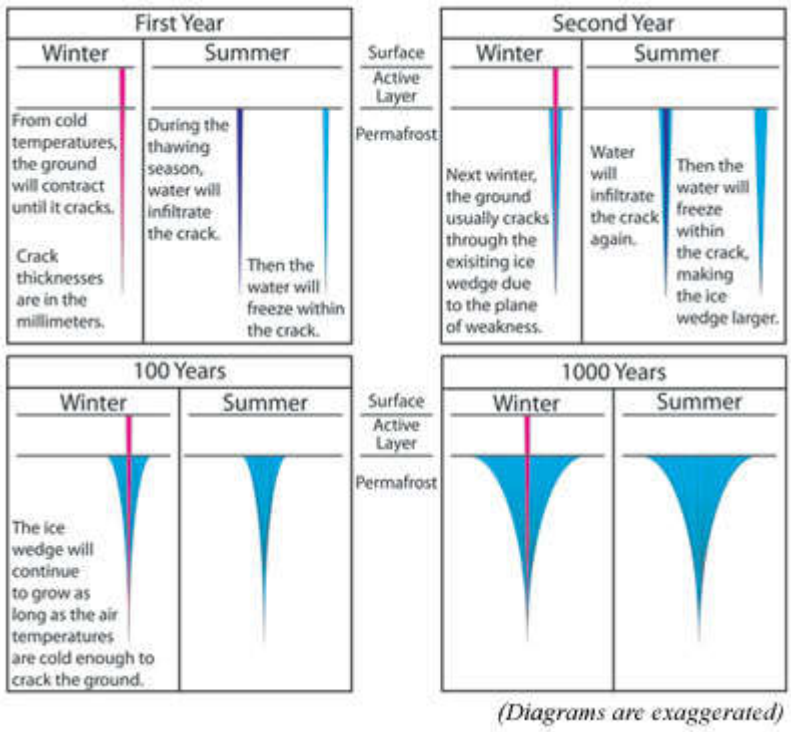

Figure 3. Schematic diagram showing the growth of an ice wedge. The addition of subsequent ice veins are shown with the lateral expansion of the ice wedge over time. Source: http://permafrosttunnel.crrel.usace.army.mil/permafrost/massive_ice.html

The frequency of thermal-contraction cracking of ice wedges is highly variable, and is loosely dependent on factors such as winter air temperatures, and vegetation and snow depth, reflecting the effects of insulation from low air temperatures and sudden changes in temperature (Mackay, 1992). In two studies by Mackay, ice wedges were shown to crack once every 1 to 50

years (Mackay, 1992), and data collected over a six-year period on Garry Island, N.W.T. showed, on average, only 40% of ice wedges crack in a given year (Mackay, 1974). With this in mind, the use of the width of an ice wedge is not useful in the determination of the age of the ice wedge due to the variance in the frequency of cracking. Following each stage of cracking, spring meltwater once again flows into and refreezes in the crack, and after many cycles, leads to the development of a wedge shape. Furthermore, because the growth of ice wedges occurs through the infilling of snow meltwater, each folia/vein preserves information about winter precipitation and thus temperatures (Meyer et al., 2002). Researchers have then used these records of the isotopic value of winter precipitation as potential proxies for paleoclimate and paleotemperatures (Lacelle et al., 2004; Lacelle et al., 2007; Kotler et al., 2010; Meyer et al., 2010; St. Jean et al., 2010; Fritz et al., 2011; Raffi and Stenni, 2011; Lachniet et al., 2012; Vasil'chuk, 2013).

Three different types of ice wedges, Anti-syngenetic, Syngenetic and Epigenetic (Figure 4) can be distinguished according to ground surface stability, and form through three different processes (Murton, 2013), of which, syngenetic and epigenetic are most common. In northern Canada and Alaska, it is believed that most ice wedges are epigenetic in origin, although small syngenetic structures have been described (Harry and Godzik, 1988). Syngenetic ice wedges are formed when thermal contraction of frozen ground and infilling occur synchronously with sediment accumulation (Murton, 2013). As the deposition of sediments, peat accumulation, burial and movements occur, the height of the ice wedge increases along with its enclosing materials (French, 2007). Therefore, in theory, ages obtained from syngenetic ice wedges should be similar those of the host sediment (French and Shur, 2010), however, this is not always the case and is discussed later on. Syngenetic ice wedges, often much larger than epigenetic ice wedges, may be up to 3-5m wide near the surface, and can extend down by as much as 10m as growth occurs over long periods of continuous sedimention (Harry and Godzik, 1988).

On the contrary, epigenetic ice wedges form in pre-existing permafrost, with little sediment accumulation (stable conditions) on the surface (Mackay, 1992), and therefore should return ages younger than the surrounding sediment (Mackay, 1990) Epigenetic ice wedges are commonly 1-1.5m wide at the permafrost table (or bottom of the active layer), and usually less

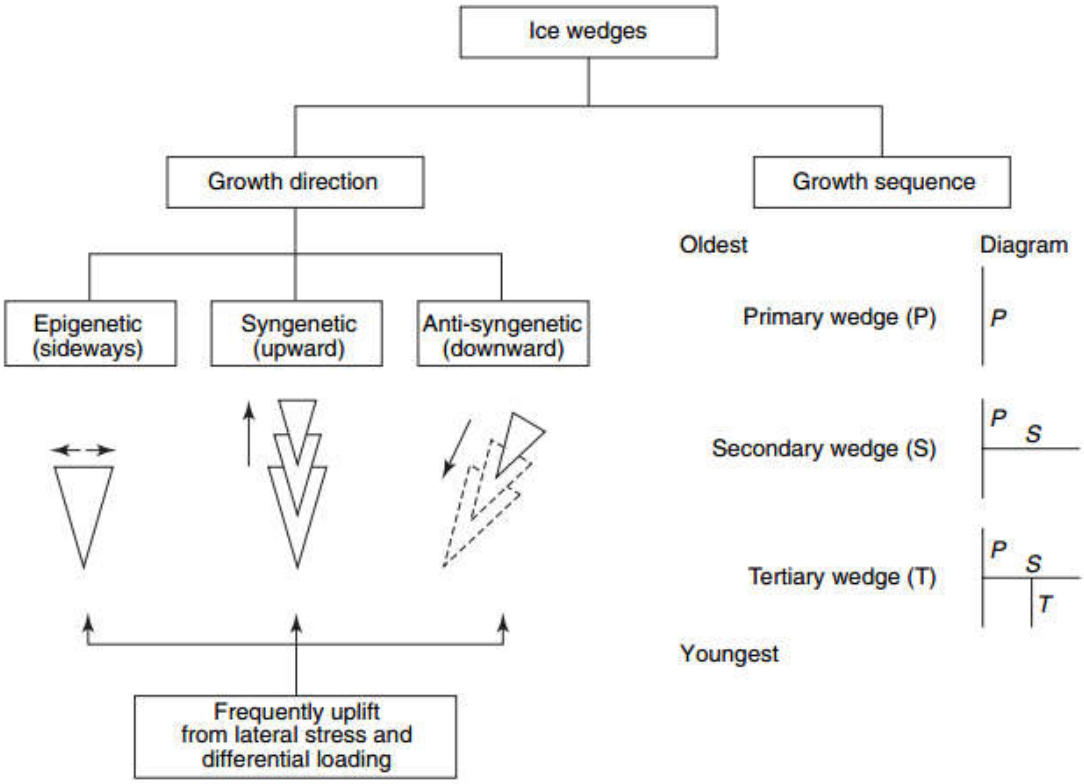

Figure 4. Classification of the different forms of ice wedges, epigenetic, syngenetic and anti-syngenetic, according to growth direction and growth sequence. Source: Mackay, 2000.

than 4m in height and is often a reflection of the mean depth of frost cracking (thermal crack). Unlike syngenetic ice wedges, they do not increase in depth, only in width as they grow (Figure 5). As such, as an epigenetic ice wedge grows and each new vein is added, older ice is moved towards the edges as younger ice is formed in the middle (French, 2007). Due the thermal expansion of water during its phase change to ice, an increase of ca. 9% volumetrically, the lateral (horizontal) pressure exerted by the ice results in the up-warping and in some cases, overturning of stratification within the enclosing sediments (Harry and Godzik, 1988). However, in some cases the lateral growth may be self-limiting in that the compressive stresses generated by the expansion of the ice wedge (Black, 1976), resulting in smaller frost cracks, as well as the ice wedge being 'squeezed' upwards above the permafrost table and subsequently truncated by thaw of the active layer (Harry and Godzik, 1988; Mackay, 2000). The combination of lateral and vertical expansion results in the upward deformation at the ground surface to form ridges up to 1m in height (Figure 5). This creates the characteristic polygonal framework associated with ice wedges, linear depressions (narrow troughs) with parallel ridges arranged in squares or hexagons with a diameter of 10-30m (Harry and Godzik, 1988; Plug and Werner, 2002). However, Plug

and Werner (2008) warn that despite numerous commonalities, ice-wedge networks may differ amongst and within sites, and can show variable frequency of fracture, growth (infilling), spacing, orientation and deformation of frozen ground around expanding wedges. Due to the complexity of the various mechanisms associated with ice wedges, Murton (2013) suggests caution when looking at initial paleoenvironmental and paleotemperature estimates in Quaternary literature.

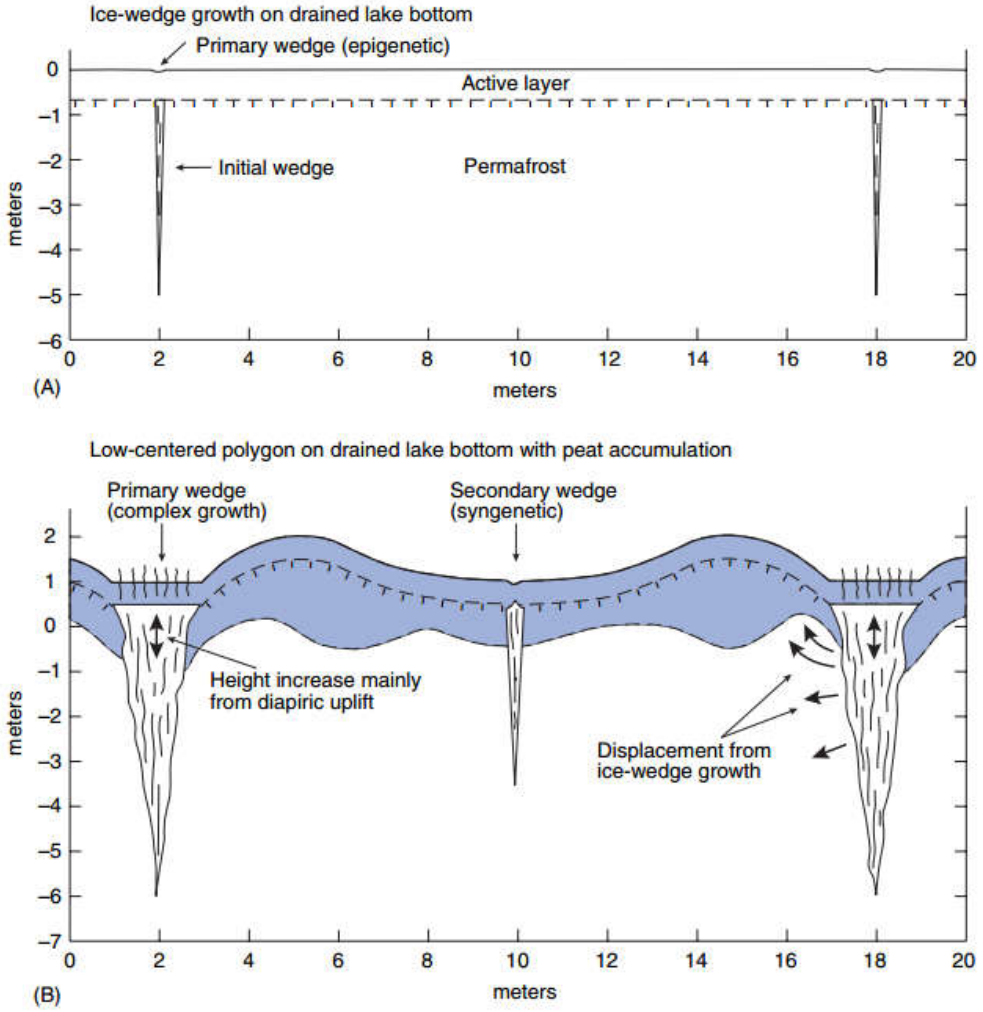

Figure 5. Schematic diagram showing the growth of primary epigenetic ice wedges and subsequent ground modifications/transformations. A) Initial growth (beginning) of an epigenetic ice wedge on a newly drained lake bottom. The tops of the ice wedges begin growth 0.7m below the zero datum of the lake bottom (i.e. depth of active layer). B) The growth of the ice wedge after several cracking and infilling cycles along with the accumulation of 1-2m of peat. The tops of the ice wedges now sit 0.5m above the zero datum of the lake bottom and at the base of the active layer. Source: Murton, 2013. Reproduced by Murton (2013) from Mackay (1992).

1.2. Stable O-H Isotopes

Atoms of each chemical element have a specific atomic number and atomic mass. An atomic mass of an element is comprised of the number of protons and neutrons, however, in some elements, the number of protons in the nucleus may remain unchanged, while the number of neutrons varies. Elements that have the same numbers of protons and electrons, but vary in neutrons are known as isotopes (i.e. ^{16}O, ^{17}O, ^{18}O). In some cases however, the presence of too many or too few neutrons in the nucleus can cause the element to be unstable (i.e. ^{14}C), resulting in the spontaneous emission of particles of energy to achieve a stable state. This process is known as radioactive decay (Further explanation in the next section). Despite the difference in the number of neutrons in a nucleus, some elements remain un-reactive and are known as stable-isotopes. The difference in the number of neutrons between different isotopes results in similar charges but different masses. As a result, it is possible to separate elements based on their atomic mass using various analytical apparatuses. Stable isotopes of interest in the study of water and ice include oxygen-18 (^{18}O) and deuterium (^{2}H), as they provide further insight into physical and chemical processes occurring in the environment.

The most common isotopes within water are ^{16}O (99.63%) and ^{1}H (99.98%). Two other isotopes exist for each element (^{18}O, ^{17}O and ^{3}H (Tritium) and ^{2}H (Deuterium)), but are much less abundant. The measure of the various different isotopes is done by the ratio of the two most abundant isotopes of a given isotope relative to the less abundant isotope (Clark and Fritz, 1997). The abundance of each isotope is expressed as the parts per thousand of difference between the sample and an internationally recognized reference, VSMOW (Vienna Standard Mean Ocean Waters), whereby;

$$\delta = \frac{(R_{sample} - R_{standard})\, x\, 1000}{R_{standard}} \qquad (1)$$

Where R is the isotope ratio: $^{18}O/^{16}O$, $^{17}O/^{16}O$ or T/H, D/H.

The changes in abundance of isotopes are referred to as delta-values that are expressed as parts per thousand (‰) differences between the sample and reference. For example, a ratio value of -10‰ has 10‰ less ^{18}O than the reference, or is depleted in ^{18}O by 10‰.

The ratio of ^{18}O and D incorporated within water molecules exhibit systematic spatial and temporal variations as they fractionate within the water-cycle. This fractionation of isotopes is due to the difference in atomic weight, where heavier water ($H_2{}^{18}O$) remains in a condensed state as more energy is required for evaporation compared to lighter water ($H_2{}^{16}O$). Therefore during evaporation, water vapour becomes enriched in ^{16}O while the remaining water becomes enriched in ^{18}O. Changes in $\delta^{18}O$ and D values of precipitation can occur as a result of Rayleigh distillation, whereby equilibrium fractionation occurs during a phase change from vapour to condensate (precipitation). As the air mass moves along it's trajectory, this phase change (Rayleigh distillation) results in the preferential depletion of ^{18}O within the air mass as a decrease in energy results in the preferential condensation of ^{18}O versus ^{16}O as more energy is required to maintain ^{18}O in an evaporated state (Figure 6). As such, as an air mass moves along its trajectory, ^{18}O becomes increasingly depleted, and each subsequent rain event becomes correspondingly depleted with respect to the remaining vapour from the previous rain event as isotopically heavier water is continuously removed from the air mass.

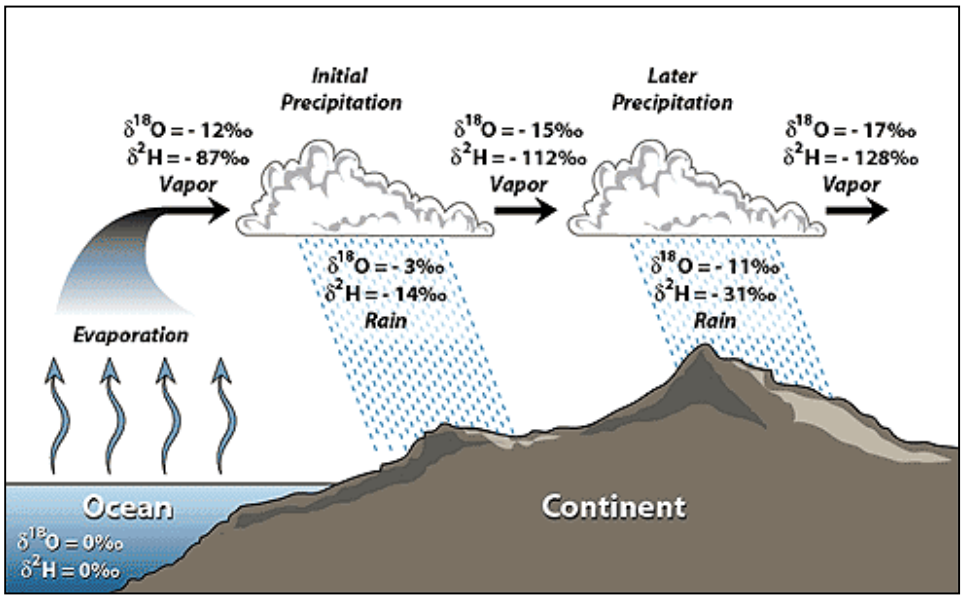

Figure 6. Rainout effect (Rayleigh Distillation) on $\delta^{18}O$ and δD values. Source: Hoefs (1997).

The most important factor controlling the isotopic composition of water is surface air temperature (Craig, 1961). This relationship exists as precipitation and rainout are driven by decreasing temperature. Water vapour in the water-cycle originates from the sub-tropical and northward oceans, and as it travels towards higher latitudes, it is cooled. As such, as an air mass

progresses towards the poles, precipitation becomes progressively depleted in ^{18}O values as air masses undergo isotopic partitioning during adiabatic cooling (Dansgaard, 1964). This process can be explained through Rayleigh distillation;

$$R = R_0 f^{(\alpha-1)} \quad (2)$$

$R=R_0f^{(\alpha-1)}$where; R is the isotopic ratio after rainout, R_o is the initial isotopic ratio, and f is the fraction of substance remaining (Clark and Fritz, 1997). The relationship between $\delta^{18}O$ and δD in most global precipitation is characterized by the Global Meteoric Water Line (GMWL) and is influenced by temperature (Figure 7). Since the inception of the GMWL by Dansgaard (1964), a vast network of stations have been set up by the International Atomic Energy Agency's (IAEA) Global Network of Isotopes in Precipitation (GNIP) to analyze the global stable isotopic composition of modern precipitation. With this, it was possible to generate a Local Meteoric Water Line (LMWL) more representative of conditions and climates specific to a region. As such, the slope and intercept of any LMWL can be significantly different from the GMWL. For example, the LMWL for two sites located within the Yukon originate from Inuvik and Mayo are;

$$\delta D_{INUVIK} = 7.3\delta^{18}O \quad 3.5\ (Lacelle\ et\ al., 2009) \quad (3)$$

$$\delta D_{MAYO} = 6.3\ \delta^{18}O \quad 36.8\ (Lacelle\ et\ al., 2009) \quad (4)$$

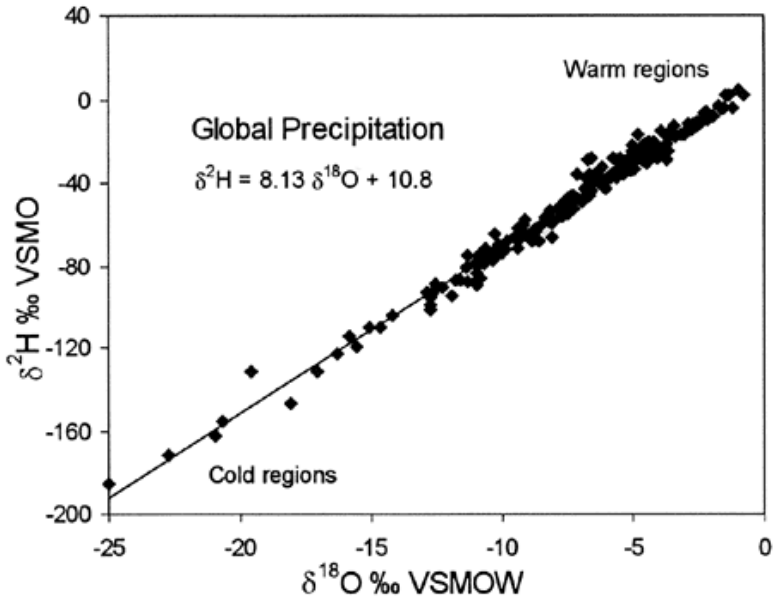

Figure 7. The relation between $\delta^{18}O$ and δD as expressed by the Global Meteoric Water Line (GMWL). Source: Clark and Fritz (1997).

1.2.1. Stable Isotopes in the Arctic

The isotopic composition of ice (single point values and regressions) can be used as an important tool to provide information about permafrost stability, paleoclimatic conditions during the formation of the ice (temperature and humidity) as well as its method of formation and source of origin. Isotopic discontinuities within sediments can be used as an indication of a changing climate, in the form of a thaw unconformity indicating permafrost degradation, or erosional event shown by the sharp change in ^{18}O signature. As previously mentioned, the isotopic composition of water is strongly controlled by temperature. Isotope ratios of $^{18}O/^{16}O$ or D/H in the water molecules of the precipitation reflect the temperature of the cloud vapour present at the time the formation of precipitation (rain or snow) and are thus representative of the air temperature. The variations in isotopes are linearly related to temperature (Dansgaard, 1964), and can be determined using the following equation;

$$\delta^{18}O = 0.695T \quad 13.6‰ \qquad (5)$$

where; T is the mean annual air temperature (MAAT) at the ground surface and $\delta^{18}O$ is the mean annual value at the site. Using this equation, it is possible to infer past winter air temperatures from the analyses of stable oxygen isotope records obtained from ground ice, such as from foliations in ice wedges, where more negative $\delta^{18}O$ values indicate colder temperatures and vice versa. In the case of ice wedges, the $\delta^{18}O$ records are thought to represent those of winter temperatures due to the infilling of ice wedge cracks by precipitation in the form of snow and snowmelt, with a strong correlation between $\delta^{18}O$ values in ground ice and average winter surface air temperatures (Lee et al., 2010).

The slope generated for an $\delta^{18}O$ vs D plot, while providing information on the $^{18}0/D$ ratio, can also be used to determine the source of origin of the ice. As many bodies of ice can be formed from different origins (i.e. buried snowback, frozen pond, remnant glacier, winter precipitation, meltwater etc.), determining the method of formation of the buried ice can provide clues on paleoclimate, glaciation and sedimention history. Kinetic processes such as evaporation at the snow surface can cause variations in $\delta^{18}O$ values, where enrichment can occur due to the isotopic exchange between vapour and snow (Clark and Fritz, 1997). Furthermore, during the melting of snow, the initial meltwater generated may be depleted in $\delta^{18}O$ values due to the preferential isotopic exchange and redistribution of ^{18}O between liquid water and ice. As $\delta^{18}O$

values increase with further melting and percolates down through the snow and in to the ground, the change in isotopic concentration can result in a decrease in the δD - $\delta^{18}O$ slope (Lee et al., 2010; Lacelle, 2011, Clark and Fritz, 1997). The freezing of water under equilibrium conditions can also result in Raleigh-type isotope fractionation between water and ice where, as freezing begins, the first ice to form will be enriched in ^{18}O by about 3‰ (Figure 8A).

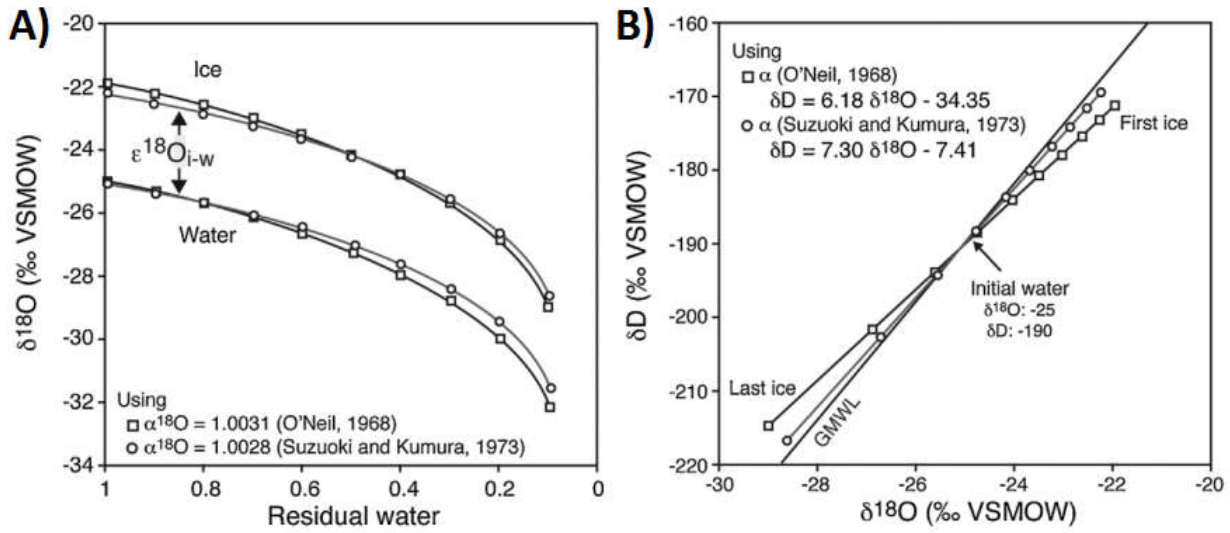

Figure 8. A) Raleigh-type isotope fractionation of $\delta^{18}O$ in water and ice during equilibrium fractionation. B)δ18O vs δD plot during equilibrium freezing of water where 'first ice' is the first ice to form from the water, and last ice is the last remaining water to freeze. Source: Lacelle, 2011.

As freezing continues, the isotopic composition of the ice formed will continue to progressively become depleted, and can be explained by Rayleigh-type isotope fractionation between water and ice;

$$R = R_0 f^{(\alpha i - w - 1)} + (\alpha_{i-w} \quad 1) \qquad (6)$$

where; R is the isotope ratio, $\alpha_{i\text{-}w}$ is the equilibrium isotope fractionation factor between water and ice and f is the residual fraction of water during freezing. On a δ18O vs δD plot, the freezing slope generated during ideal Rayleigh-type isotopic fractionation produces slopes been 6.2 and 7.3, lower than that of the GMWL (Figure 8B). This value however, is dependent on the initial isotope composition of the water, freezing rate, thickness of the boundary layer and isotope diffusion at the ice-water interface (Lacelle, 2011). With this in mind, co-isotope slopes similar to, or greater than the LMWL of 6.3 to 7.3 (Mayo and Inuvik) are likely to have originated from atmospheric sources, such as glacier ice or a buried snow bank. On the other hand, slopes below 6 would suggest the intrasedimental body of ice, such as an ice wedge or pore ice, was derived

from groundwater that formed during the later stages of closed-system freezing (Jouzel and Souchez, 1982; Mackay, 1983; Lacelle et al., 2004; Lacelle et al., 2007).

1.3. Radiocarbon

Radiometric techniques are based on the premise that certain naturally occurring elements are unstable (reactive) and will undergo spontaneous changes in their structure and organization in order to achieve more stable forms. This process is known as radioactive decay and is a time-dependent reaction, and if the rate of decay of the element is known, the age of a material can be determined.

Radioactive decay processes are governed by atomic constants. The number of transformations per unit of time is proportional to the number of atoms present in the sample and for each decay pathway there is a decay constant. In all radioactive nuclides, the decay is not linear but exponential and is usually considered in terms of the half-life (i.e. the length of time that is required to reduce a given quantity of a parent nuclide to one half). An atom that undergoes radioactive decay is termed a parent nuclide, and the decay product is often referred to as a daughter nuclide.

While the concept of radiocarbon (^{14}C) was discovered shortly after the second world war, it has been during the he last two decades of the twentieth century, characterized by a series of technological innovations, that led to significant improvements in analytical precision and brought radiocarbon to the fore-front. A major advance was the development of accelerator mass spectrometry, which not only revolutionised radiocarbon dating.

Radiocarbon (^{14}C) is one of three isotopes of carbon, the others being ^{12}C and ^{13}C. The most abundant of the carbon isotopes is ^{12}C, which makes up 98.9% of carbon, followed by ^{13}C at 1.1%, and ^{14}C, comprising of one part in 10^{10}% (only about one in a 10^{12} atoms). Both ^{12}C and ^{13}C are stable isotopes, while ^{14}C is not and decays to a stable form of ^{14}N. ^{14}C is formed in the upper layers of the troposphere and stratosphere. In this process, ^{14}N atoms in the atmosphere are exposed to cosmic ray neutrons, where by the neutrons are captured by the ^{14}N atoms, resulting in the loss of a proton, thus producing ^{14}C (Clark and Fritz, 1997):

$$^{1}n + {}^{14}N \rightarrow {}^{14}C + {}^{1}p$$

The ^{14}C that is produced oxidizes with oxygen to produce a particular form of carbon dioxide ($^{14}CO_2$), which then mixes with other forms of non- radiocarbon carbon dioxide ($^{13}CO_2$, $^{12}CO_2$) molecules in the atmosphere, and in doing so, ^{14}C becomes a part of the global carbon cycle. From the atmosphere, the majority of CO_2 (more than 95%) is absorbed into the oceans as dissolved carbonate (up take by living organisms), while the remaining is assimilated by plants through photosynthesis. The radiocarbon can then be further sequestered into the soil by the production of organic material through plant degradation and microbial activity, as well as root respiration. These organic compounds can then be further broken down and released into the soil and catchments as dissolved organic carbon (DOC). This soil-derived organic matter is most often composed of humic acids with high molecular weights (Clark and Fritz, 1997). Low molecular weight organic matter, such as cellulose (from plant matter), protein and other organic acids make up the remainder of the DOC fraction. It is there within the soils where a large quantity of ^{14}C can be stored in compared to the atmosphere, as the atmosphere contains approximately 400ppmv (P_{CO2}~$10^{-3.4}$) of CO_2, while soils, depending on the type and organic content, can contain between 3,000 to 30,000 ppmv (P_{CO2}~ $10^{-2.5}$ to $10^{-1.5}$) of CO_2.

Once the ^{14}C is assimilated into the oceans and terrestrial biosphere, it will then begin to start the decay process. That being said, although the ^{14}C being absorbed is constantly decaying, it is continually replenished by the ^{14}C that is being produced in the atmosphere, thus the ^{14}C that is stored in plant and animal tissues, and in the world's oceans (the global carbon reservoir), remains approximately constant through time. As a result of the constant uptake of ^{14}C, a position is reached where by the carbon that is used to build plant and animal tissue is in isotopic equilibrium with the atmosphere, and therefore the ^{14}C activity is the same in both. However, once an organism dies, it becomes isolated from the ^{14}C source, and thus no further replenishment can take place. It is at this point in which the 'radiocarbon clock' begins, and any ^{14}C in assimilated will begin to radioactively decay at a constant rate. By measuring how much ^{14}C remains in a sample of fossil material and comparing it to modern ^{14}C in standard material, the age of the material can be inferred. Experimental results have shown that the decay rate of ^{14}C is 1% for every 83 years, and since the decay curve (Figure 9)is not linear but exponential, this leads to a half life of 5730 years for an atom of ^{14}C. With a limit of measurement for ^{14}C activity of eight half-lives, this translates to an upper age dating limit of approximately 45,000 years.

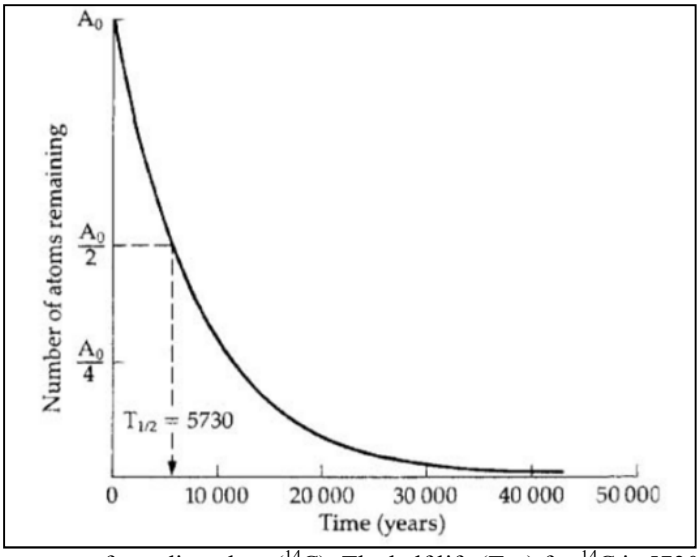

Figure 9. Radiocative decay curve for radiocarbon (^{14}C). The half life ($T_{1/2}$) for ^{14}C is 5730 years. A_0 denotes the initial quantity/concentration of ^{14}C contained within the material. Source: Walker, 2005.

Radiocarbon dating can be completed on a wide range of biogenic materials containing carbon such as wood, peat, organic lake sediments, plant remains, charcoal, shell and coral. Another source, new to the radioactive dating community, is Dissolved Inorganic Carbon (DIC) and Dissolved Organic Carbon (DOC). These two new sources allow for the dating of groundwaters and surficial water sources, and most recently ground ice. The premise behind the use of DOC and DIC as dating material is, ^{14}C is washed from soils by surface or groundwaters, where it is incorporated into the water source as DOC and DIC and remains in solution and follows the flow path of the source. However, unlike traditional dating material, the DIC and DOC within the water needs to be extracted from the water source (further about this in the methods) since it is dissolved. Furthermore, large quantities of water may be required in order to obtain enough ^{14}C material to be analyzed. In order for the material to be analyzed, the carbon source is converted to graphite pellets where they can then be dated using beta counting, or accelerator mass spectrometry (AMS). AMS employs the use of particle accelerators as mass spectrometers to count the relative number of ^{14}C atoms in a sample, as opposed to the decay products.

Normal mass spectrometers function on the basis of detecting atoms of particular elements based on differences in atomic weights. However, they are unable to discriminate between ^{14}C and other atoms of similar atomic weight (ex. ^{14}N). The creation of the AMS solved this issue, by accelerating the particles to very high speeds, and thus separating the small ^{14}C

signal (Figure 10). However, AMS does not count the absolute number of ^{14}C atoms that are being measured, but rather, determines the isotope ratio of ^{14}C relative to that of other stable isotopes of carbon (^{13}C & ^{12}C), known as isotope ratio mass spectrometry. The age is then determined by comparing this ratio with that of a standard of known ^{14}C content. Radiocarbon values are then either reported as a ratio of $^{14}C/^{12}C$ where a higher ratio represents a greater proportion of modern carbon, or as years before 1950.

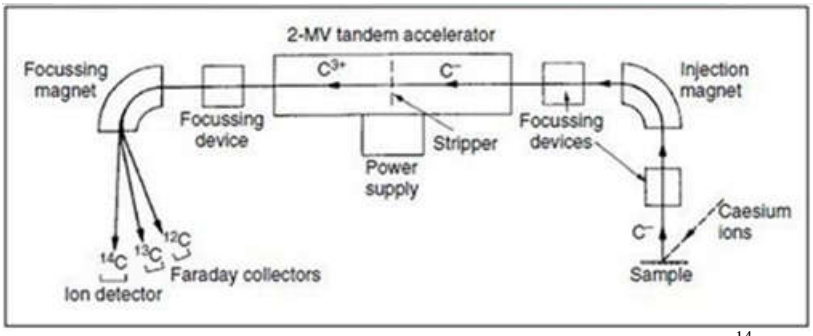

Figure 10. Schematic diagram of a tandem accelerator for the detection and counting of ^{14}C atoms. Source: Walker, 2005 (Lower).

1.3.1. Radiocarbon in the Arctic

As previously mentioned, soils play a pivotal role in the storage of carbon, with the potential to store between 7-75 times more CO_2 (in ppmv) than in the atmosphere. In Arctic regions where permafrost is present, large carbon reservoirs (including ^{14}C) have developed due to carbon being 'trapped' within frozen ground or ice and not being released back into the carbon cycle (Fritz et al., 2015). These carbon stores are often composed of carbon frozen at depth in peat deposits, the Active layer (containing 20-60% carbon) or carbon that has intermixed with mineral soils (0.1-20% carbon) (Schurr et al., 2008, Vonk et al., 2013)). When incorporated in to permafrost, this organic material can be used as dating material to infer the age of formation, either within the sediments or bodies of ice.

In this study, a focus has been on the use of DOC and DIC as the radiocarbon dating matter as opposed to the classical approach using Particulate Organic Carbon (POC). In the past, bodies of ice (pore ice, pooled ice, vein ice, massive ice & ice wedges) have been dated using particulate matter (POC) such as twigs, branches, roots, pollen and shells to determine the age of the ice in which it is embedded in (Hamilton et al., 1998; Burn, 1997; Kotler and Burn, 2000; Lacelle et al., 2004; Lacelle et al., 2007; Lacelle et al., 2009; St. Jean et al., 2011; Lachniet et al.,

2012; Vasil'chuk, 2013). This method has also been used in the dating of sediments. However, recent studies have indicated the possibility for the contamination of an organic sample by either old or modern carbon (Vasil'chuk and Vasil'chuk, 2014), that can result in radiocarbon dates that are not a true representation of the sediments or ice that is being dated.

This issue of contamination of a radiocarbon sample with old carbon has appeared in many studies, and has often been problematic for radiocarbon dating and paleoenvironmental interpretations of sedimentary sequences. This issue has also been well documented in archaeological studies with the presence of 'old-wood' and 'old-bones'. Findings in studies by Nelson et al. (1988) and Schuur et al. (2009) indicate the persistence of ancient organic material (twigs, branches, roots etc.) for thousands of years within perennially frozen sediments, and upon thawing of permafrost or ice, provide a source of old carbon contamination (Demuro et al., 2008). In a review by Vasil'chuk and Vasil'chuk (2014), the authors noted that in many cases, specifically in syncryogenic accumulation, vegetative cover is often not continuous in the area and as such, the inclusion of allochthonous organic deposits from a distance from its present position, either from fluvial disturbances or thawing of permafrost, is a common occurrence. Vasil'chuk and Vasil'chuk (2014) found this allochthonous carbon was often a source of old carbon contamination due to the very good preservation of organic materials in permafrost and the cyclical thawing and re-deposition of old carbon in the environment. Hamilton et al. (1988) obtained plant detritus of alluvial origin from within the same horizon that returned ages from 27.8 to 43.3 kyr, a difference of 12 kyr and indicating the recycling and movement of carbon of various ages. Stanley (2001) also found organic material found in the depressions of valleys and deltas was enriched in ancient organic material that had been moved from higher elevations. Another possible source for the contamination of old carbon comes from the process of cryoturbation. The constant freezing and thawing of the permafrost can result in the mixing (frost churning) of materials in the soil resulting in older carbon from deeper sediments mixing with younger carbon from above. This process can also result in organic carbon pools being moved to much deeper depths (Zimon et al., 2006), and as such can give a much older or younger age for the deposition of sediments than what is actually the case. This situation of age inversion, the irregular distribution of ^{14}C within an outcrop, has been problematic whether from cryoturbation or allochthonous material. These age inversions were seen at the Fox Permafrost tunnel in Alaska, as ages were often found out of stratigraphic order (Hamilton et al., 1988), or ages from

material trapped within a body of ice found to be much older than the actual formation of the body of ice (Griffing et al., Hamilton et al., Lachniet et al., 2013). In a review on the strategy and choice of valid ^{14}C dates in syngenetic permafrost, Vasil'chuk and Vasil'chuk (2014) suggest that these anomalous dates or inversion of dates within bodies of ice or stratigraphic layers are not an exception, but rather a rule.

The type of material being used as the radiocarbon material (i.e. insects vs. pollen vs. woody material vs. bones, etc) was also found to be problematic and shown to return differing ages (younger and older) despite being found within the same deposit (Kennedy et al., 2010, Vasil'chuk and Vasil'chuk, 2014). The various size fractions has also been shown to be a possible source of contamination. Nelson et al. (1988) collected a large sample of allochtonous peat and separated the material in to different size fractions, with each fraction dated on its own. The results from the subsequent dating provided ages ranging from 13,250 to 30,260 years BP, with size fractions becoming older as size increased, thus concluding the smaller the fossil size, the older the date.

While it has been shown that radiocarbon dating can be subject to certain limitations as well as the potential for reduced reliability, it never the less can be used as a powerful dating tool when used properly and under the right strategy for the choice of dating material. Vasil'chuk and Vasil'chuk (2014) suggest that when selecting the dating material, the fluvial origins (precipitation outwash, melting of snow, rivers etc.) should be taken into consideration. Furthermore, the youngest of the ^{14}C dates obtained from the particular horizon should be considered closest to the actual time of accumulation and freezing as new material can no longer be incorporated after freezing.

A new method for radiocarbon dating of ice, although used for decades in the dating of groundwaters, is the use of Dissolved Organic Carbon (DOC) as the dating material. As opposed to detrital matter (POC) commonly used, DOC has shown potential to be a more reliable dating material (Lachniet et al., 2012). The formation of ice wedges occurs through the infilling of cracks in the ground by meltwater. This meltwater is derived from atmospheric sources that have come in contact with vegetation and sediments on the surface, and in some cases organic matter within the active layer, prior to infiltrating frost cracks (Opel et al., 2011). As this meltwater is often spring snowmelt, it is considered to be pristine/pure and as a result, is able to attract and

leach considerable amounts of highly bioavailable DOC and other elements/ions from relatively young surface organic matter (Guo et al., 2007; Lachniet et al., 2012; Fritz et al., 2015). Lachniet et al. (2012) have shown that $\delta^{13}C$ values of DOC are nearly identical to that of POC, and therefore support the notion of the dissolution of organic matter found on the ground surface and within the active layer during periods of thaw as the source of DOC material. Recent studies had shown massive ground ice to contain large stores of DOC, with ice wedges containing the greatest potential for DOC storage of all massive ground ice types. Concentrations within ice wedges from multiple studies have shown to range from 8.8-68.5 mg/L (Vonk et al., 2013; Lachniet et al., 2012; Douglas et al., 2011; Fritz et al., 2015), offering the potential for a significant source of material required for radiocarbon dating.

In a recent study, Lachniet et al. (2012) compared POC radiocarbon dates obtained from an ice wedge and its surrounding sediments from a previous study, to newly obtained radiocarbon dates using DOC and CO_2 as the dating material. Radiocarbon dating based on POC ^{14}C originally assigned an age of Marine Isotope Stage (MIS) 3 (34 to 41ka cal BP) to the ice wedge, while recent dates from DOC and occluded CO_2 gas returned significantly younger dates between 22 to 28 ka cal BP. This age disparity indicated the persistence of old carbon in the environment causing anomalously old ages when dating POC, bringing in to question the true age of ice wedges and timing of events in Central Alaska. By dating the occluded CO_2 gas, Lachniet et al. (2012) were able to model the age of the CO_2 by calculating the fraction of respired CO_2 and the age of the respired CO_2. The modeled ages, although younger than the obtained CO_2 ages, produced ages near DOC ages. Due to the close ages between modelled and obtained CO_2 ages and DOC ages, Lachniet et al. (2012) concluded that DOC ages could be used as more reliable dating material than POC. With the these new ^{14}C dates, along with previous work that had investigated stable isotopes ($\delta^{18}O$ δD) of the ice wedge ice, Griffing (2011) was able to newly constrain the age of formation to Heinrich event 2 during MIS 2. However, Lachniet et al. (2012) do note there are limitations to the use of DOC. There is the potential for old carbon to be stored in the active layer from which DOC can derive (Nelson et al., 1988; Schuur et al., 2009; Abbott and Stafford, 1996), and thus can only be used as maximum limiting ages. In the unlikely case that DOC is derived solely from contemporary soil carbon and vegetation living during ice wedge growth, DOC presents the opportunity to accurately represent the true age of the ice. However, there is no data that presently compares the proportion of 'new'

versus 'old' carbon within the active layer and its subsequent contribution to DOC and DIC fractions. Despite this uncertainty, Lachniet et al. (2012) do point out that that it is striking that DOC ages are still thousands of years younger than POC dates despite the complexity of carbon-cycle dynamics at the ground surface. As such, they recommend the use of DOC and CO_2 within the ice as a the source of 14C dating material to constrain the timing of ice wedge activity, with the caveat that these ages may themselves still be too old.

While uncertainty remains regarding the contribution of 'old' carbon to DOC and DIC, the use of DOC and DIC offers a unique opportunity to explore the possibility of the use of DOC and DIC in cases where POC may not easily be obtained. Furthermore, under the assumption that the source of DOC and DIC is from the surface or active layer from recent material that has not been affected by the 'recycling' of carbon often seen in the Arctic, the ages obtained from DOC and DIC potentially offer a more accurate age that is reflective of the true formation of the ice wedge. Nevertheless, until the contribution of 'old' carbon to DOC and DIC can be determined, dates obtained from DOC and DIC will still be considered maximum limiting ages.

1.3. Purpose

This thesis has two primary goals. The first goal was to test and incorporate new analytical techniques in the radiocarbon dating of ice wedges using Dissolved Inorganic Carbon (DIC) and Dissolved Organic Carbon (DOC) as dating sources contrary to the classical use of Particulate Organic Carbon (POC) as the dating source. The second goal of this thesis was to investigate the Paleoclimate, Glaciation and Sedimentation history of the region surrounding Two Moose Lake. This will be accomplished using the new dating techniques along with a variety of other analysis including stable isotopes and granulometry. These results will then be compared to other studies from the surrounding region in an effort to improve on the paleoclimate and glaciation history in the central Yukon.

2. Study Area

2.1. Overview of Area

The study area is situated at Two Moose Lake (64°44'06''N, 138°21'55''W, 1300-1400 m.a.s.l.) on the Blackstone plateau, central Yukon (Figure 11). The Blackstone plateau (ca. 1050 m.a.s.l), which measures approximately 200km long, and up to 65km wide, is bound to the North and South by the Ogilvie Mountains (1900-2000 m.a.s.l). The plateau is dissected by the Blackstone and East Blackstone rivers, located 200m to the east of Two Moose Lake, and is underlain by poorly resistant Palaeozoic metasedimentary, ultramafic and sedimentary rocks and is intruded by Cretaceous porphyritic syenite (Green, 1972). With heights of 2500m a.s.l., the intrusive rocks form the highest peaks in the area.

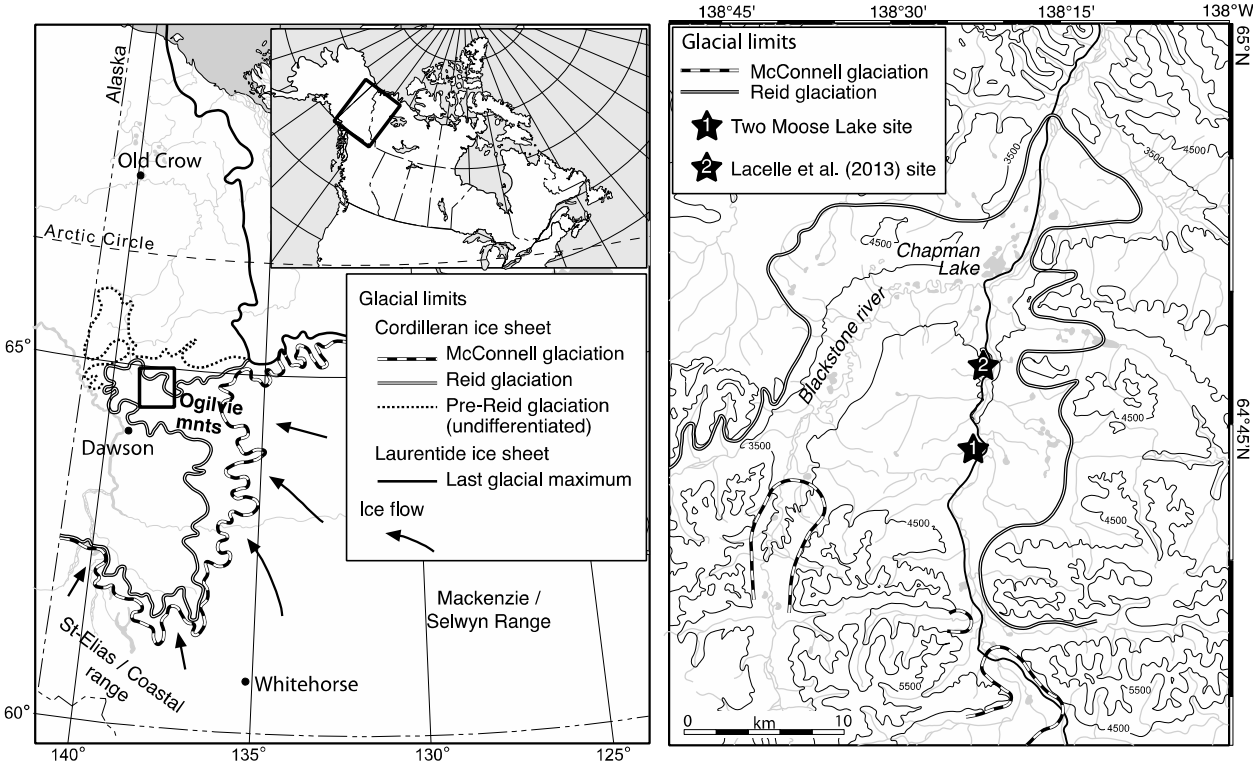

Figure 11. *Left:* Map showing the location of the study area in Yukon Territory, Canada. Quaternary glacial limits are indicated on the map. Map obtained from Lacelle et al. (2013) *Right*: Location of the slump exposure at Two Moose Lake (1). The location of the Chapman Lake study (2) by Lacelle et al. (2013) is also indicated, along with the glacial limits of the McConnell and Reid glaciations. Source: Adapted from Lacelle et al. (2013).

2.1.1. Surficial Geology

The Blackstone Plateau is long with undulating slopes, creating a subdued topography with northward draining hills and slopes. The surface sediments on the Blackstone Plateau, derived predominantly from the sedimentary rock located within the region, reflect the glacial and fluvial history, with unconsolidated glacial till occupying much of the lower laying area (Vernon and Hughes, 1996). Alluvial deposits occupy the river valleys. The glacial and alluvial deposits are comprised of a mixture of sand and silt, with a loose texture and irregular lenses of washed gravel. While the actual depth of the glacial sediments is not known, it is possible for them to be up to 30m thick. Discontinuous thin veneers of glacial deposits are also found on the upper slopes of the valleys in the region. The unglaciated highlands are covered by colluvium, namely carbonates sand and black chert and shale to support varying vegetation depending on slope orientation.

The Blackstone Plateau has a hummocky moraine morphology dotted by numerous kettle lakes, Chapman Lake, located ca. 10km north of Two Moose Lake, being the largest. Some of the landscape is also occupied by polygonal terrain underlain by ice wedges (Figure 12A). The study site is situated at Two Moose Lake, a small thermokarst lake situated at km104 of the Dempster Highway, a gravel permafrost road traversing northern Yukon and open year round. In summer 2013, a small thaw slump was discovered along the western shore of the lake. The slump (Figure 12B) likely formed as a result of thermo-erosion along the lakeshore. This process appears to have previously occurred at Two Moose Lake as there is evidence of a slump scars next to the current slump that has stabilized and been re-vegetated. The thaw slump exposes multi-tiered ice wedges and bodies of tabular massive ground ice. However, the slump appeared to have stabilized by the summer of 2015, as the overhang above the headwall had collapsed, and vegetation began to re-grow. This study investigates will investigate the origin and age of the ground ice bodies exposed in the headwall of the thaw slumps, which will help constrain the timing of glacial advances on the Blackstone Plateau and allow reconstructing the history of permafrost in the region.

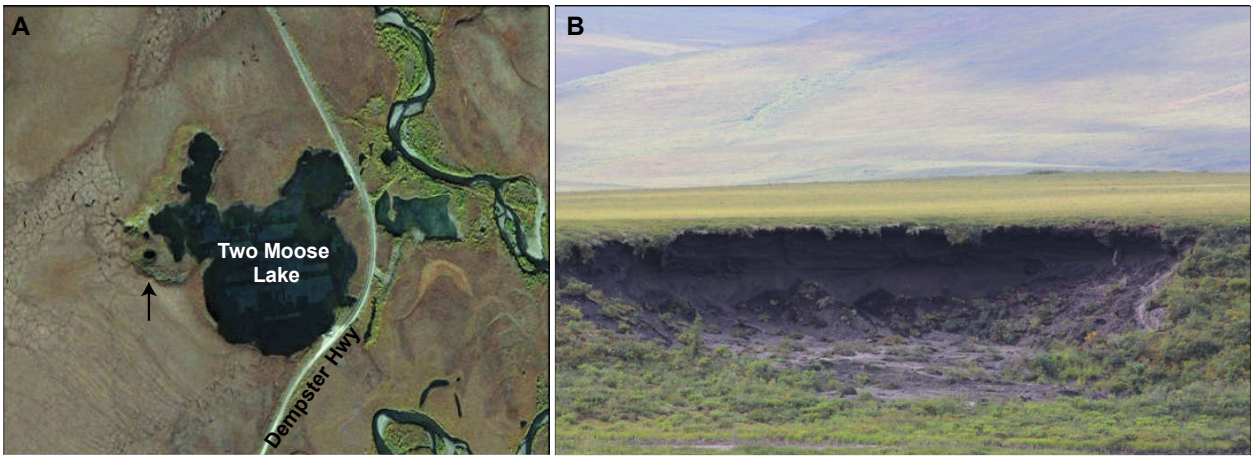

Figure 12. A) Satellite view of Two Moose Lake. The Sampling location is indicated by the arrow. The Dempster highway can be seen passing on the eastern (right) side of Two Moose Lake, and the Blackstone river on the other side of the Dempster Highway. Polygon squares (ice wedges) can be seen on the western and southern sides of the Lake (Image Source: Google Maps/Earth, 2016). B) Outcrop/slump at Two Moose Lake, August 2013. The photo was taken from across Two Moose Lake from the Dempster Highway, facing in the southwest direction.

2.1.2. Bedrock Geology

Surrounding the area of Two Moose Lake, various geological bedrock units are present (Green, 1972), where by the age of the unit decreases with unit number (Figure 13). To the north and northwest, Ordivician/Silurian carbonates (Unit 8) supporting little vegetation, and Devonian/Carboniferous aged black chert (Unit 13) and shale covered with moss are present. To the east, Devonian/Carboniferous aged black chert (Unit 13) is present. To the south, Precambrian volcanic rocks (andesite) (Unit 4) that are highly calcareous, and Ordivician/Silurian shales and carbonates (Unit 9) with heavy vegetation can be found. To the west, Proterozoic sedimentary rocks (Unit 2) composed primarily of weathering dolomite with thin layers of dark shale and slate occurring. While the specific geology surrounding the region is not directly pertinent to the study, knowledge of the local geology could be used indirectly as an indicator of the source of the till and material within bodies of ice to determine the source of the ice, whereby material similar to the local geology would suggest origin from a local glacier.

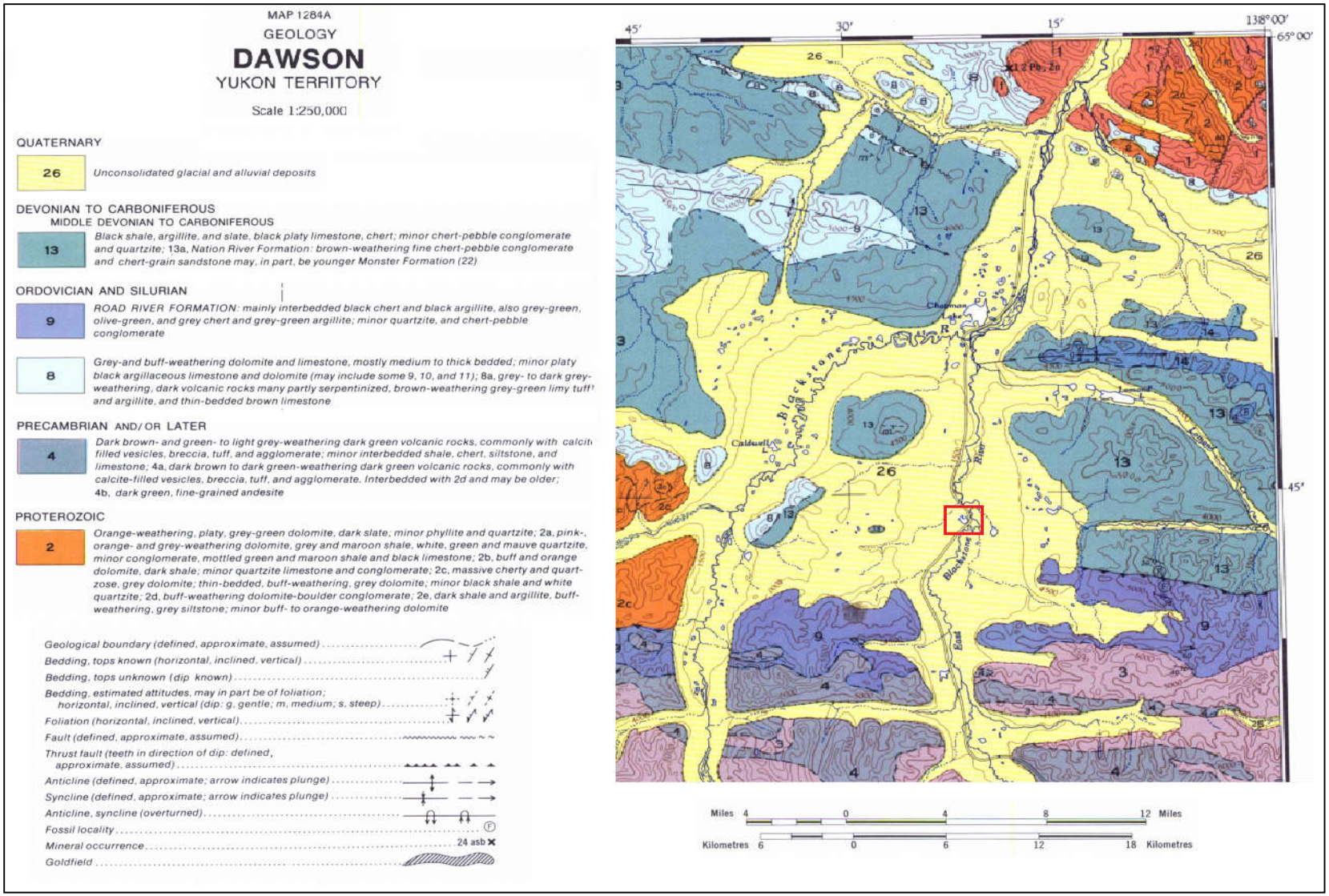

Figure 13. Geological units surrounding Two Moose Lake (identified by the red box), Yukon Territory. Source: Modified from Geological *Map 1284A - Geology of Dawson, Yukon Territory* (Geological Survey Canada, 1972).

2.2. Glacial History

2.2.1. Late Pleistocene: Pre-Reid Glaciations

The glaciation history of Yukon is highly variable, with vast areas being glaciated by the Cordilleran ice sheet while others remaining unglaciated, and the extent and timing of each often debated. Although often referred to as an ice sheet, Ward et al. (2007) and Demuro et al. (2012) describe the Cordilleran sheet rather as an ice complex, composed of a series of coalescing valley glaciers and piedmont lobes controlled strongly by topography. In southern and central Yukon, Bostock (1966) recognized a series of four regional Cordilleran glaciations and local montane glaciers in the region, with each subsequent glaciation less extensive than the previous (Figure 14). The decrease in the extent of each glaciation is attributed to, beginning in the late Cenozoic (ca. 2.7 million years BP), the uplift of the St. Elias Mountains and coastal range creating an orographic obstacle, and thus a decrease in supply of Pacific moisture, creating drier conditions in southern and central Yukon (Harris, 2005). The two oldest glaciations as determined by Bostock (1966), the Nansen and Klaza (often referred to as Pre-Reid glaciations) are poorly defined in terms of extent and age in central Yukon, but Froese et al. (2000) believe them to be greater than Late Pliocene (>2 Ma) in age. However, in recent publications, authors have suggested anywhere from 4 to 6 pre-Reid glaciations (Ward et al., 2007, Beierle, 2002, Duk-Rodkin et al., 1996), ranging from Late Pliocene (ca. 2.7 Ma) to middle Pleistocene.

2.2.2. Middle to Late Pleistocene: Reid and Gladstone Glaciations

The Reid glaciation (Figure 14), known as the penultimate glaciation, represents the most extensive Middle to late Pleistocene glaciation in southern and central Yukon, as represented by oldest traceable terminal moraine systems (Duk-rodkin et al., 2004). The Reid glaciation was originally constrained by fission track dating of Sheep Creek tephra (SCt) overlying a Reid moraine at the Ash Bend site in central Yukon to Marine Isotope Stage 8 (MIS 8) (190±20 ka; Hughes et al., 1987; Berger et al., 1996) and by a maximum age of 311±30 ka by Ar–Ar dating (Huscroft et al.,2004) of basalt underlying Reid glacial deposits along the Yukon River downstream of Fort Selkirk, south-central Yukon. However, new OSL dates by Westgate et al. (2008) have shown that the Sheep Creek tephra is actually composed of several

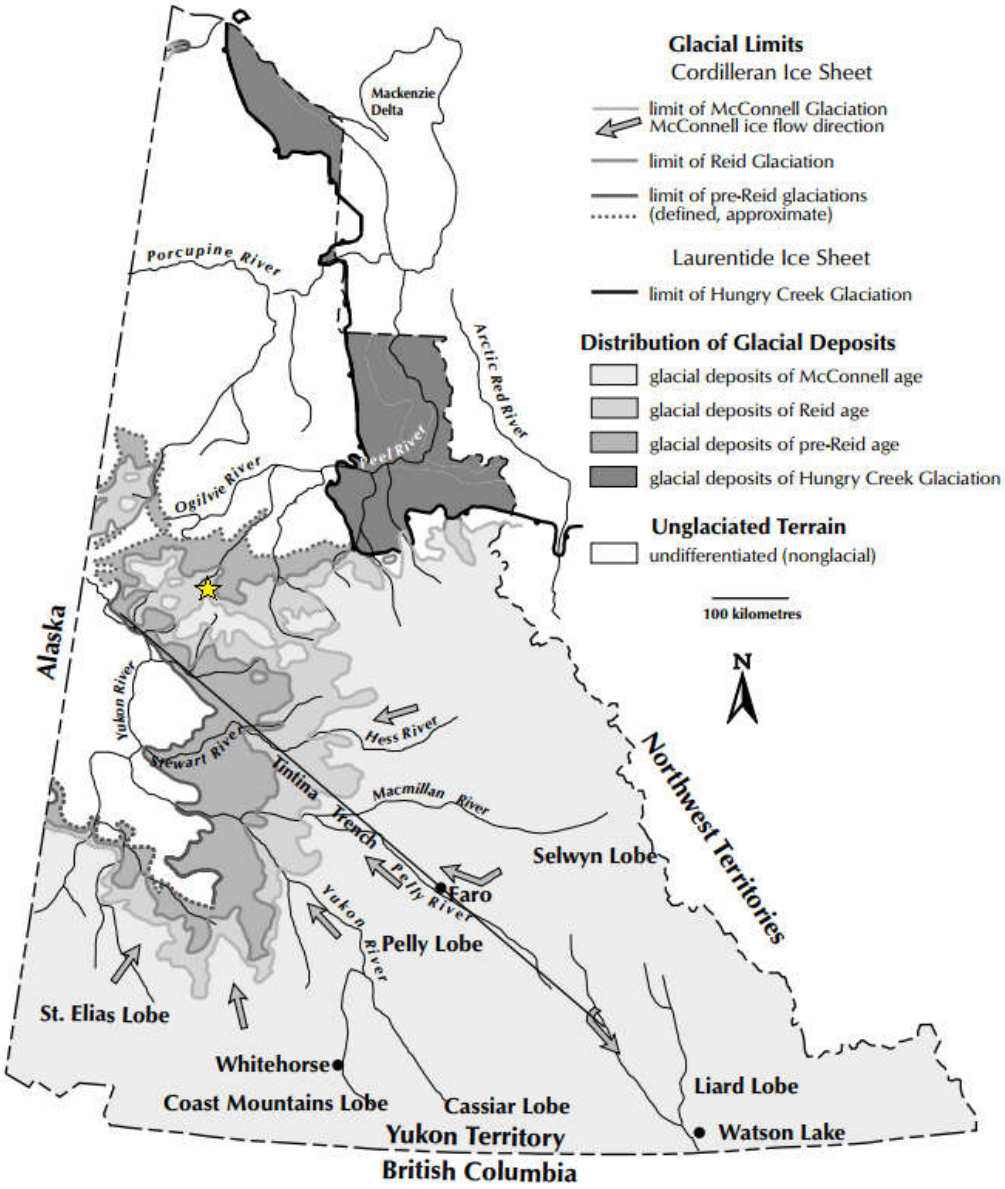

Figure 14. Glacial limits map of Yukon (after Duk-Rodkin, 1999). Source: Modified from Bond (2004).

stratigraphic units, and the SCt in Fairbanks (SCt-F, ca. 200ka) is in fact older than that in western Yukon (SCt-C, SCt-K and SCt-A, ca. 80ka), thus suggesting the Reid Glaciation in the central Yukon is more likely of MIS 6 age than MIS 8. The MIS 6 age of the Reid glaciation was further supported by OSL dates of silts containing Old Crow Tephra (OCt) overlying deglacial Reid Gravels. Ward et al. (2008) obtained ages of OCt from Pelly River in central Yukon originally dated to 140±10 ka, and later revised to 124±10 ka by Preece et al. (2011). On the first combined minimum and maximum chronological constraint on the Reid glaciation of the

central Yukon Territory, Demuro et al. (2012) obtained two OSL ages of 132 ± 18 ka and 158 ± 18 ka for the gravel units underlying and overlying the Reid till in the Stewart river valley.

Recent analysis, however, have shown that central Yukon may have been glaciated between the Reid glaciation and the most recent McConnell glaciation. Cosmogenic exposure dating on boulders in central Yukon by Ward et al. (2007) obtained ^{10}Be ages between 51-51 ka (n=4), the first MIS 4 (early Wisconsin) age for glaciation, proposing this glaciation be known as the 'Gladstone glaciation'. Further support for this glaciation can be found in adjacent Alaska, where TCN exposure dating on moraine boulders in the Yukon-Tanana Upland in east-central Alaska by Briner et al. (2005) obtained an age of to 53.1±15.9 ka, lending support to a local glaciation in the region during MIS 4. Ward et al. (2007) suggest the Gladstone glaciation is a result of the extension of the St Elias and Cassiar lobes of the Cordilleran ice sheet, while the Reid glaciation a result of the extension of the Selwyn Mountain lobe. Samples in southwest Yukon may further support this with tills represented by MIS 6 and MIS 4 ages (Turner et al., 2013).

2.2.3. Last Glacial Maximum: McConnell Glaciation

The most recent glaciation in southern and central Yukon, the McConnell glaciation, occurred during the late Wisconsin (MIS 2, ca. 30ka BP) glacial stage, terminating ca. 13-14ka BP (Figure 14). The McConnell glaciation was the least expansive of the glaciations in the Quaternary period, restricted mainly to southern (Cordilleran Ice Sheet) and eastern Yukon (Laurentide Ice Sheet), and represented by the innermost (youngest) major moraine system in Yukon (Bieirle, 2002, Bostock, 1966, Duk-rodkin, 1996). Evidence from midden assemblages (^{14}C dating) indicated that glacial conditions were established by 29ka BP, and full force by 24.5ka BP with the disappearance of spruce trees and a change to steppe-tundra ecosystems (Zazula et al., 2006; Zazula et al., 2007). Radiocarbon dating (^{14}C) of plant, wood and fossils underlying McConnell glacial sediments from the Mayo area indicated that periglacial climate and glaciation began ca. 29.6ka BP (Matthews et al., 1990). However, the extent and coverage of the McConnell glaciation is often debated, as expansive glaciers remained in mountainous areas in southern and eastern Yukon, while montane valley glaciers were contained to major valleys, with minimal expansion into the Blackstone plateau region in central Yukon (Jackson et al., 1991; Hughes et al., 1989; Duk-Rodkin et al., 1996). Lacelle et al., (2007) has suggested that ice

that covered the Blackstone Plateau (and remnant buried ice) is correlated to the Reid Glaciation, as the McConnell glaciation was restricted to minor advances in some valleys. Furthermore, Lacelle et al. (2007) go on to suggest that the lack of absolute dates of material of the local glacial chronology, and rather the use of soil development, relative weathering and stratigraphic positions of moraines has led to difficulty in deciphering between Reid and McConnell deposits, and thus the expanse of the glaciations. In a study by Beierle (2002) it was suggested that Chapman Lake, located ca. 10 km to the north of Two Moose Lake, may have been ice-covered during the McConnell glaciation, as an age of 13.2±0.3 ^{14}C ka BP was obtained from basal lacustrine sediments, suggestive of McConnell glaciation deposition of the Chapman Lake Moraine and deglaciation by 13ka BP. Further evidence for full deglaciation of Yukon was supported by radiocarbon ages of 13,660 ± 180 years BP lacustrine sediments in the terminus area of the St. Elias mountains piedmont lobe complex in west-central Yukon (Jackson et al., 1991) and data from lakes and pollen from southern Yukon (Bunbury and Gajewski, 2008).

2.3. Description of Outcrop

The study site, an exposed slump located on the western shore of Two Moose Lake, is ca. 60m wide and exposed to a depth of ca. 4m below the surface in the winter, and ca. 7m in the summer, where the bottom of the outcrop is covered by slumped debris forming the base of the outcrop in the spring/summer and by snow in the winter. The headwall is also covered by an overhang that extends ca. 1-2m depending on the location. The slump developed on a north-facing slope in response to thermo-erosion along the shore of Two Moose Lake. With the occurrence of the slump, many permafrost and ice features were exposed. Based on visual observations of the headwall, four horizontal stratigraphic units were delineated, as well as two distinct sets of ice wedges. During the summer months, access to the site was achieved through walking across the hummocky terrain as well as canoeing, and in the winter months, Two Moose Lake remains frozen and therefore can be crossed.

All units extend horizontally across the entire extent of the outcrop, with the thickness of each remaining relatively uniform throughout the outcrop. The upper most layer of the outcrop, ca. 0.5m thick (0-0.5m depth), is comprised of an organic rich Active Layer and frozen peat layer. The second layer, composed of frozen Sandy Silt Loam and silt with organics, is ca. 1.25m

thick (0.5-1.75m depth), and overlays a ca. 1.4m thick (1.75-3.15m depth) silt layer. The lowest layer, composed of a mixture of ice and till, extends downwards ca. 1m (3.15-4.15m depth), although it is unknown if or how much deeper the layer may penetrate as its lower contact was not exposed due to coverage by slumped debris and snow. The contact between the ice/till layer and silt layer was sharp, suggesting an erosional surface or thaw unconformity.

There are two distinct sets of ice wedges exposed in the headwall. The shoulders of the first set of ice wedges (N=5) extend from the base of the Active layer, ca. 0.25m below the surface, cross-cutting downwards to the base of the exposed ice/till layer. These ice wedges are assumed to be of Holocene age, and here on forth referred to as Holocene ice wedges. The Holocene ice wedges have near vertical lamination, are composed of clear/white ice containing minimal sediments, vary in width at the top of the ice wedge from 0.75m to 3m, and taper with depth. The second set of wedges (N=4), thought to be of Pleistocene age, and here on forth referred to as Pleistocene ice wedges, occur solely in the ice/tille layer. The Pleistocene ice wedges varied in thickness from 0.5m up to ca. 3m in diameter, and had a darker hue than those of Holocene age due to the higher sediment concentration. It is not known how deep the ice wedges penetrate due to slumped debris covering the lower contact, however, all of the ice wedges in this layer were truncated at the same height as the top of the ice/till layer and bottom of the silt layer. This further supports that the sharp contact between the massive ice layer and silt layer is an erosional surface or thaw unconformity.

2.4. Climate: Late Pleistocene to Today

2.4.1. Late Pleistocene and Holocene Climate

Throughout its history, much of the Yukon has been subject to many glacial and interglacial periods, however, some regions have remained ice free during these periods. Starting approximately 30,000 years ago, the maximum age from samples in this study, North America, as well as the rest of the world, was experiencing the effects of a glacial period, the Wisconsinan glaciation, that began ca. 107ka BP. At this point, much of North America and Greenland was covered in various ice sheets (Coordilleran, Innuitian, Greenland, and Laurentide), with the onset of the McConnell glaciation (MIS-2, late Wisconsinan, 29ka BP) covering parts of Yukon (Beierle, 2002). However, much of central Yukon during the period remained unglaciated by

major ice sheets, during which Matthews et al. (1990) concluded that much of central Yukon was dominated by a tundra environment and thus suggested temperatures as much as 5°C lower along with dryer conditions (Lacelle et al., 2009) than today. Reasoning for the lack of glaciation in central Yukon has often been attributed to the St. Elias Mountan range.

Starting in the late Cenozoic, and continuing through the Quaternary, the region was slowly uplifted, leading to drainage systems carving extensive valley systems, plateau regions of the central Yukon being gently elevated (millimetres per thousands of years) and finally, in the southwestern Yukon, the rapid uplift of the St. Elias Mountains (metres per thousands of years). It was the uplift of the St. Elias Mountains (and uplift of the Wrangell Mountains in Alaska, USA at the same time), that would have a dominant and controlling effect on the climate experienced in central Yukon and Alaska for the next 2 million years (Harris, 2005) . The St. Elias Mountains are a major orographic obstacle, as they are more than 4000 m.a.s.l (max elevation: Mount Logan, 5.959 m.a.s.l.), and as a result, obstruct to the westerly air flow across the subarctic Pacific Ocean and are also located at the end-point of extratropical Pacific storm tracks (Orlanski, 2005). With the westerly air flows blocked by the St. Elias, this led to dry conditions over central Yukon, and thus minimal precipitation for glacier developments, leading to the central Yukon remaining unglaciated (Edwards et al., 2001).

At the culmination of the Last Glacial Maximum (LGM- Clark and Mix, 2000), ca. 24 to 21ka BP, the McConnell Glaciation was also at its maximum expanse (Matthews et al., 1990) while insolation reached a minimum at 21ka BP (Dyke et al., 2002). Much of Alaska and central Yukon continued to be unglaciated, forming the most recent Beringia land bridge (22 to 17ka BP) from which humans migrated from Asia to the Americas. Conditions at this point were much colder, up to 4°C colder than present, as well as much drier than present, thus leading to the region to remain unglaciated (Viau et al., 2008). Following the LGM, temperatures continued to remain colder than present, reaching as low as 5°C cooler than present between 17 to 15ka BP (Kurek et al., 2009). By ca. 14.5ka BP, rapid temperatures increases across the Yukon saw temperatures reach modern values, coinciding with the start of the Bølling Allerød interstadial period (McBean et al., 2005, Kurek et al., 2009). This warm period, lasting less than 2 thousand years, ended with a sudden plunge back into a new and very short-lived cold event known as the Younger Dryas at ca. 12.5ka BP (McBean et al., 2005), however records for this period in the

central Yukon are few (Kurek et al., 2009). Temperatures during this period, potentially reached in less than 100 years, were up to 2°C cooler than present, coinciding with the advance of ice sheets (McBean et al., 2005).

The next major change in climate in the central Yukon began approximately 11.3 ka BP (Kaufman et al., 2004) years ago, with an increase in temperatures during the transition from the late Pleistocene to the Early Holocene. This transition to a warm period, known as the Holocene Thermal Maximum (HTM), was driven by Milankovitch orbital forcing that peaked between 10 and 9ky BP (Ritchie et al., 1983), whereby precession-determined maximum insolation led to an increase in total annual insolation of 1 Wm^{-2} higher than present at 60N, and increasing to as much as 5 Wm^{-2} at the poles (Berger and Lourtre, 1991). Due to the tilt of the earth towards the sun, maximum insolation occurred during the summer solstice (up to 10% greater than present (Kaufman et al., 2004)), and minimum insolation slightly lower than present at the winter solstice, leading to higher seasonality changes (Viau et al., 2008) with summer air temperatures up to 5°C warmer than present-day by 8ka BP, while winter air temperatures decreased from their maximum at 12ka BP (Clark et al., 2004, Kaufman et al., 2004, McBean et al., 2005, Viau et al., 2008), and drier conditions (60-90% of present day) (Edwards et al., 2001, Lauriol et al., 2002, Kaufman et al., 2004). The timing of the HTM was significantly different spatially, with central Yukon and surrounding Beringia experiencing the HTM 2 ka to 3 ka years prior to the rest of North America, with Greenland, regions downwind of the Laurentide Ice Sheet (eastern North America) and even Europe not warming until after 8 ka BP (McBean et al., 2005). The earlier warming in central Yukon and Beringia has been attributed to two physiographical features, the vastness of the unglaciated area in Beringia, leading to the absorption of more insolation by land as opposed to being reflected by ice (such is the case for the rest of North America), and the breadth of shallow continental shelves surrounding Beringia. Furthermore, the expansion of forests over tundra further reduced surface albedo, leading to a positive feedback (Kaufman et al., 2004).

Following the HTM, a further warming of 2°C (reaching 7°C above present) occurred between 10 and 8 ka BP (Kaufman et al., 2004, Clark et al., 2004), with July temperatures increasing, January temperatures decreasing and precipitation above present (Viau et al., 2008), followed by a severe cold and dry event starting ca. 8.2ka BP lasting for less than a century

(McBean et al., 2005; Fisher et al., 2008, Bunbury and Gajewski, 2008). Following the 8.2ka BP event, temperatures increased rapidly to pre-event temperatures, followed by the subsequent cooling to near-present temperatures until ca. 4.5ka BP, coinciding with decreasing insolation in the Northern Hemisphere insolation (Zdanowicz et al., 2014). During this cooling, July temperature conditions continued to increase, January temperatures decreased and precipitation decreased, all to near-modern temperatures (Viau et al., 2008).

The most significant cooling event of the Holocene began ca. 4.2ka BP, coinciding with neoglacial and wet conditions (Menounos et al., 2009), supported by a sharp decrease in $\delta^{18}O$ of 6.5‰ in the Mt. Logan (St. Elias mountains, southwest Yukon) Ice core (Zdanowicz et al., 2014; Fisher et al., 2008). Polen records indicate a decrease in temperature of up to 1.5° dropping below present temperatures from 4.2 to 2ka BP (Kurek et al., 2009; Bunbury and Gajewski, 2008), However, polen records from this period, and continuing to 1ka BP, show conflicting trends between warm and cold, and wet and dry periods. This trend however is reflected in ice cores from the St. Elias ice range and peat bog inception dates (Fisher et al., 2008). Following the 4.2ka event, ice cores from the St. Elias Mountains show large amplitude variations in $\delta^{18}O$ of up to 8‰, strikingly different from cores from the high Canadian Arctic and Greenland Holocene records, implying abrupt changes of more than 10°C during these oscillations (Zdanowicz et al., 2014). However, Zdanowicz et al. (2014) indicate there are no equivalent trends in the North Atlantic region ice cores and are in anti-phase with these cores and other proxy temperatures from northwestern North America. Fisher et al. (2004) propose that the shifts in $\delta^{18}O$ reflects abrupt past changes in the large-scale atmospheric circulation over the North Pacific, and thus reflect changes in atmospheric moisture related to the ENSO regime.

Climate within the past millennium was affected by the Medieval Warm Period (MWP) from ca. 800 to 1200 AD (1.1ka BP to 0.75ka BP), Little Ice Age (LIA) from 1450 to 1800AD (0.5ka BP to 0.15ka BP), and finally the most recent warming in the 20th century. During the MWP, pollen records indicated much of the Arctic experienced warmer conditions than present (Bunbury and Gajewski, 2008), however, temperatures in the central Yukon were still -0.5 to -1°C cooler than present (Viau et al., 2012). Immediately following the MWP, the Earth as a whole plunged into the LIA, reaching temperatures (inferred from pollen samples, Bunbury and Gajewski, 2008) as low as -2°C cooler than present (Viau et al., 2011) and during which

glaciers advanced on all continents (McBean et al., 2005). According to Bradley (1990) and Bourgeois et al. (2000), this period may have been the coldest period of the Holocene. Following this period, there was an abrupt reversal in trend, with temperatures increasing, reaching temperatures last seen during the HTM (Zdanowicz et al., 2014).

2.4.2. Present Climate

The study area is located in a region that is part of the continental sub-Arctic climate regime, which is characterized by low precipitation and a wide temperature range. Winters in the region are cold and long, while summers are short and cool. Spring and fall are short with quick transitions from the proceeding and upcoming seasons (Green, 1972). Regional climate conditions can be assessed from 2 nearby meteorological stations (Environment Canada, 2010): Dawson (1981-2010), Mayo (1981-2010) (Table 2). Mean annual air temperature recorded at Mayo and Dawson were -2.4°C and -4.1°C respectively. Due to their locations within deep valley bottoms, the air temperatures at Dawson and Mayo are affected by topographically controlled temperature inversions in the winter, therefore leading to warmer winter conditions and higher summer maxima, where as temperatures at higher elevations(i.e. highlands) may be up to 5°C cooler (Burn, 1994).Total annual precipitation received at Dawson and Mayo exceeds 300mm (300-500mm/yr) and precipitation is mostly of orographic origin.

Table 2. Winter, Summer and MAAT for meteorological stations located within 150km of Two Moose Lake.

Meteorological Station	Coordinates	Distance from Two Moose Lake (km)	January(°C)	July(°C)	MAAT (°C)
Dawson[1]	64°02N, 139°07W	125 (South)	-26.0	15.7	-4.1
Mayo[1]	63°37N, 135°52W	150 (Southeast)	-23.1	16.1	-2.4

[1]Average temperature values were based on 30-year climate normals calculated by Environment Canada from 1981-2010

2.4.3. Climate Change Since 1950

Over the past few decades, the change in climate, as well as the impacts of climate change, have bas been well documented worldwide, and more specifically in the Arctic. In the most recent report released by the IPCC, AS5 (2013), it was concluded that the Global Mean Surface Temperature has increased since the late 19th century, with each of the past three

decades being successively warmer at the Earth's surface than all the previous decades in the instrumental record, and the first decade of the 21st century having been the warmest. Globally, there has been a warming of 0.85°C (±0.2°C) over the period 1880-2012, with much of the warming (0.72°C) occurring over the period 1951-2012 (Hartman et al., 2013). However, Canada has warmed at a rate double that of the global average, warming by 1.3°C since 1948 (Barrow et al 2004). The Arctic, one of the coldest and driest places in Canada, has seen an increase in both temperature and precipitation over the past century, warming 2.1°C in the Yukon and Mackenzie Delta region from 1948 to 2007 (Environment Canada, 2007) (Figure 15). While MAAT have increased over the past 50 years, the variation in between seasonal changes is much more dramatic, with winter temperatures in northwestern Canada having increased by as much as 3-4°C in the past 50 years, while only increasing 1-2°C in the Summer (ACIA, 2004; Hengeveld et al., 2005).

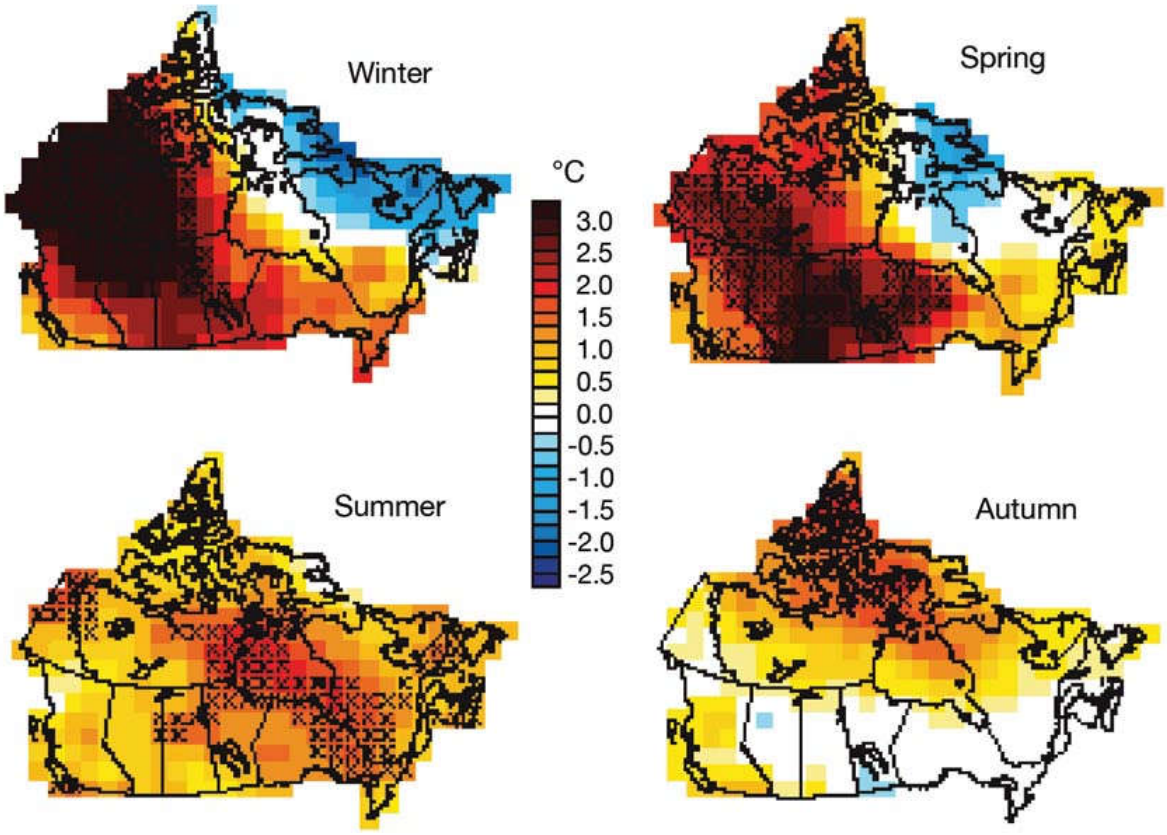

Figure 15. Regional distribution of seasonal temperature trends (°C) observed across Canada from 1948 to 2003. "X" symbols overlaying areas indicate locations where the temperature trend is statistically significant. Source: Modified from Hengeveld et al. 2005.

2.4.4. Climate for the Next Millennium

While climate change over the past century has been well documented, as well as the effects it has had, researchers are currently trying to project, using various models, how the climate may change in the future, and the potential effects it may have. In the near future, current projections by the IPCC using the CMIP5 multi-model ensemble show temperatures continuing to rise over the next few decades, rising by as much as 1-1.5°C (Figure 16) from 2016-2035 relative to 1986-2005 under the RCP4.5 scenario (Kirtman et al., 2013; Collins et al., 2013). Projections by the Arctic Climate Impact Assessment (ACIA) using the lowest emissions scenario and the model that generates the least warming response, project that the Earth will warm twice as much in this century as it warmed over the past century (ACIA, 2004). However, this scenario is highly unlikely and temperatures are likely to increase at a much greater rate. Five ACIA climate models running the B2 emissions scenario (resulting in a temperature rise slightly below the middle of the range of IPCC scenarios), have projected average annual increases of roughly 3-5°C (Figure 16) from 1990-2090, double that of what will be seen in the rest of the world, and winter temperatures rising significantly, increasing by as much as 4-7°C.

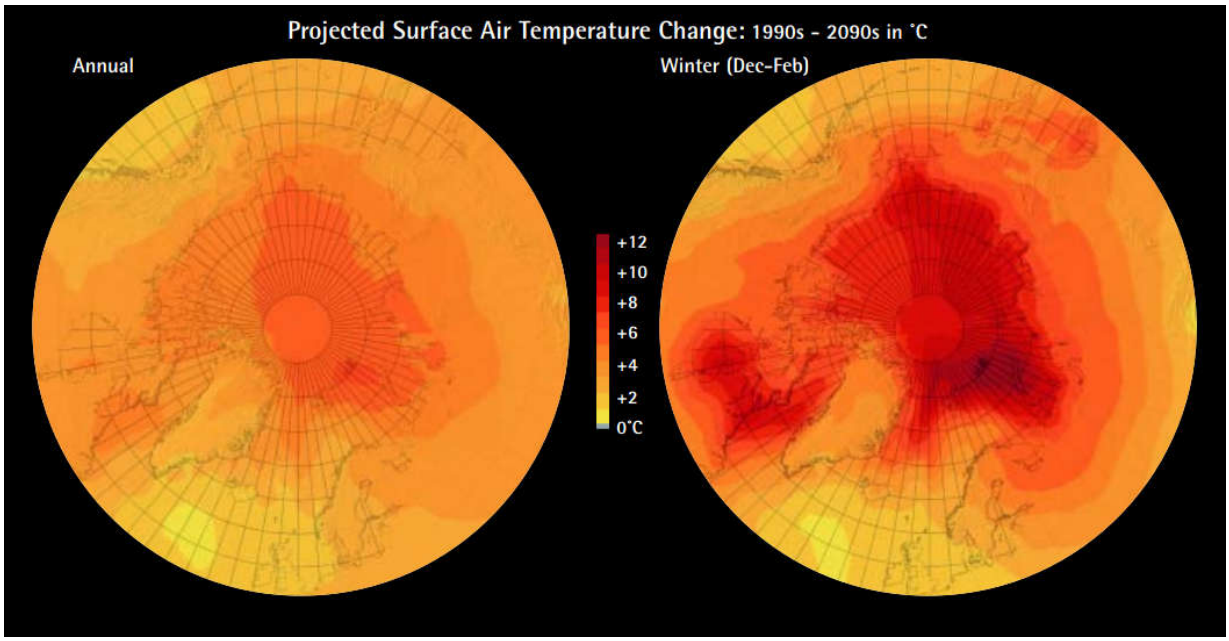

Figure 16. Projected annual (left) and Winter (Right) temperature change from the 1990'2 to 2090's based on the average change calculated using five ACIA climate models using the lower B2 emission scenario. Image obtained from ACIA, 2004.

2.5. Permafrost and Ground Ice Conditions

The Blackstone Plateau is located on the northern boundary of the extensive discontinuous permafrost zone (50-90%) (Figure 17). In nearby Dawson, permafrost reaches depths of 60 m, where a mean annual near-surface ground temperature of -1.7°C had been measured (Smith and Burgess, 2000). Due to the high altitude (>1000m) on the Blackstone plateau and cooler climatic conditions (near surface temperatures below -4°C, (Kojima, 1996)), permafrost coverage is more extensive and deep, especially on north facing slopes where peat is able to accumulate (Heginbottom et al., 1995). In some cases, permafrost exceeds 120 m (Green, 1972). However, permafrost is less extensive on well-drained south-facing slopes and in the proximity of major rivers; such is the case for Two Moose Lake.

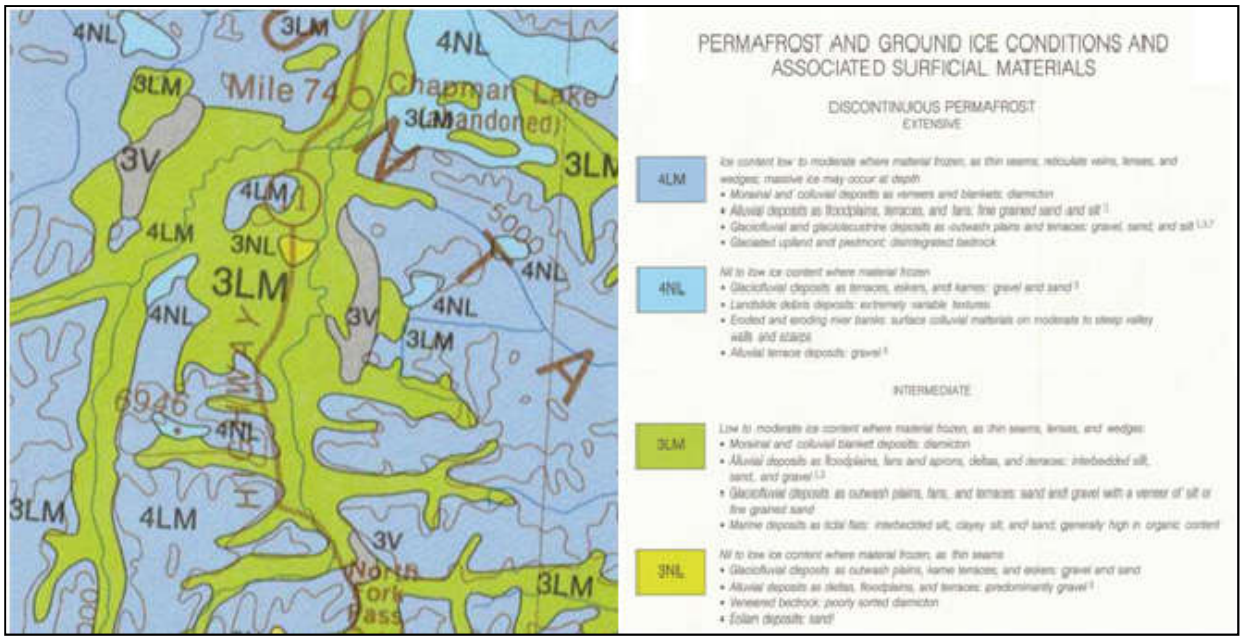

Figure 17. Permafrost and Ground Ice Conditions surrounding Two Moose Lake. Two Moose lake is located in 3LM permafrost (located in the center of the map) just south of the yellow region (3NL) (Modified from Geological Map*1691A - Permafrost and ground ice conditions of northwestern Canada* from Heginbottom & Radburn, 1992).

Two Moose Lake site is located within discontinuous permafrost (~50%) with low to moderate ice content. The active layer in the region can reach thicknesses of 0.5-1m on mineral soil (Burn et al., 1986), but during the field season in August 2013, a thaw layer of only 0.25m was observed.

Geomorphic features associated with the presence of permafrost in the study area include: (1) solifluction lobes, (2) patterned ground and (3) thaw slumps, all of which are present at Two Moose Lake, where ice wedges were exposed in a thaw slump (Green, 1972). Solifluction lobes are often an indication of high ice content below the surface, as sufficient meltwater is required for slumping to occur. Extremely prevalent in the area was the presence of polygonal terrain (Figure 12A), where a network of ice wedges occupies the troughs up to 3-4m wide and 1-2m deep. The polygonal terrain covers much of the landscape in the region, and is often found in current or relic drainage channels, and thus have developed in alluvial sediments. Finally, a few thaw slumps can be found along lakeshores, such as at Two Moose Lake, or along road bluffs. These features are indicative of the presence of tabular massive ice bodies (origin of which can come from various sources, i.e. relic snowbanks, glacier ice, injection ice, ice wedges etc. For example, Lacelle et al. (2007) documented the presence of buried glacier ice in a thaw slump found 10km north of Two Moose Lake.

Similar to the increasing surface air temperatures seen across the globe and arctic, there has been an increase in the near-surface permafrost temperatures and is likely to continue to increase in the near future (Smith et al., 2010). Ground temperatures measured by Burn & Kokelj (2009) at upland and tundra sites within the discontinuous permafrost zones, such as seen at Two Moose Lake, have warmed during the past 25 years by as much as 1-2°C since the early 1970's. At sites where the Mean Annual Ground Temperature (MAGT), measured at the top of permafrost, is less than -1°C, ground temperatures have increased by ca. 0.2°C per decade, however, the absolute rate has decreased in recent years (Smith et al., 2010). It is possible to attribute the recent decrease in rate to temperatures due to the phase change that occurs as the permafrost approaches 0°C. As a result of the latent heat effects, crossing the 0°C barrier into positive temperatures is difficult, preventing permafrost thawing and allowing permafrost to persist over extended periods of time even in a warming climate (Smith et al., 2010). As a consequence to the thawing of permafrost and thickening of the active layer, there had been an increase in thermokarst activity in northwestern Canada, with more pronounced effects at sites containing excess ice, ice wedges and massive ice (Burn, 1997; Murton and French, 1994, Lacelle et al., 2004, Lacelle et al., 2010, Lacelle et al., 2015). Furthermore, increased precipitation has increased the amount of water saturated in thawed layers, further increasing thermokarst activity (Kokelj et al., 2015)

2.6. Surficial Vegetation

The landscape within the uplands is often devoid of timber, except for the presence of small pockets of dwarf birch, stunted black spruce and scattered willows (Green, 1972). Most of the north-facing slopes within the region are underlain by permafrost, and therefore only allow for small and sporadic pockets of stunted spruce, usually located in close proximity to drainage channels, but none-the-less, the slopes are heavily covered in moss. In the small valleys (often containing rivers and streams that incise them) at lower elevations, vegetation is dominated by dwarf birch (although still sparse), dense willow thickets, with dense pockets of moss and lichen. On the broad basins (between the small valleys and slopes), much of the area is formed on soft shales and underlain by permafrost, therefore supporting little vegetation (Kojima, 1996). The vegetation that does occur takes the form of wet, spongy, hummocky vegetation, creating an uneven surface. Much of the vegetation is made up of tussocks, 0.5-1 m in diameter and height, composed principally of sphagnum moss, a variety of sedges, and minor dwarf bushes such as blueberry (Figure 18).

Figure 18. *Left*: Vegetation at Two Moose Lake. The landscape is dominated by hummocky material and brush, with small pockets of stunted birch. *Right*: Blueberry bushes with lichens and moss surrounding.

3. Methods

3.1. Field Investigation and Sample Collection

Fieldwork at the Two Moose Lake thaw slump was completed in summer 2013 (August 1st to 25th, 2013) and spring 2014 (April 14th to 25th, 2014) (Figure 19). During the first field season, 281 samples were collected from the headwall of the slump, while 161 samples were collected during the second field season, comprising of ice wedge ice, pore ice and sediments/permafrost.

Active layer (upper 0.25m) and permafrost (>0.25m in depth) samples were sampled for determination of ice content (gravimetric water content (GWC) and volumetric water content (VWC)), grain size distribution and $\delta^{18}O$-δD stable isotopes of pore ice and pooled ice. The active layer and permafrost samples were collected using various tools and methods. During the summer 2013 (Figure 19A, Figure 20), active layer and ice-bearing permafrost samples from the upper 3.7m of the outcrop (from the top of the active layer to ice layer) were collected at various sampling intervals and placed in a sealed Ziploc bag. Permafrost samples in the upper 1.9m were collected using a Hilti power drill with an 8cm diameter core barrel with diamond-impregnated cutters (Figure 20A & B). Samples were extracted vertically with the core barrel positioned perpendicularly to the headwall, with each sample having a slight overlap to produce a continuous sampling record for the layer (no crossing over of samples occurred as the lower portion of each sample had already been removed), and therefore each sample is representative of an ~7cm section of the outcrop (Figure 20B). Prior to samples being collected, ca. 10cm of material was removed from the surface to remove any possible contaminants (sediments or organic material) that may have fallen from the thawed overhang, as well as to remove meltwater that may have refrozen on the surface of the headwall which could give an altered isotope signal that is not representative of the original permafrost and ground ice (Lacelle, 2007). Between each sample, the inside of the core barrel was rinsed with water and dried to ensure that there was no cross-contamination between samples. Due to the much higher ice content below 1.9m, the permafrost samples were collected using an ice pick and sampled at larger intervals; diamond-impregnated cutters do not function properly in ice-rich material (Calmels et al., 2005). Similar to the previous samples, ca. 10cm of material was removed prior to extraction.

Figure 19. Panoramic view of an ouctrop exposed by a slump at Two Moose Lake, Canada in August 2013 (A) and April 2014 (B). A) The effects of the air temperatures above 0°C in August 2013 are evident as the outcrop is in a dynamic state with melting of the headwall occurring, leading to the covering of otherwise white ice wedges (as seen during the winter) with sediments to alter their appearance, as well as the generation of mud flows at the base of the headwall. Furthermore, the stratigraphy within the outcrop is much less visible, and sampling conditions much more difficult due to the unstable nature (water saturation) of the materials located at the bottom of the outcrop. B) Stratigraphy of the outcrop is visible as the outcrop is frozen, and therefore in a stable state. The individual ice wedges, those extending from the bottom of the active layer and those truncated lower in the outcrop are much more apparent. Sampling conditions are much more stable during this time, although the lower extent of the outcrop is covered by frozen sediments and snow.

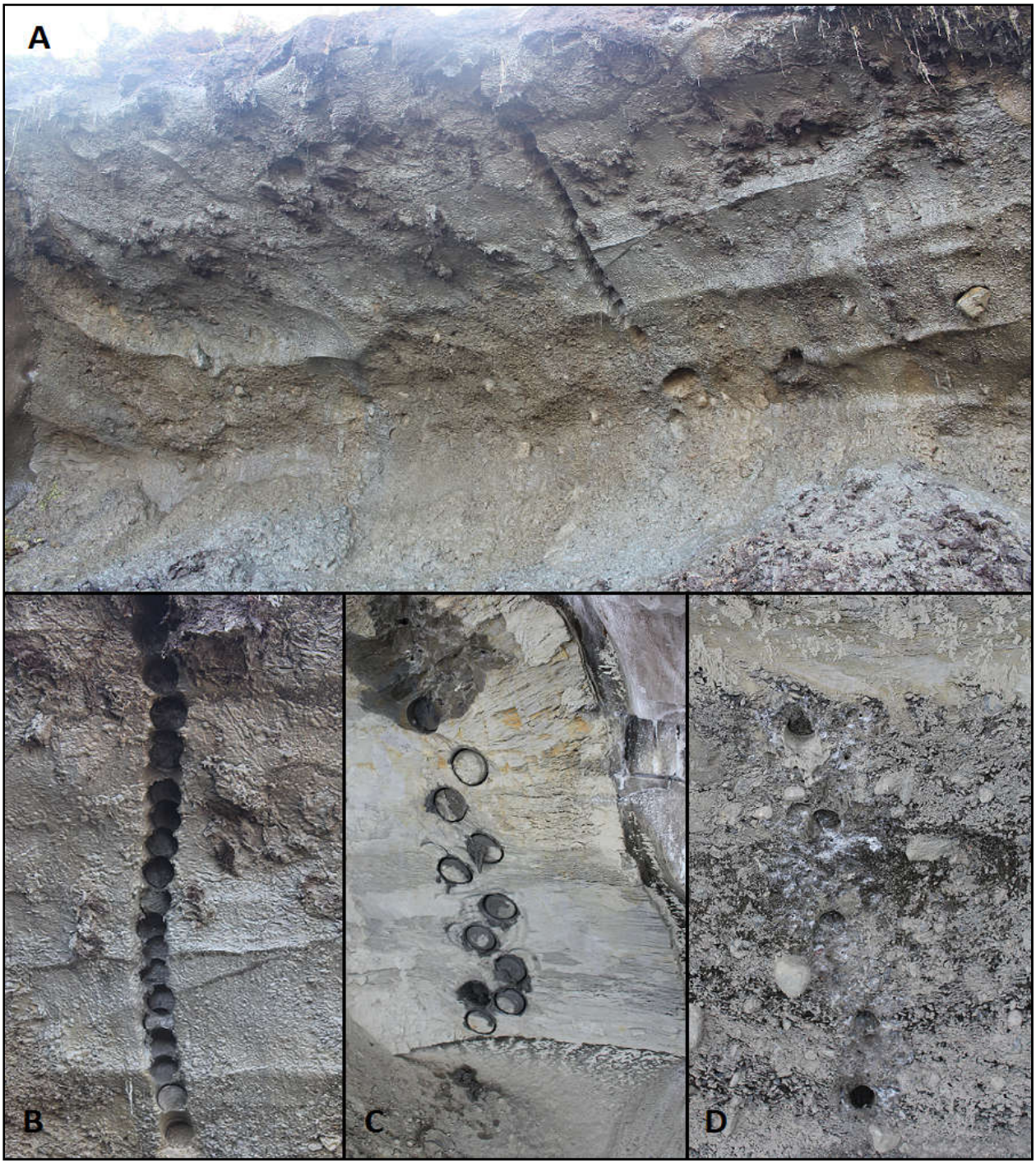

Figure 20. Sample extraction from the headwall at Two Moose Lake during August 2013 (A & B) and April 2014 (C & D). A) Headwall showing the location of sample extraction using a Hilti power drill with a 8cm diameter corer with diamond-embedded cutters (0.25-1.9m). Samples below 1.9m were removed using an ice pick (not visible). Sample extraction using a Hilti power drill from B) 0.25-1.9m showing the slight overlapping of samples during August 2013; C) 1.75-3.15m during April 2014 and; D) 3.15-4.35m (lowest exposed unit) from April 2014.

All permafrost samples were placed in a sealed Ziploc freezer bag (double bagged in order to prevent leakage/loss of sample) and allowed to melt in the field.

During the second field investigation in April 2014, the lower portion of the outcrop (ca. 1.75m to 4.35m) was re-sampled due to more favourable sampling conditions (Figure 19B, Figure 20C &D),, for determination of ice content (GWC and VWC), grain size distribution and δ^{18}O-δD stable isotopes of pore and massive ice. Samples were extracted vertically at various intervals using the same Hilty power drill (Figure 20C&D) with an 8cm diameter core barrel with diamond-impregnated cutters and handled in the same manner as August 2013. Similarly, ca 5-10cm of the outer of each core sample was removed to prevent contamination, and the inside of the core barrel wiped clean with paper towel between samples. Samples were then placed and stored in Ziploc Freezer bags (double-bagged to prevent leakage) and remained frozen until laboratory analysis.

In total, six ice wedges were sampled along the headwall, two during the first field investigation in August 2013 (Figure 21A), and five in April 2014. Samples from the six ice wedges were collected for δ^{18}O-δD and grain size analysis analyses: four of which were truncated immediately below the active layer (0.25m below the surface and extending to >3m depth), whereas two were truncated at 3.2m depth (Figure 19A & B). Similar to the outcrop permafrost samples, ca.10cm of the surface of the ice wedges was first removed using a chainsaw to remove surface contamination. For $^{18}O/^{16}O$ and D/H samples, the ice wedges were sampled horizontally across the wedge orthogonal to the nearly vertical lamination (suggestive of an epigenetic ice wedge) (Figure 21B, C and D). During the first sampling season (August 2013), large blocks of ice (ca. 30-50cm in width) were first cut from the ice and then sub-sampled across by cutting 1-3cm wide slabs of ice to 3/4 of the depth of the ice block (Figure 21D), with the remaining 1/4 not used in order to prevent contamination from water from previous ice blocks cut on the tarp. Due to the mechanical failure of the chainsaw, approximately 30 samples from Ice Wedge #2 were collected using an ice screw (Figure 21B, right side of ice wedge). During the second sampling season, due to more stable sampling conditions, individual samples/slabs of ice were cut directly from the ice wedges (Figure 21E). Each ice wedge sub-sample was then placed in a sealed Ziploc bag (double bagged in order to prevent lose of sample due to leakage), and allowed to melt in the field. Upon melting, samples were agitated and

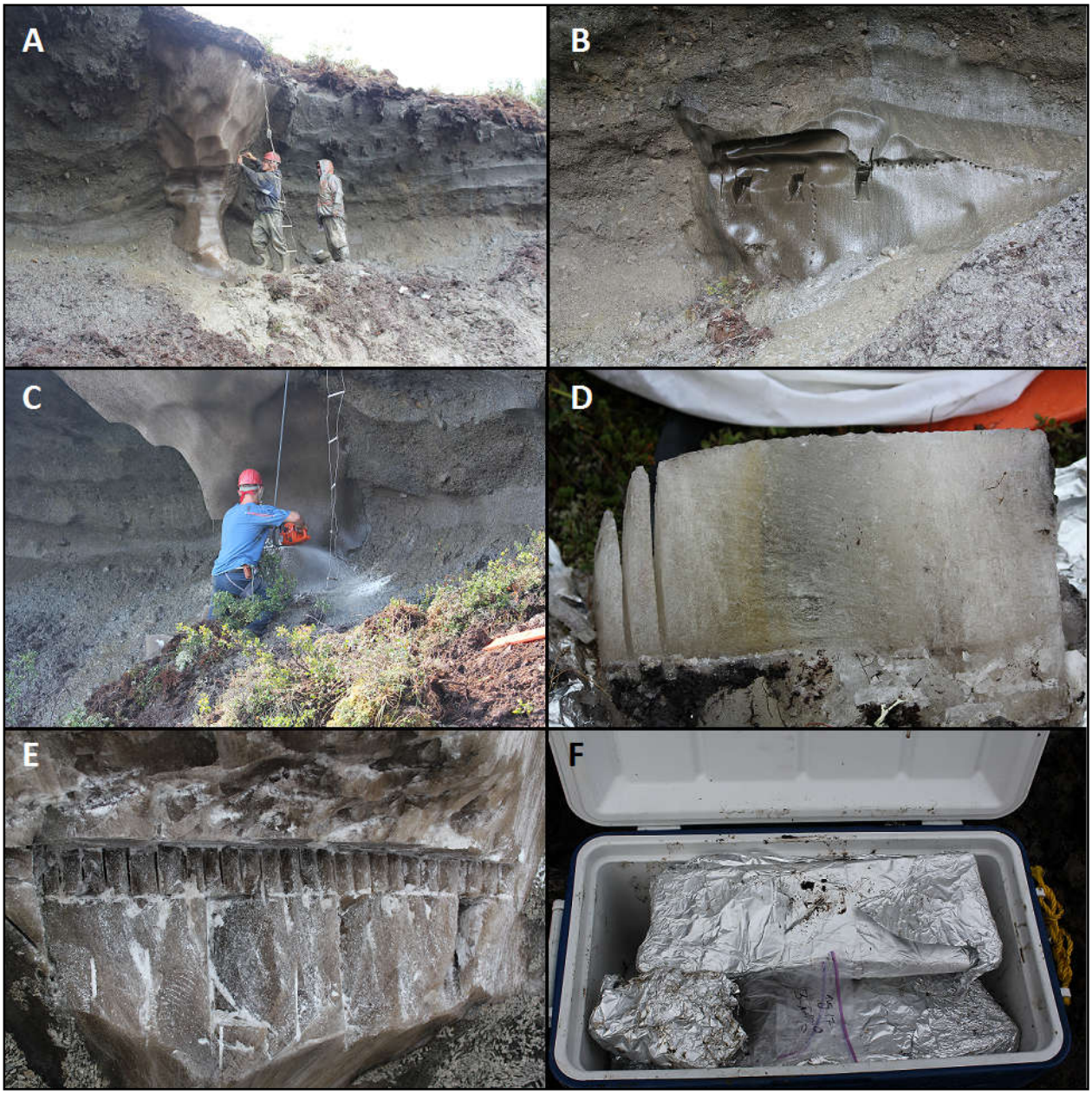

Figure 21. Stable Isotope and Radiocarbon sampling. A) Sampling of an Ice wedge truncated immediately below the Active layer (0.25m-3.2m) during August 2013. Vertical sampling with an ice screw for stable isotopes can be seen; B) Sampling of an Ice wedge truncated below 3.2m (August 2013). Stable isotope samples were removed horizontally from the middle cut/hole (in line with the ice screw holes), while radiocarbon samples were removed above (continuous sequence, remained frozen) and below (individual blocks, melted in field); C) Mechanical removal of an ice block from an ice wedge truncated immediately below the Active layer using a chainsaw (August 2013); D) Example of subsampling (ice slabs) of ice blocks removed from ice wedges for stable isotope analysis; E) Example of stable isotope sub-sampling (upper vertical cuts, ice slabs removed directly from ice wedge) during April 2014. Radiocarbon samples were removed directly below the stable isotope samples as large blocks; F) Storage and transportation of Radiocarbon ice block samples extracted from the ice wedge seen in B). Blocks were wrapped in tin foil and stored in a cooler in order to remain frozen.

transferred to 50mL falcon tubes.

The above six ice wedges were also sampled for $^{14}C_{DIC}$ and $^{14}C_{DOC}$ analysis, including an additional ice wedge that was truncated below 3.2m. For radiocarbon analysis, ice blocks were cut from ice wedges using a chainsaw (Figure 21B and D), ranging in size from ca. 0.2 to 0.3m^3 for each sample to ensure enough water would be available to obtain the required amounts of DIC and DOC to produce CO_2 for graphitization. For each ice wedge, blocks were extracted horizontally across the wedge to determine the direction of growth, as well as to determine the initiation age (Figure 21B & E). Each ice block was handle with sterile nitrile gloves and surface-cleaned by wiping with paper towel and rinsing with DI water in order to remove possible organic contaminants from the chainsaw (oil) and surficial material. Each sample was stored in large Ziploc bags (double bagged) during melting. Upon melting, samples were transferred to pre-cleaned and sterilized 500mL and 1L Nalgene bottles, and filled to the top to ensure there was minimal headspace. Unthawed ice block samples were obtained with the same method, but after rinsing, were wrapped in aluminum foil as an insulator (St. Jean et al., 2011), kept frozen in a cooler and stored in a -20°C freezer in Dawson city until departure (Figure 21F).

All samples were shipped to the Advanced Research Complex (ARC) at the University of Ottawa by freight (melted samples) and by air (frozen samples). Ice was shipped with the melted samples in order to keep them refrigerated. Upon arrival at the ARC, frozen samples were stored in walk-in freezer at -20°C, while melted samples were stored in a fridge at 4°C.

3.2. Laboratory Analysis

During laboratory analysis, samples were processed through a series of steps in order to obtain the appropriate results. The first step, in which all samples (excluding radiocarbon samples) were subject to, involved the determination of the total weight of the sample (liquid and solid). With the wet weight determined, excess water (volume of water in the sample which exceeds the total pore volume that the sample can hold) from each sample was removed for δ18O-δD analysis, and the remaining sediments following the procedures for gravimetric water content, organic and inorganic content, and grain size distribution outlined below. Samples obtained for radiocarbon analysis were subject to an independent analysis outlined below.

3.2.1. Ground Ice, Organic Matter and Inorganic Carbon Contents:

The Volumetric water content (VWC) of the active layer, permafrost and ice wedge samples were determined in the laboratory and calculated using the following equation:

$$VWC(\%) = \left(\frac{Volume\ of\ water\ (g)}{Total\ volume\ of\ Sample\ (g)}\right) x\ 100 \quad (7)$$

Samples were first weighed (for determination of the gravimetric water content), then allowed to melt in plastic Ziploc bags. Samples were then transferred to 50mL centrifuge tubes (in some cases requiring more than one tube) to determine the total volume of sample. In an attempt to separate the liquid and solid phases as best as possible, as well as to prevent as much sediment/organic matter being transferred to the liquid phase and for ease of water transfer, samples were centrifuged at 2400rpm for 15 minutes with the intent of expulsing as much water from within the sediments or organic matter found in active layer, permafrost and ice wedge samples. Excess water was then removed from the samples (poured into a separate beaker or centrifuge tube), and the volume recorded.

Following the determination of the VWC, the gravimetric water content (GWC) of the active layer, permafrost and ice wedge samples was determined and calculated using the following equation:

$$GWC(\%) = \left(\frac{Weight\ of\ water\ (g)}{Dry\ Weight\ of\ Sample\ (g)}\right) x\ 100 \quad (8)$$

As previously mentioned, samples were initially weighed (wet weight) prior to removal of water, re-weighed after the removal of water, then baked at 105°C for 24 h. After baking, samples were then weighed again (dry weight).

The organic matter and inorganic carbon contents of the sediments were measured to determine changes in the respective contents that could potentially suggest different sedimentation conditions or environments. The organic matter and inorganic carbon components of the samples were determined though the loss of ignition method (LOI) (Heiri et al., 2001). The previously dried sediments were first ground up to break up blocks of dried 'mud' created from drying during baking at 105°C (GWC) and then shaken in bags in an attempt to homogenize the samples. Multiple aliquots were then taken from the sample, creating a composite sub-sample of the original sample, with shaking/mixing of the sample in between each

aliquot in order to attempt to obtain a homogenous and representative sample. The organic matter content was calculated using the following equation:

$$Organic\ Matter\ Content\ (\%) = \left(\frac{DW_{105} - DW_{550}}{DW_{105}}\right) \quad (9)$$

where DW_{105} represents the weight of a subsample (~8g of the previously dried sample) that was re-dried at 105°C for 24hr, and DW_{550} the weight of the sample after combustion at 550°C for 3h.

The Inorganic carbon content was determined by heating the sample at 950°C for 3 hours to decompose any carbonate minerals, and calculated using the following equation:

$$InorganicCarbonContent\ (\%) = \left(\frac{DW_{550} - DW_{9\ 50}}{DW_{105}}\right) \quad (10)$$

where DW_{950} represents the weight after heating at 950°C for 3h.

3.2.2. Grain Size Analysis of Sediments and Muck

The analysis of grain size distribution of the sediments was undertaken to help differentiate and distinguish between the various layers within the outcrop in conjunction with LOI results. Prior to grain-size analysis, all samples were analyzed for organic carbon content to determine if any samples contained high organic content that could potentially cause a skewing in the grain size distribution. In the case of this study, organic carbon content was found to be minimal and therefore no pre-treatment of samples prior to grain-size analysis was required. Grain-size analysis was achieved through one of two methods, in some cases both, the use of a Particle Size Analyser (PSA) or by wet-sieving. Samples with sediments finer than sand (< 1Φ, or 0.5mm) were analyzed using a Microtrac S3500 laser particle-size analyser at the University of Ottawa. The laser particle analyzer uses tri-laser light scattering, with a multi-detector, multi-angle optical system.

Similar to the determination of organic/inorganic carbon content, sediments from the samples were mixed in sample bags, from which multiple aliquots taken per sample to form a composite sub-sample (whole sample not analyzed), with shaking/mixing of the sample in between each aliquot in order to attempt to obtain a homogenous and representative sample. Samples were then dispersed using sodium hexametaphosphate, allowed to sit for 24hr in a

fridge at 4°C for maximum dispersion of the sediments, then analyzed for grain size distribution with the PSA. For sediment samples that contained material coarser than sand, grain size distribution was determined by a combination of laser particle analysis (for material finer than sand) with wet sieving methods (material coarser than sand). Prior to analysis and contrary to laser particle analysis, the entire sample of sediments was weighed, shaken and the large cobbles scrapped in order to remove clay caked to the surface of them. Aliquots of the finer components (< 1Φ, or 0.5mm) of the sample were collected to create a composite sample of the finer components of the sample to be analyzed by the Laser Particle Size Analyzer and analyzed in the same method as highlighted above. The remaining large sediments (>1Φ) sediments were soaked overnight in deionized water to remove the clay attached to the larger sized sediments. After soaking for 12h, the sample was poured onto a 2Φ (>0.25mm) sieve and rinsed with water to remove sediments smaller than 0.25mm. The remaining sediments were baked for 24h to evaporate the water. The dried sediments were sieved using a sieve stack (-2Φ, -1Φ, 0Φ, 1Φ and 2Φ sieves) and shaker. The sediments from each sieve were collected and weighed. The weighs of each sieve size were then manually input into the software employed by the Microtrac S3500 laser particle-size analyser, from which the data from wet sieving and particle size analysis were joined to determine the particle size distribution.

3.2.3. Stable O-H Isotopes

Over three hundred melted ground ice and ice wedge samples were returned to the G.G. Hatch Isotope Lab (University of Ottawa) for determination of stable isotope ratios of oxygen ($^{18}O/^{16}O$) and hydrogen (D/H). Prior to analysis, pre-treatment of the excess water extracted from the samples was required. Each sample was filtered using 0.45µm nitrocellulose filters (Whatman, WCN) to remove particulate matter and sediments, transferred to falcon tubes and subsequently stored in fridges at 4°C. Upon analysis, 1mL aliquots of sample were extracted and transferred to 2mL vials with septa for analysis.

Simultaneous direct measurements of $^{18}O/^{16}O$and D/H were measured by Laser Absorption Spectroscopy (LAS) using a Los Gatos Research (LGR) Triple Water Vapour Isotope Analyzer (model IWA-45EP) with off-axis integrated cavity output spectroscopy (OA-ICOS). This instrument uses near-infrared tunable diode laser absorption spectroscopy with the laser coupled off-axis, relying on spatial separation of reflections from highly reflective mirrors

installed within the high-finesse optical cavity (Berman et al., 2013). Direct water samples without conversion, were introduced into the OA-IOCS via a CTC LC-PAL autosampler equipped with a heated (≈85 °C) injector block, where the H_2O samples were evaporated for isotope analysis directly on the H_2O_{vapor}. Results were calibrated and normalized to internal laboratory water standards that were previously calibrated relative to Vienna Standard Mean Ocean Water (VSMOW). Furthermore, high-spectral contamination Identifier software was used, and determined that no spectral contaminants were present in the analyzed samples. The results are presented using the δ-notation, where $\delta^{18}O$ and δD represent the parts per thousand differences for the composition of $^{18}O/^{16}O$ or D/H in a sample with respect to VSMOW. Measurement precision for δ18O is ±0.25 per mil, while precision for δD is ±1 per mil. The complete measurement procedure and performance of the liquid water analyzer is described in Lis et al. (2008).

3.2.4. Radiocarbon Dating of Ice Wedges

In this study, it was decided to use Dissolved inorganic carbon (DIC) and Dissolved organic carbon (DOC) as the radiocarbon (^{14}C) dating material as opposed to usual method of using Particulate Organic Content (POC) that has been used in many studies for the dating of ice (Burn (1990), Fritz et al. (2012), Kotler and Burn (2000), Lacelle et al. (2004), Lacelle et al. (2007), Lacelle et al. (2013), Shur et al. (2004), St-Jean et al. (2011), Vasil'chuk et al. (2004), Vasil'chuk (2014), Vermaire and Cwynar (2010), Bray et al. (2006)). There was a three-fold reasoning for this. In a study by Lachniet et al. (2012), the authors found that DOC produced a more representative, as well as a younger ages, than POC and CO_2 samples analyzed for radiocarbon. Secondly, it was found that the larger organic matter classically dated (i.e. twigs, roots, branches etc.) was not necessarily placed in situ, and rather could be old recycled carbon, often referred to as 'old carbon' (Vasil'chuk and Vasil'chuk, 2014). Lastly, upon visible analysis of the ice layers and ice wedges, there was found to be little or no visible pieces of organic matter inter-dispersed in the ice. This was found to be true when samples were melted and little to visibly there was no larger fragments of organic matter found in the sediments.

A main issue that arose prior to preparation of water samples for CO_2 extraction, was the potential of carbon leaching from the filters. In practice, the use of a filter should neither introduce any artefacts to the analysis, nor affect the analytical procedure (Khan and

Subramania-Pillai, 2007). Since nitrocellulose filters are made of organic matter, there was concern that leaching of material from the filters could cause interference in the analysis. The inclusion of material from the filter can become a significant source of error when the carbon in the sample is converted to CO_2 (and on to graphitization) for radiocarbon analysis. The degree to which the result could be affected is dependent on several factors: the original/actual age of the carbon in the water (sample), the concentration of carbon in the water, the amount of carbon leached from the filter, as well as the age of the carbon in the filter.

In the case of this study, samples were filtered using 0.45µm nitrocellulose filters (Whatman, WCN), and in select cases, 0.70µm glass filters (Whatman GF/F). Laboratory tests by Khan and Subramania-Pillai (2007) showed that the DOC in deionized distilled waters (DDW) increased after being filtered with both the 0.45µm nitrocellulose filter and 0.70µm glass filter. In their study, up to 300mL of DDW was filtered with each filter, collecting samples in 50mL increments and analyzing for Total Organic Content (TOC). Both filters showed that after the first 50mL there was in fact some leaching, with DOC concentrations just below 1mg/L. However, after the second increment (100mL total water filtered), there was a negligible increase in the DOC. It was thus recommended by Khan and Subramania-Pillai (2007) that prior to filtration of the sample, that the filters be pre-washed with at least 150mL of DDW in order to leach as much of the material from the filter as possible in order to prevent contamination. However, this appears to be a procedure that is seldom used by researchers, with many researchers opting to not pre-wash the filters at all, or using less than 100mL of DDW for rinsing (Karanfil et al., 2003).

Accordingly, 0.45µm nitrocellulose filters were rinsed with at least 150mL of DDW prior to use. The nitrocellulose filters ensure that the true DOC of the sample is measured, which is operationally defined as the organic carbon in water that has passed through a 0.45µmfilter (USEPA, 1999). Furthermore, glass filters currently only go to the lowest pore size of 0.70µm, and therefore wouldn't be a true representation of the DOC component of the waters. However, select samples were filtered using both filters (separately) in order to assess if there was a major difference between the results for [DOC], as well as to view the affect that the nitrocellulose filters may have on the age of the water compared to those of the glass filters. The 0.70µm glass

filters were treated for contamination by baking them at 550°C for 3h to burn off any organic matter, then further rinsed with 150mL of DDW prior to use.

Prior to radiocarbon analysis, the concentrations of DIC and DOC were analyzed at the G.G. Hatch Lab (University of Ottawa) using an OI Analytical Aurora Model 1030W TIC-TOC Analyzer to determine ppm carbon (ppmC). Samples were filtered using a 0.45μm nitrocellulose filter into 40mL amber borosilicate EPA vials with septum liners and no headspace. The OI Analytical analyzer uses sequential acidification and oxidation to produce CO_2 for concentration and $\delta^{13}C$ analysis. An aliquot of water is drawn up via a needle, and acidified using 5% H_3PO_4, releasing inorganic carbon (DIC) in the form of CO_2.The gases are purged from the vial using ultra-pure helium and pass through water traps as well as an in-house designed scrubber-conditioning interface in order to remove any water vapour (H_2O_{vapour}). The CO_2 is then measured by a non-destructive infrared (NDIR) detector. After all of the inorganic carbon has been consumed, a persulphate reagent ($[SO_5]^2$ or $[S_2O_8]^2$) is added to release the organic carbon in the water (DOC), producing CO_2 again, and analyzed in the same manner as DIC. Data is then normalized using three different internal standards, with an analytical precision of 2% (±0.002 ppmC) for carbon concentrations (ppm).

Once the concentrations of DIC and DOC were determined, the amount of water required for analysis (^{14}C radiocarbon) was calculated. For Accelerator Mass Spectrometer (AMS), the amount of carbon required for analysis can be as low as 0.5mg to achieve a reliable result, although greater amounts were preferred for these potentially old samples. In the case of radiocarbon samples for this project, it was suggested (verbal communications with the A.E. Lalonde AMS Laboratory - Radiocarbon Laboratory, University of Ottawa) that a higher quantity of carbon would be preferred as the age of the carbon was unknown, although hypothesized to be of Pleistocene origin. Reasoning was that if the age of the water (ice) was in fact found to be old (>15-20,000 years), the amount of ^{14}C remaining in the sample would be exponentially lower (less than 15% of the original ^{14}C), and therefore the amount of ^{14}C available for counting in a 0.5mg sample would be much lower than for a larger sample. As a result, it was decided that the maximum amount of carbon, 4mg, would be the desired amount required for analysis.

In preparation for CO_2 extraction from DIC and DOC samples, 1L glass bottles were baked for 4h at 600°C in order to combust and remove any organic material on the surface. The first step in CO_2 extraction involved the combustion of DIC within the waters. After pre-treatment (baking), 3mL of orthophosphoric acid was added to the bottles, capped with caps containing a butyl rubber septa, and evacuated under vacuum to remove atmospheric gases. The pre-filtered sample was then injected into the glass bottle through the septa using a needle attached to a syringe. Samples were then baked at 70°C for 12h to facilitate the conversion of DIC within the sample to $CO_{2\text{-DIC}}$.

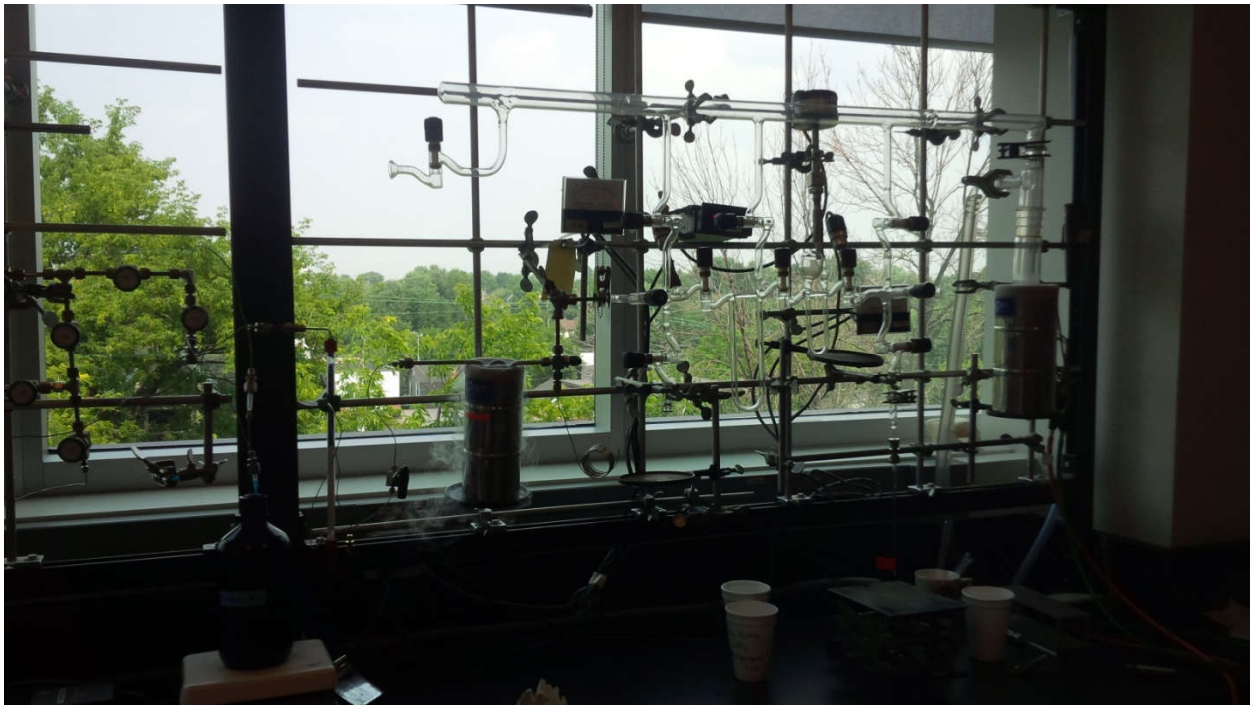

Figure 22. Set-up of the Ice-line extraction apparatus at the G.G. Hatch Stable Isotope Laboratory, University of Ottawa. The Ice-line was used for the extraction of $CO_{2\text{-DIC}}$ and $CO_{2\text{-DOC}}$ from water (ice) samples that were subsequently used for conversion to graphite and radiocarbon analysis. Samples progressed from the left-side (amber bottle), through a series of cold-traps, with the final capture occurring in pre-evacuated breakseals (red tape, bottom right).

After baking, samples were connected to the Ice Line at the G.G. Hatch Stable Isotope Laboratory (University of Ottawa), where the CO_2 was extracted and collected through a series of cold traps (Figure 22). The method for CO_2 extraction was based on a method devised by Leonard et al. (2013), with further modifications through consultation with Paul Middlestead (G.G. Hatch Stable Isotope Laboratory, University of Ottawa). The final collection of the extracted $CO_{2\text{-DIC}}$ was captured in pre-baked (600°C for 3h) and evacuated breakseals.

After collection of the DIC-CO_2 component from the water, the only remaining carbon in the water should now only reside in the organic components, from which the DOC component of the water can now be extracted. Samples were placed in a fridge overnight to fully cool to 4°C. After cooling, samples were sparged from 20 minutes with He to expulse any remaining CO_2 in the water. With He flowing, approximately 1.5g of $KMnO_4$ of was poured into the bottle and immediately re-capped. The bottle was then placed under vacuum and evacuated to negative pressures. During this process there is no loss of CO_2 from DOC, as higher temperatures are required to release the organic content to CO_2. The sample was heated at 98°C for 20 minutes to facilitate the combustion of DOC to CO_2. Following heating for 20 minutes, the samples were connected to the Ice Line, and $CO_{2\text{-DOC}}$ extracted in the same manner as for the $CO_{2\text{-DIC}}$. Blanks of only 3mL of orthophosphoricacid were run each day prior to CO_2 extraction to ensure that there was no residual CO_2 or leaks in the line, and also to ensure there is no organic contamination of the acid solution. Furthermore, the Ice Line was pumped under vacuum between each sample in order to remove any CO2 or other contaminants remaining from previous samples to prevent cross-contamination.

Upon the completion of the capture of all of the CO_2 samples (DIC and DOC components), graphitization of CO_2 to graphite (pure carbon) took place. Samples were connected to the automated graphitization line at the Radiocarbon Lab (A.E. Lalonde AMS Laboratory, University of Ottawa) through specially designed ports (Figure 23). Iron (Fe) powder (~4mg) was added through a second port, where, once the reaction was under way, it was used as a catalyst to reduce the CO_2 in breakseals to graphite (C) under an H_2 environment. Standards of oxalic acid were provided by the Radiocarbon lab and run simultaneously with each batch of graphitization.

Graphite samples were then pressed in to sample targets and subsequently run on an Accelerator Mass Spectromete (AMS) at the A.E. Lalonde AMS laboratory (Advanced Research Complex, University of Ottawa) for ^{14}C analysis (Figure 24). Radiocarbon results were returned in both an uncalibrated ^{14}C BP as well as $F^{14}C$ format. These results were subsequently calibrated to calendar years before present (present=AD 1950) using the freely available OxCal version 4.2 calibration program (Bronk Ramsey, 2009) and the IntCal13 calibration (Reimer et al., 2013). Ages for the samples from the various ice wedges were reported as median ages with

2 sigma uncertainty, along with age probability distributions (youngest to oldest) to a 95.4% Confidence Interval.

Figure 23. Automated Graphitization line at the Radiocarbon Lab (A.E. Lalonde AMS Laboratory, University of Ottawa) used in the reduction of CO2 to graphite for subsequent analysis on AMS.

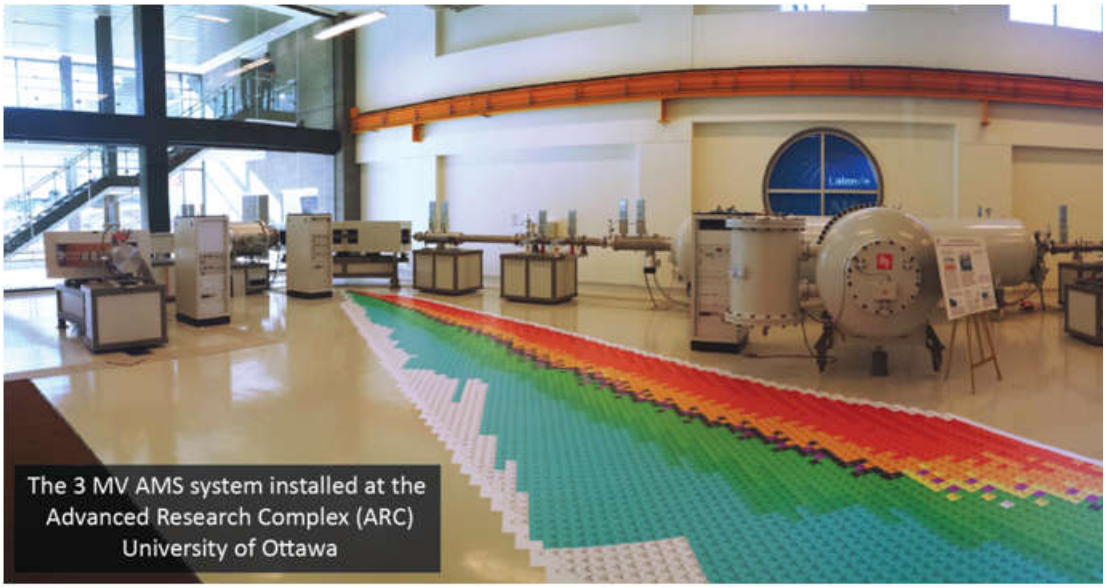

Figure 24. Accelerator Mass Spectrometer (AMS) used in this study and located at the A.E. Lalonde AMS Laboratory, Advanced Research Complex, University of Ottawa, Canada. Lower: Source: http://www.ams.uottawa.ca/.

4. Observations/Results

4.1. Cryostratigraphy & Stratigraphy

The study site, an exposed thaw slump, is ca. 60m wide and exposed to a depth of ca. 7m below the surface in the summer with the lower limits covered by slumped debris and only to ca. 4m in the winter whereby the lower contact is covered by snowpack. The headwall of the slump was delineated into four horizontal stratigraphic units based on visual aspects, sediment content/grain size, organic content and ice content (Figure 25).

All units in the headwall extend horizontally across the entire extent of the outcrop, with the thickness of each remaining relatively uniform throughout the outcrop. The first unit (Unit 1), the upper most layer of the outcrop, is ca. 0.5m thick (0-0.5m depth) and comprised of an organic rich Active Layer (AL) and frozen peat layer (Figure 26A). Unit 2 is composed of frozen Silty Loam with ice veins, further divided into an upper portion and lower portion by organic content, and is ca. 1.25m thick (0.5-1.75m depth) (Figure 26B). Unit 3 is a silt layer with vertical and horizontal ice veins and ca. 1.4m thick (1.75-3.15m depth) (Figure 26C and D). The lowest layer, Unit 4, is a massive ice body with interdispered till that extends downwards ca. 1m (3.15-4.15m depth), here on forth referred to as the Ice/Till (I/T) layer (Figure 25B and Figure 29). The contact between the I/T layer and the overlaying silt layer was sharp, suggesting an erosional surface or thaw unconformity.

Also present within the outcrop are two distinct sets of ice wedges (Figure 30). The first set of ice wedges (N=5), determined to be of Holocene age through radiocarbon dating in this study and here on forth referred to as Holocene ice wedges, were distinguished from the second set of ice wedges by their vertical extent, extending from the bottom of the Active layer (Unit 1), cross-cutting through Units 2 and 3, and tapering off in the I/T layer (Unit 4). The second set of wedges (N=4), determined as late Pleistocene age in this study and here on forth referred to as Pleistocene ice wedges, occur solely in the I/T layer. It is not known how deep the ice wedges penetrate due to slumped debris covering the lower contact. Similar to the I/T layer, the tops of the ice wedges were also truncated, suggesting an erosional surface or thaw unconformity.

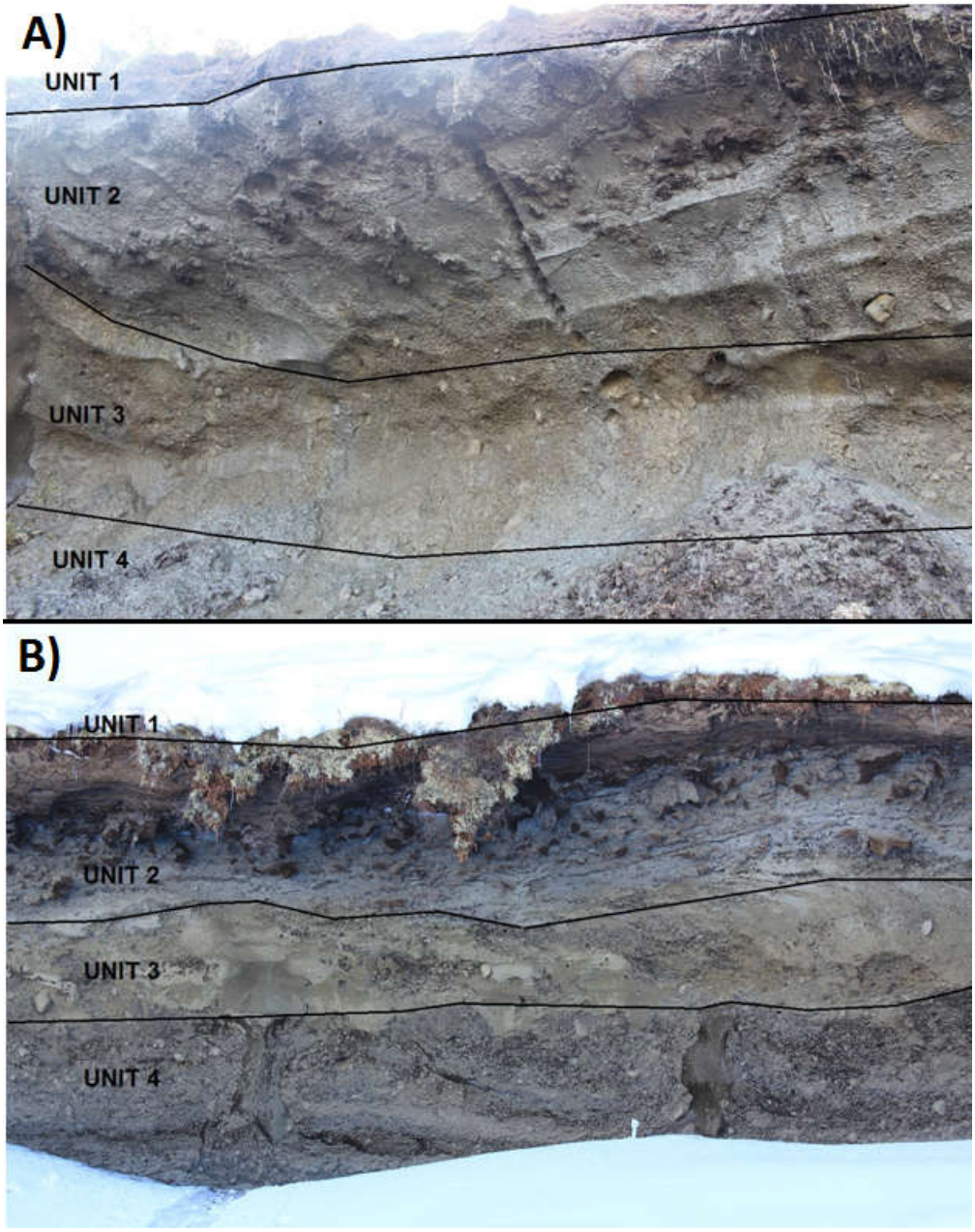

Figure 25. A) Exposed outcrop located at Two Moose Lake, Yukon from August 2013 showing the 4 stratigraphic units. Image was taken from the sampling location of the outcrop located to the right of ice wedge IW1. Vertical sampling of the upper transect using the Hilti drill and core barrel can be seen in Unit 2. B) Exposed outcrop during April 2014. Image was taken from the middle of the outcrop where ice wedges IW4 (Right) and IW5 (Left) can be seen in Unit 4.

Unit 1: Active & Peat Layer (0-0.5m)

The upper portion (0-0.5m) of the outcrop is comprised of two layers: the Active layer and Peat layer (Figure 26A), and is distinguished from the layers below by higher organic content. In the Active layer, organic content (LOI analysis) makes up ca. 50% of the material, decreasing to 13% in the Peat layer (Figure 27A). At the time of sampling, the active layer was ca. 0.25m

thick (thawed) and contained no excess ice (or excess water due to absorption by the peat) as represented by a volumetric water content (VWC) of 0%. As the layer was thawed, sediments were easily removed using a shovel and were composed of a mixture of loosely packed peat and plant material (rootlets, branches, etc.). The presence of frozen and unfrozen ground was used to distinguish the boundary between the Active layer and Peat layer, with the VWC increasing from 0% to ca. 90% at ca. 25cm below the surface (Figure 27B). Despite the lack of excess ice, the gravimetric water content (GWC) still represented ca. 100 to 200% of weight in the Active layer.

The peat layer, extending from the bottom of the Active layer (0.25cm) to ca. 50cm below the surface, was frozen at the time of sampling. It is possible that the peat layer may have been part of the active layer in previous years, as Lacelle et al. (2007) reported an active layer depth of 0.3-0.4m at a site ca. 10 km north of Two Moose Lake ca. 10 years prior. Similar to the Active layer, the Peat layer contained peat and plant material, but differed in that it remained frozen, with ice making up between 46% to 93% of the volumetric water content (VWC). Due the higher ice content, the GWC content in the Peat Layer was much greater than the active layer, ranging between 130 to 370% GWC (Figure 27B).

Unit 2: Silt Loam with Organics Layer (0.5-1.75m)

The second layer of the outcrop, composed of Silt Loam w/ organics (0.5 to 1.75m), was differentiated from the layers above and below (Figure 25 and Figure 26B) by the change in organic content (LOI), decrease in GWC and change in grain size. The upper portion of the layer contained visible patches of organic matter (between 5-12%) that are made up of a mixture of peat, rootlets and other organic material that were mixed with sand and silt (Figure 27A). In the lower portion of the layer, the presence of patches organic matter is much more sporadic and less common, represented by the lower organic content of 3-5%. The layer as a whole remained cryogenically frozen at the time of sampling and contained visible ice in the form of ice veins, pore ice, and in some cases pooled ice. However, the density of ice is sporadic and not uniform across the layer, and is reflected in the highly variable VWC, with values ranging from below 15% to as high as 90% and showing no trend with depth. However, despite the sporadic nature of visible ice, there was a decrease in the water content (GWC) with depth, from 150-200% in the upper portion, to below 80% in the lower portion (Figure 27B).

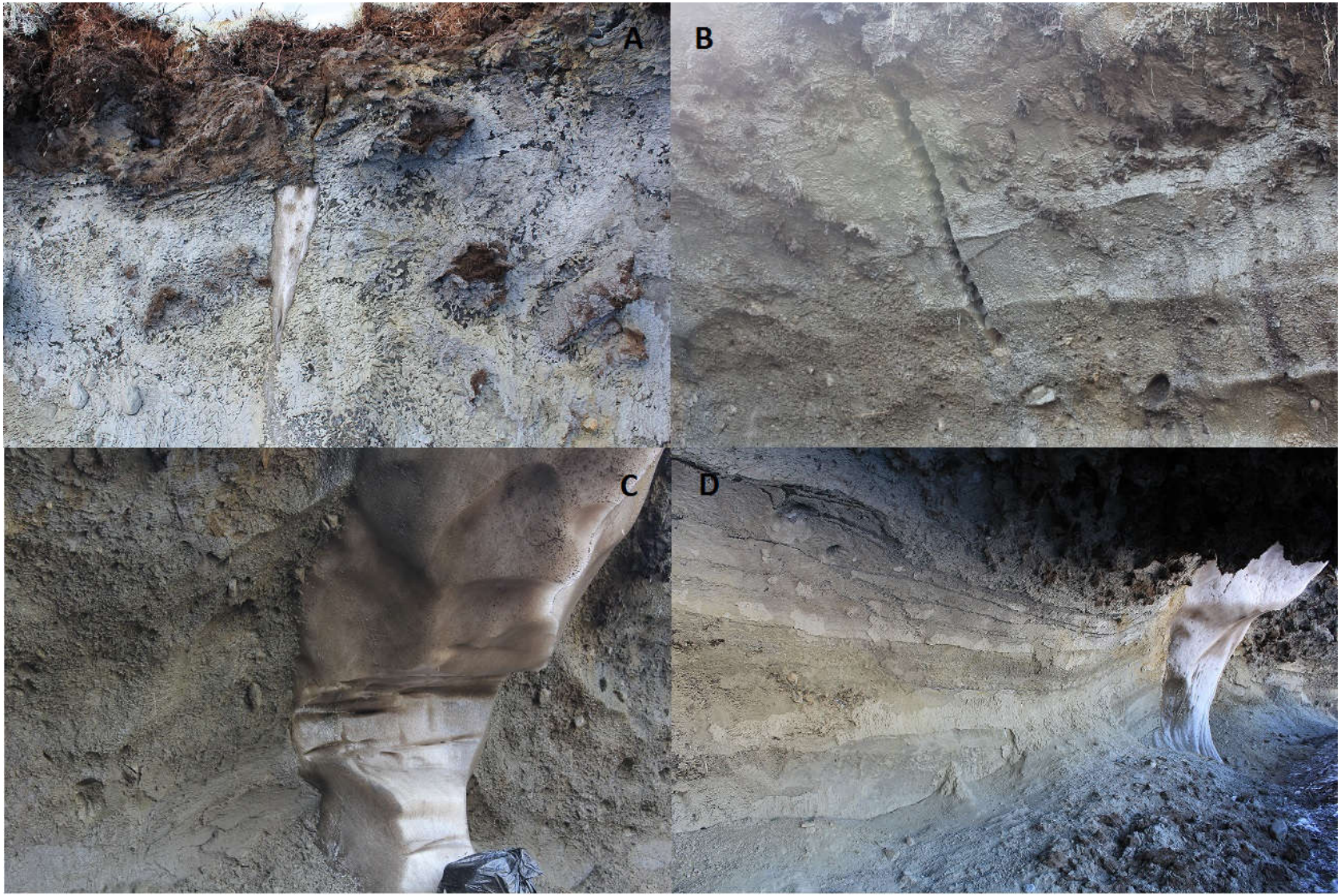

Figure 26. A) Unit 1 showing the Active Layer (Light brown/orange) and Peat Layer (Dark brown) in the upper portion of the outcrop. B) Unit 2 showing Silty Loam and Silt with organics layer. The transition between higher to lower organic content can be seen with a decrease in depth. The location of the samples is shown by the core marks (August 2013). Unit 3, silt layer, to the left of ice wedge IW1 in C) August 2013 and; D) April 2014. The vertical and horizontal ice veins can be seen frozen in the silt layer in April 2014.

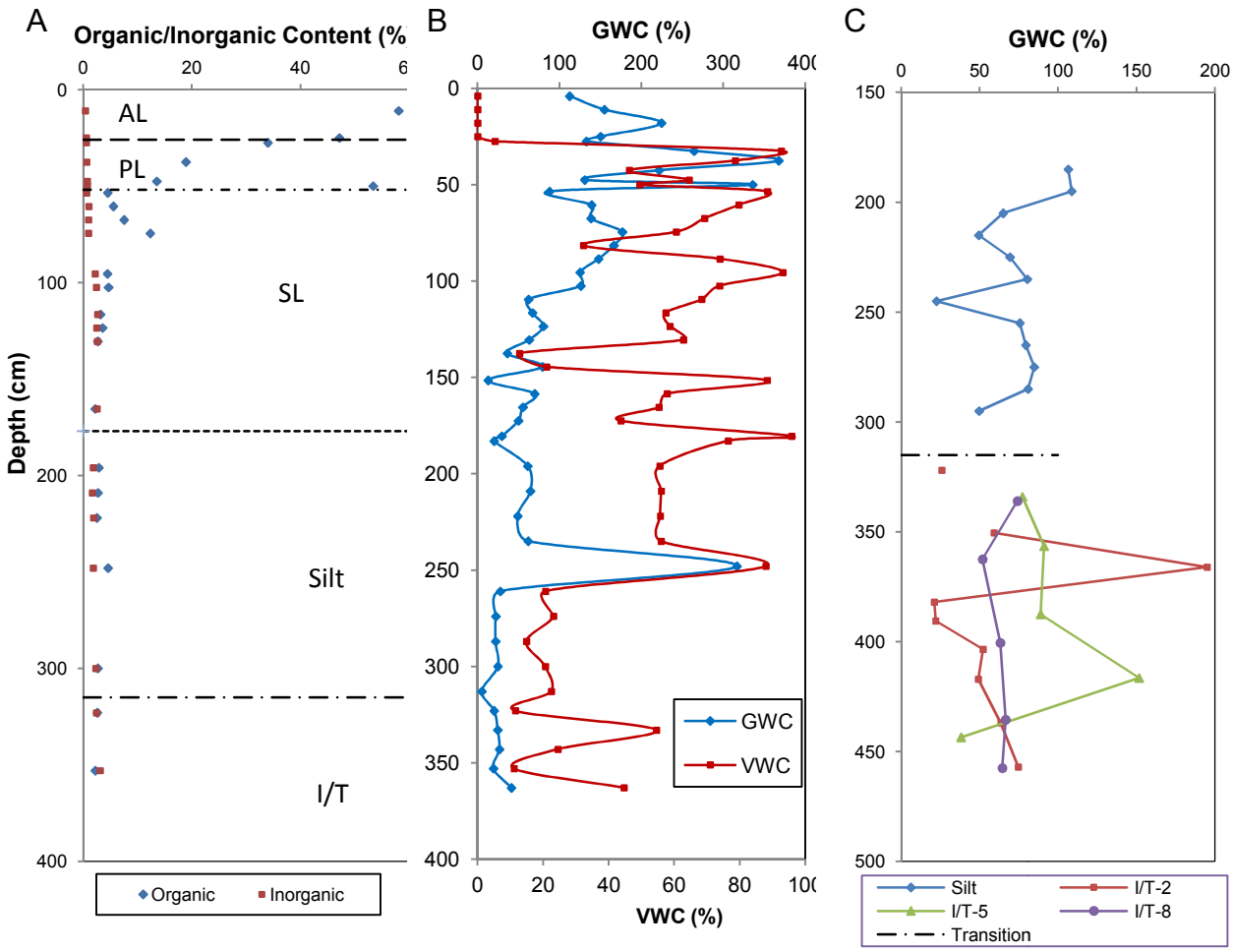

Figure 27. A): Inorganic and Organic content; & B) Gravimetric Water content (GWC) and Volumetric Water Content (VWC) profile for the exposed outcrop located at Two Moose Lake (August 2013). C) GWC for the Silt and Ice/Till Layer (April 2014). Where, AL=Active Layer (N=4), PL= Peat Layer (N=6), SL=Silt Loam w/ organics (N=18), Silt (N=12), and I/T=Ice/Till (N=5).

Unit 3: Silt Layer (1.75-3.15m)

Visually the silt layer (Figure 25, Figure 26C and D), ca. 1.5m thick, is easily distinguished from the layers above and below it by its light-brown hue compared to the grey appearance of the layers above and below. Soil texture analysis on sediments within the layer returned a uniform composition of sandy silt (Folk's classification) throughout the layer. Sediments composition was made up mainly of silt (>75%), with lesser proportions of sand (<20), and clay (<5%) (Table 3, Figure 28A & B.). Organic content within the layer was nearly non-existent, comprising of less than 3% of the material. Sediments are horizontally stratified and inter-bed in a matrix of ice. Ice veins (mm to cm thick), with a larger abundance in the upper portion of the

layer, occur sporadically within the layer and run horizontally to the bedding, and in some cases short vertical veins connect veins at different depths (Figure 26D). Samples for the layer were collected both in 2013 and 2014, however the results for GWC differ between the two years. Samples from 2014 were on average double the GWC those of 2013. Samples from 2013 had a GWC between 5 to 65%, with more than half of the samples below 30% (Figure 27B). One sample produced a GWC of 316%, however it is likely that this sample contained an ice vein, and not representative of the layer as a whole. On the other hand, the GWC of samples from 2014 were on average higher than the highest GWC value from 2013, ranging from 50 to 109%. The difference between years can likely be attributed to the different sampling conditions, as samples from 2013 were obtained during the summer when temperatures were higher, during which melting of the headwall was taking place, and thus decreasing the amount of water (in the form of ice) relative to the amount of sediment. VWC was determined for samples from 2013 only. While the GWC may not necessarily reflect the visual ice content, results from VWC are more indicative of it. Samples in the upper portion of the layer had VWC between 55-95% (Figure 27B), a reflection of the higher abundance of ice veins, while VWC for samples in the lower portion ranged between 15 to 23%. The largest VWC (95%) occurred at the top of the silt layer, and it is possible that this large value, along with a higher density of ice in the upper portion of the layer, would suggest pooling (and refreezing) or water that had percolated to the silt layer during warmer conditions, suggesting a potentially deeper thaw depth.

Unit 4: Ice/Till layer (3.15-4.35m)

The Ice/Till (I/T) Layer is the lowest of the exposed layers (Figure 29), occurring across the entire extent of the outcrop. Due to the large extent and continuity of this I/T layer across the outcrop, this layer is assumed to be a stratigraphically significant layer as opposed to localized pooling of water. The I/T layer was not visually apparent until the second field season (April 2014), as warmer temperatures during the first field season (August 2013) led to meltwater covering the headwall and base of the headwall with sediments/mud that had melted from the headwall as well as from material that had fallen from the overhang. These deposits

Table 3. Grain size distribution for the Silt and Ice/Till layer.

Sample ID	Depth (cm)		Gravel (%) (≥2mm)[a]	Sand (%) (2mm-≥62.5um)[a]	Silt (%) (62.5-≥3.9um)[a]	Clay (%) (<3.9um)[a]
Silt						
14-MG-31	195		-	20.18	75.12	4.7
14-MG-36	245		-	17.86	78.28	3.86
14-MG-40	285		-	19.07	76.56	4.37
		average:	-	19.04	76.65	4.31
I/T - Left IW2						
14-MG-56	335.5		9.03	24.99	54.35	11.64
14-MG-60	390.5		69.26	11.28	14.41	5.05
14-MG-63	437		37.23	21.2	27.13	14.44
		average:	38.51	19.16	31.96	10.38
I/T - Left IW5						
14-MG-65	334		31.15	33.08	21.91	13.88
14-MG-67	387.5		18.08	20.89	35.93	25.11
14-MG-69	443.5		48.35	12.95	24.29	14.39
		average:	32.53	22.31	27.38	17.79
I/T - Right IW8						
14-MG-70	336		27.54	26.26	30.9	15.28
14-MG-72	400.5		28.72	22.17	29.52	19.59
14-MG-74	457.5		32.12	23.83	26.81	17.26
		average:	29.46	24.09	29.08	17.38

[a]Grain size classification based on Wentworth (1922).

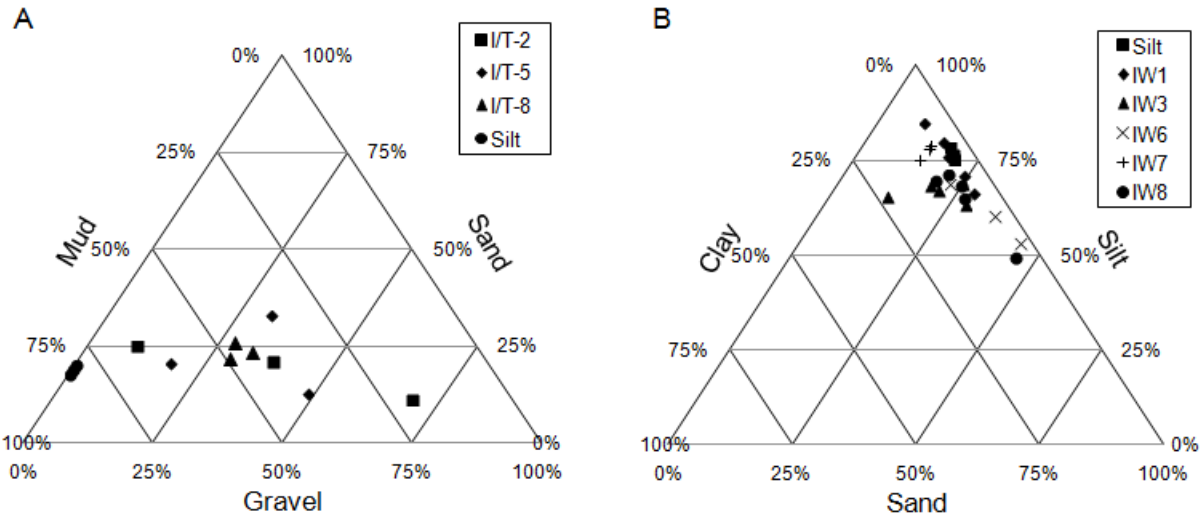

Figure 28. Tertiary diagram for sediments enclosed in the A) Silt and Ice layer, & B) Silt and Ice wedges at Two Moose Lake, Yukon. Mud in A) represents a combination of Clay and silt. Classification for the different sediment types are as follows and based on Wentworth (1922): Gravel: ≥2mm, Sand: <2mm to ≥63um, Silt: <63um to ≥3.9um, clay: <3.9um.

also made sampling of the lower extremities of the headwall difficult due to the constant flow of meltwater and mud down the base, increasing the potential for contamination of any material obtained from the lower portion of the outcrop. Furthermore, these wet conditions made sampling of this layer difficult and as result minimal exploration and samples were taken from this layer during the first field season. Initial samples that were obtained from this layer suggested the potential for a sediment rich ice wedge due to the high ice content of a few

samples obtained using an ice pick, as well as the presence of other ice wedges in the layer. Field exploration during April 2014 revealed the presence of at least an ca. 0.75-1m thick mixture of ice and till below the Silt layer, however its lower contact was not exposed and thus it was not possible to determine if the layer extended any deeper.

The I/T layer does not appear to have any form of stratigraphy as it is composed of a heterogeneous mixture of randomly orientated sediments and ice. The ice within the layer has a clear-like nature unlike those of the ice wedges (discussed later), as it appears as though the finer sediments (silt and clay) within the layer have formed as conglomerates, whereby the sediments seem to have been expulsed from the ice and formed as a cluster/ball of sediment (Figure 29). GWC in the layer was highly variable ranging between 20 to 200% with no horizontal or vertical trend. The high variability in GWC (ca. average of 70%) supports the initial visual determination of the heterogeneity of the layer (Figure 27B and Figure 29). Further exploration was completed by analyzing 3 vertical transects in the I/T layer to determine if there was any stratigraphy to the layer. GWC for the 3 transects produced variable results (Figure 27C), with a high variability within and between the transects. Similar to GWC, grain size distribution within each transect is highly variable with no vertical trend, as grain sizes varied by as much as 50% between samples in a transect (Table 3Figure 28). Comparisons of samples taken at the same height but at different locations within the layer also showed high variability in grain size distribution between samples, further building on the heterogeneity and lack of stratigraphy within the layer (Table 3). On average approximately one third of the sediments in the layer was composed of gravel, followed closely by silt (ca. 30%), with lesser amounts of sand (ca. 22%) and clay (ca. 15%), and classified (Folk's classification) as a mixture between muddy gravel and gravelly mud. Furthermore, results for gravel comprised of all sediments >2mm, however, there was a large variation in the size, with 'gravel' composed of a mixture of granules (2-4mm), pebbles (4-64mm) and cobbles (64-256mm), although the exact proportion of each was not analyzed. However, it was not possible to extract cobbles as they were often larger than the diameter of the core barrel (8cm), but should be noted that cobbles of various sizes were in fact present. Similar to the silt layer, the organic content in the ice layer was below 3%.

Figure 29. Upper: Ice/Till layer (Unit 4), shown between the two horizontal black lines, at Two Moose Lake, April 2014. Ice Wedge IW4 is shown located in the middle of the image within the I/T layer. B) Zoomed in image of the I/T layer showing the various sediment sizes, clay conglomerates and clear nature of the ice.

Within the I/T layer, there were two unique features. First, a thaw unconformity can be seen across the layer, where a sharp contact is present between the Silt and I/T layers (Figure 29Upper, upperline). The boundary can also be distinguished by a change in grain size, as no sediments larger than >2mm were found in the silt layer (present in the I/T layer), the I/T layer contained >50% less silt and contained 2 times the amount of clay. Furthermore, the I/T layer

also contained five ice wedges that were also truncated at the same height of the thaw unconformity, further supporting the notion of an unconformity between the silt and I/T layer and also suggesting the unconformity occurred after the penetration of the ice wedges.

4.2. Ice Wedges

4.2.1. Holocene Ice Wedges (0.5-ca. 4m)

The most noticeable feature of the outcrop is the presence of five ice wedges (IW1,3,6,8 and 9) extending from the lower contact of the active layer (Unit 1; 0.5m depth) down into the I/T layer (Unit 4) at the bottom of the outcrop (Figure 30), spanning a depth of 3-4m. The width of the ice wedges varies from 1m to over 3m wide at the upper contact, narrowing in width with depth. The ice within the ice wedges was whiter in colour, suggesting a composition of mainly ice with minimal amounts of sediments within them. This is supported by the GWC, where values for the ice wedges ranged between 19294 to 47076%, and a VWC between 98.4 to 99.57%, indicating that less than 1% by weight, and less than 2% by volume of the ice wedges are composed of sediments (Table 4). Lamination within the ice wedges is nearly vertical, suggestive of epigenetic ice wedges, and therefore likely formed after the deposition of the layers in which they penetrate. This notion is further supported by the large ratio in width between the top of the ice wedge and the bottom, differing from the syngenetic ice wedges that have a similar width at the top and base (Murton, 2013). Furthermore, the sediment layers in contact with the sides of the ice wedge were tilted upwards (relative to their original position in the layer) by as much as 45° (Figure 30B-E). The tilting of the layers in contact with the sediments occurs as a result of the horizontal expansion of the ice wedge during freezing of melt water in the crack, and would only occur if sediments/layers were already previously in place.

Soil texture within the ice wedges was composed only of sediments smaller than 2mm in size, with the silt comprising between 60-75% of the sample, followed by various amounts of sand (19-35%) and clay (5-12%) (Table 5, Figure 28). Sediment composition horizontally across each ice wedge was highly variable, with changes in sediment sizes by as much as 100% between samples, reflecting potentially different conditions during the lifespan of formation

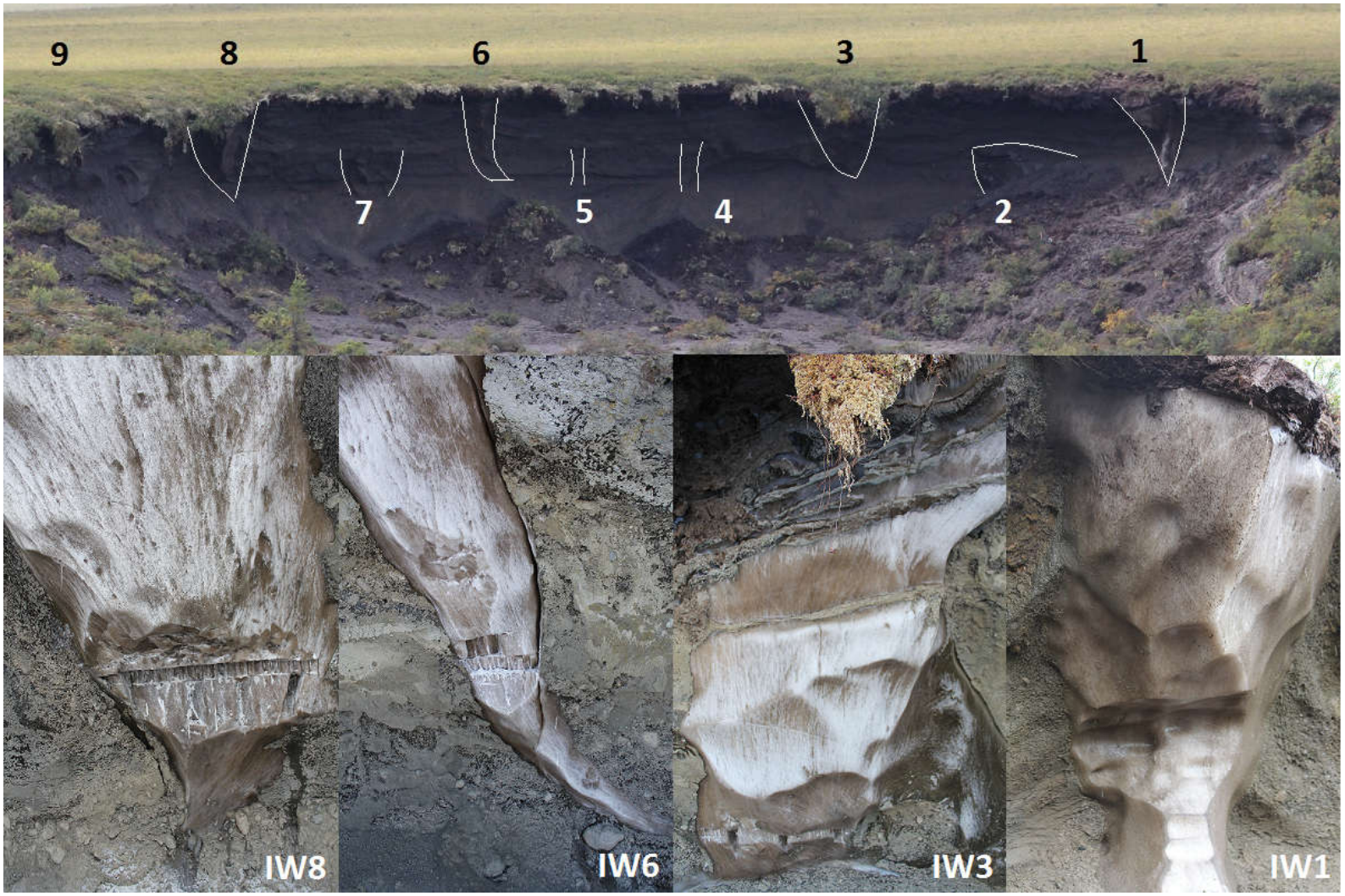

Figure 30. UPPER: Location of Holocene and Pleistocene Ice wedges in the headwall at Two Moose Lake, August 2013. Ice wedges are indicated by why lines, whereby Holocene Ice wedges (N=5, IW9 not shown or analyzed) are indicated by black numbers above and white lines that intersect at the bottom and Pleistocene Ice wedges (N=4) are indicated by white numbers below and white outlines that do not intersect at the bottom. LOWER: Close up images of the various Holocene Ice Wedges from April 2014 (IW3,6, 8) and August 2013 (IW1). Stable isotope, grain size analysis and LOI sampling locations are indicated by the continuous band cut out across the length of the ice wedge while larger holes (above, below and within the continuous band) indicate where large blocks were extracted for radiocarbon analysis.

Table 4. Wet- & Dry-Gravimetric water content (GWC) and Volumetric water content (VWC) for the Ice wedges at Two Moose Lake, Yukon.

Ice Wedge	Age	Wet-GWC (%)	Dry-GWC (%)	VWC (%)
IW1	Holocene	20507	99.03	98.39
IW2	Pleistocene	6676	98.16	94.67
IW3	Holocene	19294	99.31	99.43
IW6	Holocene	21322	99.36	99.57
IW7	Pleistocene	9193	98.63	97.04
IW8	Holocene	47076	99.60	99.46
Average	*Holocene*	*27050*	*99.33*	*99.21*
Average	*Pleistocene*	*7935*	*98.40*	*95.85*

Table 5. Grain size distribution for the Holocene and Pleistocene ice wedges.

Sample ID	Horizontal Distance (cm)	Sand (%) (2mm-≥62.5um)[a]	Silt (%) (62.5-≥3.9um)[a]	Clay (%) (<3.9um)[a]
IW1 - Holocene				
14-MG-1	115.5	28.63	66.06	5.31
14-MG-5	97.5	24.25	70.75	5
14-MG-14	54.5	18.53	75.96	5.51
14-MG-20	29.5	9.46	84.6	5.94
14-MG-24	4.5	15.55	79.63	4.82
	average:	19.28	75.40	5.32
IW3 - Holocene				
14-MG-152	44.85	28.35	63.22	8.43
14-MG-159	76.05	25.08	68.64	6.28
14-MG-166	99.45	18.77	68.59	12.64
14-MG-172	122.85	20.91	67.09	12
14-MG-174	130.65	11.57	65.63	22.8
	average:	20.94	66.63	12.43
IW6 - Holocene				
14-MG-105	3.5	22.39	68.88	8.73
14-MG-111	18	35.54	60.43	4.03
14-MG-116	31.25	44.4	53.21	2.39
	average:	34.11	60.84	5.05
IW7 - Pleistocene				
14-MG-120	12.5	13.4	78.08	8.52
14-MG-129	40	12.84	75.23	11.93
14-MG-136	63	13.08	79.01	7.91
	average:	13.11	77.44	9.45
IW8 - Holocene				
14-MG-80	3	20.81	71.26	7.93
14-MG-88	53	24.77	68.51	6.72
14-MG-96	103	27.12	65.22	7.66
14-MG-102	141	45.47	49.45	5.08
14-MG-103	147	19.23	69.79	10.98
	average:	27.48	64.85	7.67

[a]Grain size classification based on Wentworth (1922).

of the ice wedge. Furthermore, the distribution of grain size composition between the various ice wedges was also varied. These changes in sediment make-up can give indications on the prevailing conditions at the time of formation of the ice wedge, as well as the source of infilling. Organic content within the samples was below 3%, suggestive of an arid environment with little vegetation.

4.2.2. Pleistocene Ice Wedges (3.15-?m)

In all, four ice wedges were discovered within the I/T layer (Unit 4), one (IW# 2) during the first field season and three more (IW# 4,5 and 7) during the second field season (Figure 30, Figure 31) when conditions were more conducive to their appearance. These four ice wedges were determined to be of Pleistocene age (Determined in this studied and discussed below), and were all truncated in line with the top of the I/T layer (Figure 29). The depth to which they penetrated is unknown as slumped material covered the lower contact, however, based on visual comparisons between 2013 and 2014, it is possible that ice wedge IW2 extends further below what is exposed.

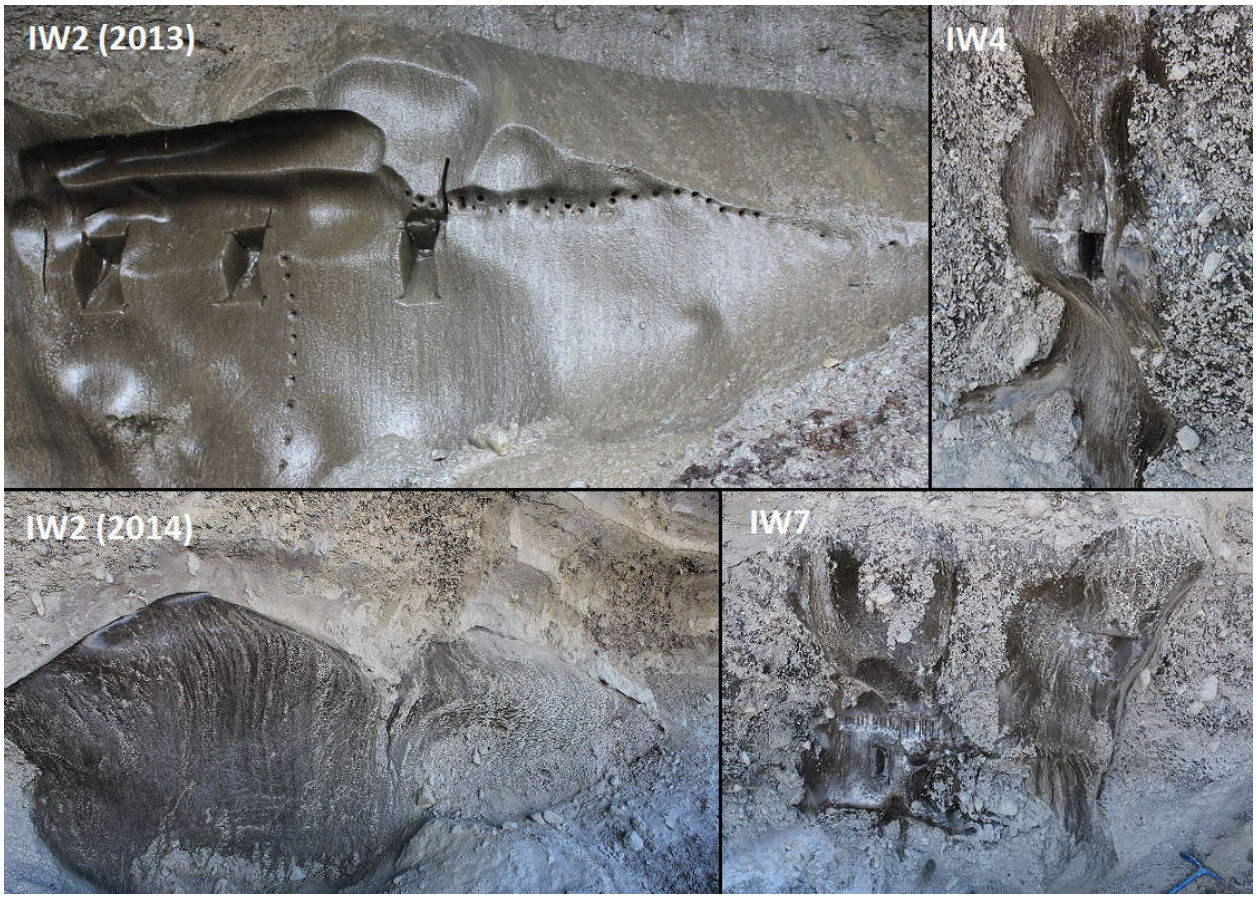

Figure 31. Pleistocene ice wedges sampled during August 2013 (IW2) and April 2014 (IW2, 4 and 7). Stable isotope, grain size analysis and LOI sampling locations are indicated by the continuous band cut out across the length of the ice wedge while larger holes (above, below and within the continuous band) indicate where large blocks were extracted for radiocarbon analysis.

The Pleistocene ice wedges contain a much darker appearance than those of Holocene age ice wedges which can be attributed to the higher sediment content compared to the Holocene ice wedges. The higher sediment content is supported by the higher GWC than seen in Holocene ice wedges, with values between 6676 to 9193%, indicative of 1-2% by weight of sediments and

double that of Holocene ice wedges (Table 4). Furthermore, the VWC of the Pleistocene ice wedges (95.85%) was 5 times lower than that seen in the Holocene ice wedges (99.21%) and would further explain the darker hue.

Lamination within the ice wedges was nearly vertical with thin bands of sediment separated by layers of ice of variable thickness (Figure 31). The vertical lamination would suggest that the ice wedges are epigenetic, and therefore the ice layer would have been in place prior to the formation of the ice wedges. Further evidence supporting the ice wedges as epigenetic ice wedges is seen by the tilting of the ice layers upwards along the sides of the ice wedges, having only occurred if the ice layer was already in place at the time of ice wedge formation. Sediments from ice wedge IW7 were analyzed, and shown to be composed predominantly of silt (77.44%), with lesser amounts of sand (13.11%) and silt (9.45%), giving a more silty character than those the Holocene ice wedges (Table 5, Figure 28). Furthermore, had the Pleistocene ice wedges been formed at the same time as the ice layer (syngenetically), the sediment composition enclosed in the ice wedges and I/T layer should have been similar. This does not appear the case, as the I/T layer contained sediments larger than 2mm while none of the ice wedges contained any coarse fragments and contained lesser amounts of silt (29%) in comparison to the of the ice wedges (77.44%), as well as half the amount of sand and clay, and therefore suggesting different conditions of formation.

4.3. Stable Isotopes (δD & $\delta^{18}O$)

4.3.1. Permafrost

The $\delta^{18}O_{ice}$ composition of ice in the permafrost (Figure 32A) decreased from -19.96‰ at the top of the headwall in the Peat layer (Unit 1, 0.25m depth) to -27.07‰ at the base of the exposed I/T layer (Unit 4, 4.35m depth). The $\delta^{18}O_{ice}$ composition of the upper portion of the outcrop, from the Active Layer to Silt loam w/ Organics (Unit 1 & 2, 0.25 to 1.75m depth), was determined using samples from 2013, while samples from 2014 were used for the silt and Ice/Till layer (Unit 3 &4, 1.75m to 4.35m depth). The reasoning for the use of samples from different years was due to potential surface contamination of samples in the Silt and I/T layer by melt water dripping down the vertical headwall and from the overhang above due to the warmer conditions in 2013. In contrast, the headwall was frozen in 2014 and therefore the outer 10cm of ice/sediment was removed without any contamination of exposed surface by melting water and

sediments. While there were inter-layer variations in $\delta^{18}O$, there was an overall depletion in $\delta^{18}O$ with an increase in depth, suggestive of cooler conditions prevailing at deeper depths, and hence an amelioration in climate during the deposition of sediments. $\delta^{18}O$ Values in the Peat layer (Unit 1, 0.25-0.5m) averaged -20.35‰, decreasing to an average of -21.21‰ in the Silt Loam w/ organics layer (0.5-1.75m) (Table 6, Figure 32A). The $\delta^{18}O$ values in the upper portion of the outcrop are on average, more enriched than modern precipitation at Mayo (-22.32±3.06‰; IAEA/WMO, 2015), suggesting that the deposition of these layers occurred during more favourable conditions than present. In the silt layer, $\delta^{18}O$ values averaged -22.62‰, whereby $\delta^{18}O$ values decreased from -22.35‰ at upper boundary to -23.7‰ at the lower boundary. The increase in $\delta^{18}O$ from the lower contact of the layer to upper contact would suggest a amelioration in conditions over the deposition of the layer to those similar to present day Mayo (-22.32‰). In the Ice/Till layer, $\delta^{18}O$ values averaged -24.33‰, decreasing from -21.94‰ at the upper contact to -27.07‰ at the lower contact. Similar isotopic values were obtained by Kotler & Burn (2000) from a pre-Late Wisconsinan deposit in the Mayo region, with values between -28 to -26‰. A unique feature seen in the Ice/Till layer is the oscillation of $\delta^{18}O$ in the layer (Figure 32A), potentially suggestive of changes in the freezing rate/pattern, or the input of new waters or precipitation. Furthermore, at the boundary between the Silt layer and Ice/Till layer, a 3‰ difference occurs between the lower contact of the silt layer and the upper contact of the I/T layer, whereby the Silt layer is less enriched in $\delta^{18}O$ relative to the Ice/Till layer. The large difference in $\delta^{18}O$ between the two layers supports the previously mentioned notion of an unconformity between the Silt and Ice/Till layer, also seen with the truncated ice wedges in the Ice/Till layer.

On a δD vs. $\delta^{18}O$ plot, the relationship between δD and $\delta^{18}O$ can sometimes be used as a diagnostic of the origin of the water (ice), and any modifications by post-depositional processes. By comparing the regression line of a δD vs. $\delta^{18}O$ plot from a set of samples to the regression lines from local and global sources (local and global meteoric water lines), it is possible to determine if the ice that has formed was a result of precipitation (in the form of snow leading to firnification), or the re-freezing of precipitation or from groundwater. On a δD vs. $\delta^{18}O$ plot for the outcrop at Two Moose Lake as a whole (Unit 1 to Unit 4), a regression of

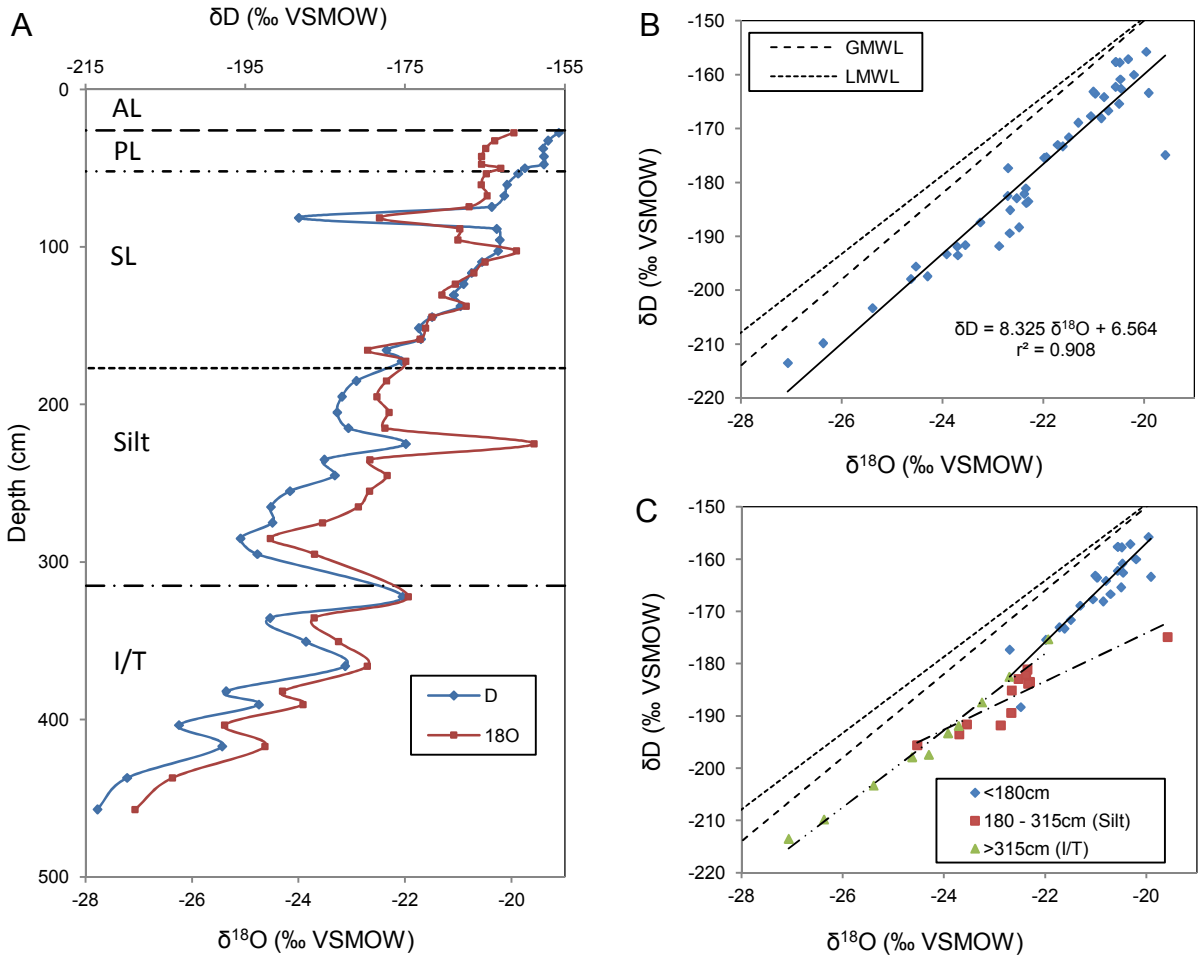

Figure 32. A) Stable Isotope (^{18}O, D) profile for the outcrop at Two Moose Lake (<180cm=August 2013, >180cm=April 2014). Where, AL=Active Layer, PL= Peat Layer, SL=Silty Loam w/ Organics, I/T=Ice/Till. δ^{18}O values represent single point data. B) δD vs. δ^{18}O plot for the outcrop as a whole (GMWL: δD= 8 δ^{18}O+10; LMWL (Iunvik): δD= 7.3 O^{18}δ-3.5). C) δD vs. δ^{18}O plot for the upper portion (<180cm), Silt layer and Ice/Till Layer. The following regressions were obtained: $\delta D_{<180cm}$=9.442 δ^{18}O+31.89 (r^2=0.807), δD_{Silt}=4.635 δ^{18}O-81.41 (r^2=0.806), and $\delta D_{I/T}$=7.351 δ^{18}O-16.37 (r^2=0.985).

Table 6. Summary of Isotope Data for the Outcrop and Ice wedges.

		δ18O (‰)			δD (‰)		
	Age	Average	Max	Min	Average	Max	Min
Outcrop							
Upper portion (<180cm)[a]	Unknown	-20.95	-19.91	-22.70	-165.89	-155.75	-188.30
Silt[b]	Unknown	-22.62	-19.58	-24.53	-186.28	-174.90	-195.60
Ice/Till[b]	Unknown	-24.33	-21.94	-27.07	-195.23	-175.30	-213.50
Ice Wedges							
IW1[b]	Holocene	-22.72	-22.29	-22.99	-193.53	-190.08	-196.92
IW2[a]	Pleistocene	-28.51	-24.66	-30.92	-230.01	-216.16	-241.34
IW3[b]	Holocene	-23.94	-22.64	-26.50	-201.54	-196.92	-208.04
IW6[b]	Holocene	-23.12	-22.52	-23.40	-195.91	-191.21	-198.14
IW7[b]	Pleistocene	-26.42	-25.52	-26.98	-226.87	-221.50	-230.35
IW8[b]	Holocene	-25.59	-25.15	-26.33	-200.99	-197.55	-204.79

[a]Samples obtained in August 2013.
[b]Samples obtained in April 2014.

$\delta D=8.325\ \delta^{18}O+6.564$ ($R^2=0.908$) was obtained (Figure 32B). This slope is above both that for the global meteoric water line (GMWL: $\delta D= 8\ \delta^{18}O+10$) and the local meteoric water line for Inuvik (LMWL: $\delta D= 7.3\ O^{18}\delta-3.5$). (Lacelle et al., 2007). However, as earlier results from this study suggests different conditions and times of formation for each of the layers, individual regression lines were generated for each layer (Figure 32C). The upper portion of the outcrop (Active Layer to Silt loam w/ Organics layer) produced a slope ($\delta D_{<180cm}=9.442\ \delta^{18}O+31.89$, $r^2=0.807$) well above the GMWL and LMWL, suggesting that perhaps the layer was deposited during warmer conditions that currently, as supported by the less depleted $\delta^{18}O$ values compared to modern values at Mayo (Figure 32A, Table 6). The slope for the silt layer ($\delta D_{Silt}=4.635\ \delta^{18}O-81.41$, $r^2=0.806$) was well below both the GMWL and LMWL and would indicate that the ice within the layer was likely water that had infiltrated the layer and refrozen. Finally, the slope of the Ice/Till layer ($\delta D_{I/T}=7.351\ \delta^{18}O-16.37$, $r^2=0.985$), produced a slope similar to the LWML at Inuvik, and suggests there was no post-modification that occurred, and therefore it is possible that the layer is the remnant of a buried snowbank or potentially buried relict basal glacier ice.

4.3.2. Holocene Ice Wedges

In general, the formation of ice wedges occur during climatic conditions producing a mean annual air temperature (MAAT) below -4°C, and require a rapid decrease in temperature to below -20°C for ground cracking to occur (Harry & Gozdzik, 1988). These cracks are then filled by either 1) winter precipitation in the form of snow, or 2) refrozen $\delta^{18}O$-depleted snow meltwater, from which the $\delta^{18}O$ from the ice can be used to determine the prevailing climatic conditions at the time of formation, as well as surficial conditions. In the outcrop at Two Moose Lake, the $\delta^{18}O$ composition of the Holocene ice wedges varies, however there is a clear distinction between the $\delta^{18}O$ of Holocene (N=4) age ice wedges in comparison to Pleistocene (N=2) age ice wedges, as the Pleistocene ice wedges are more depleted in $\delta^{18}O$ (Table 6).

The lowest $\delta^{18}O$ values recorded in the Holocene ice wedges occurred in the two smallest ice wedges, IW1and IW6, with average $\delta^{18}O$ values of -22.72‰ and -23.12‰ respectively (Figure 33A and Figure 34A; Table 6). Variation in $\delta^{18}O$ horizontally across IW1 and IW6 was less than 1‰ with no apparent trend in $\delta^{18}O$ across the ice wedges. The $\delta^{18}O$ values for IW1 and IW6 fall within the range of modern precipitation at Mayo (-22.32±3.06‰; IAEA/WMO,

2015). A site just ca.10km north at Chapman lake produced an $\delta^{18}O$ value of -22.4±0.5‰ from a modern ice wedge (Lacelle et al., 2007), between IW1 and IW6 at Two Moose Lake.

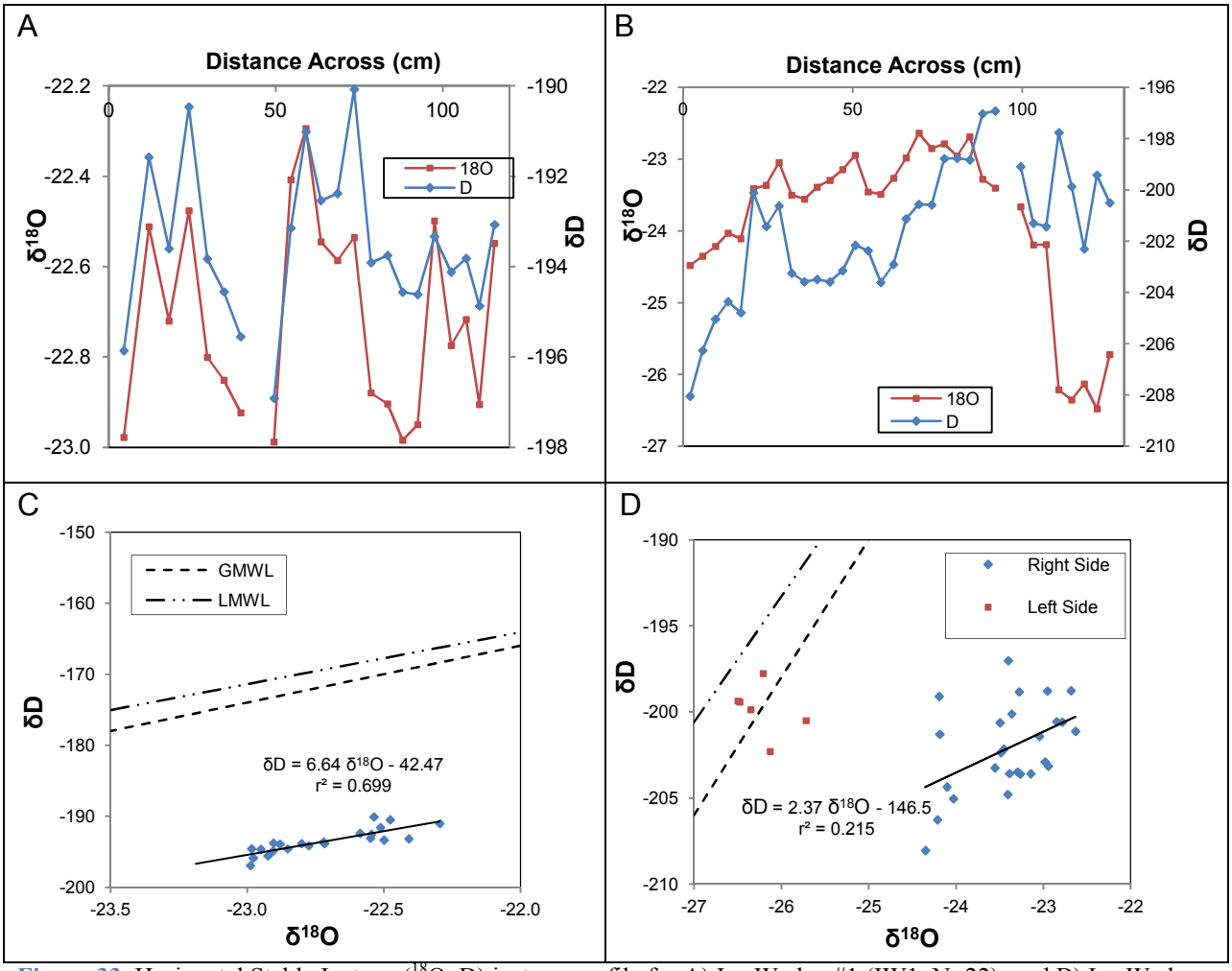

Figure 33. Horizontal Stable Isotope (^{18}O, D) isotope profile for A) Ice Wedge #1 (IW1, N=22); and B) Ice Wedge #3 (IW3, N=34). δD vs. $\delta^{18}O$ plot for C) IW1; and D) IW3. GMWL is the Global Meteoric Water Line (δD= 8 $\delta^{18}O$+10), and LMWL is Inuvik's Local Meteoric Water Line (δD= 7.3 $\delta^{18}O$-3.5). $\delta^{18}O$ values

Furthermore, a failed re-initiated ice wedge of similar age at site in the Mayo region produced an $\delta^{18}O$ value of -23.1‰ (Burn et al., 1986). Ice wedge IW3, the largest of the Holocene ice wedges, produced an average $\delta^{18}O$ of -23.94 (Table 6). Upon further review however, there appears to be two distinct portions to the ice wedge. On the right side of the ice wedge, $\delta^{18}O$ values were below -26‰ (Figure 33B), where at ca. 30cm from the right contact of the ice wedge, there is a 3‰ jump in $\delta^{18}O$, with $\delta^{18}O$ values on the left side (<110cm) of the ice wedge ranging between -22.5 to -24.5‰ . A possible explanation for the difference can be due to a sudden

change in climate resulting in ameliorating conditions and therefore being less depleted in $\delta^{18}O$. With this in mind, the left side (<110cm) and right side of ice wedge IW3 were analyzed separately due to the sudden change, resulting in the left side of the wedge producing an average of -23.48‰, a value closer to the that seen at a modern ice wedge near Mayo by Burn et al. (1986). Conversely, ice wedge IW8 produced the most depleted $\delta^{18}O$ values of the Holocene ice wedges, with an average $\delta^{18}O$ of -25.59‰, with sample values ranging between -25.15 to -26.49‰ (Table 6, Figure 34B). The $\delta^{18}O$ of IW8 are ca. 2-3‰ more depleted than those at present-day Mayo (-22.32±3.06‰; IAEA/WMO, 2015). A modern ice wedge in the Mayo region produced an $\delta^{18}O$ value of -26‰, slightly less depleted than that of ice wedge IW8 (Burn et al., 1986), while at a site ca. 10km south of Two Moose Lake, St. Jean et al. (2011) uncovered a channel of underground ice wedges with $\delta^{18}O$ values of ca. 25‰.

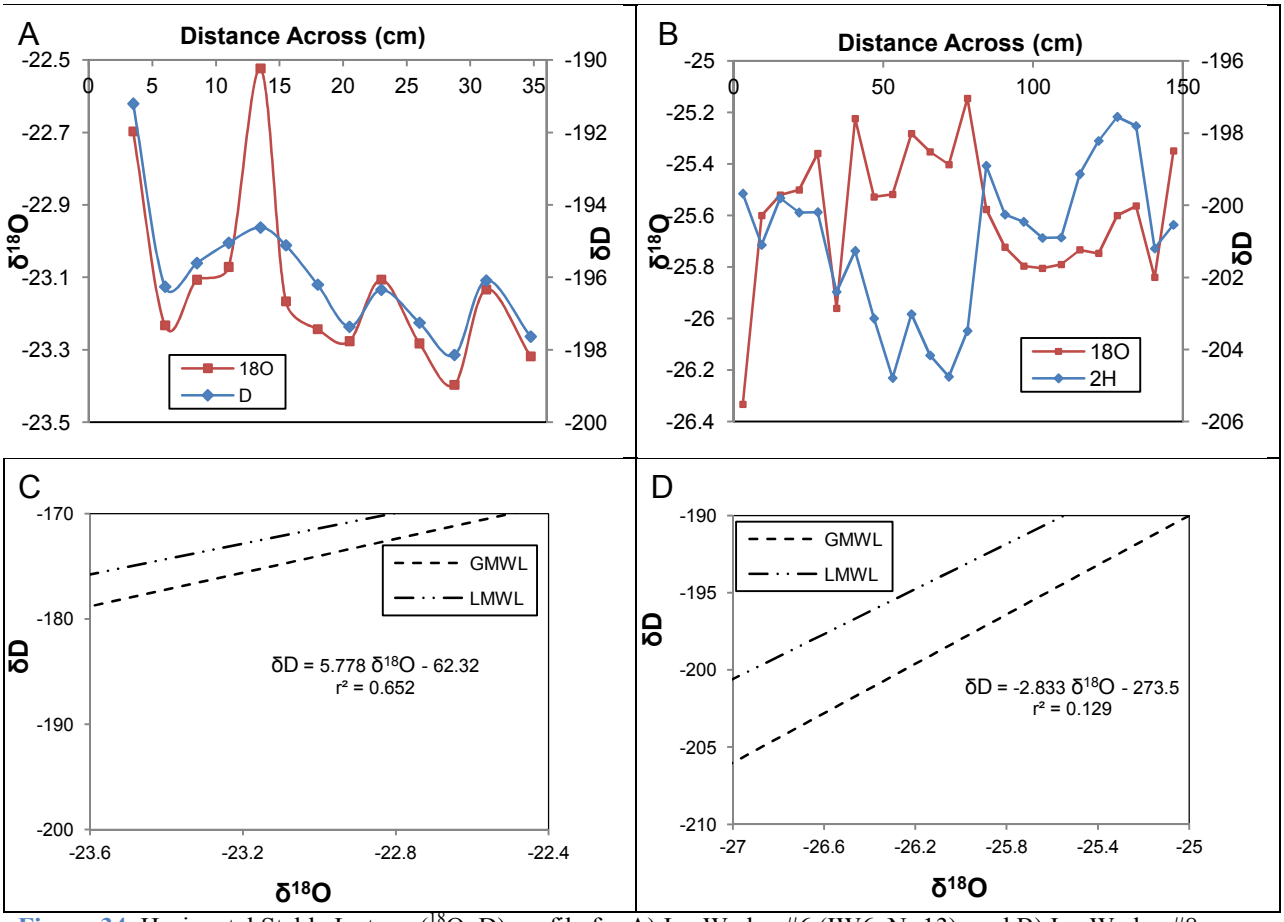

Figure 34. Horizontal Stable Isotope (^{18}O, D) profile for A) Ice Wedge #6 (IW6, N=13); and B) Ice Wedge #8 (IW8, N=24). δD vs. $\delta^{18}O$ plot for C) IW6; and D) IW8. GMWL is the Global Meteoric Water Line (δD= 8 $\delta^{18}O$+10), and LMWL is Inuvik's Local Meteoric Water Line (δD= 7.3 $\delta^{18}O$-3.5).

It is often assumed that when an ice wedge cracks, it does so in the middle of the wedge, as so often expressed in visual representations of ice wedge growth. Accordingly, each half of an ice wedge should in theory produce mirror images in stable isotope profiles from the centre outwards on either side. However, this does not appear to be the case as seen in the stable horizontal profiles for all of the Holocene ice wedges (IW1 & 3, Figure 33A and B; IW6 & 8, Figure 34A and B). It should be first mentioned, that during extraction of samples from each of the ice wedges, the intention of sample extraction was to sample across the entire diameter of the ice wedge to determine if there was in fact a trend. However, while this was the intention, it is impossible to know for certain whether the horizontal transect was in fact through the center of the ice wedge, or if it may have occurred off-center, without completely digging out the material surrounding the ice wedge. With this being accounted for, the following analysis was concluded based on the assumption that the horizontal transect was a representation of the diameter of the ice wedge. In the case for each of the ice wedges (Figure 33A and B; IW6 & 8, Figure 34A and B), there is no apparent trend across the horizontal extent of the ice wedge, with large flunctuations in $\delta^{18}O$ values. One ice wedge, IW8, does show somewhat of a trend, with $\delta^{18}O$ decreasing from the exterior (youngest) towards the interior (oldest). However, despite this lack of trend, according to Michel (1982) horizontal isotope profiles are useful in indicating that change in $\delta^{18}O$ over shorter periods of time, and therefore can be used to look at variations in temperature over time, and can be used in conjunction with radiocarbon dates for determination of a climate at a specific time.

On a δD vs. $\delta^{18}O$ plot, ice wedge IW1was the only ice wedge to plot (Figure 33C) near the LMWL ($\delta D = 7.3\ O^{18}\delta - 3.5$) with of slope of $\delta D = 6.64\ O^{18}\delta - 42.47$ ($r^2 = 0.699$), slightly below the LMWL, while ice wedge IW6 plotted (Figure 34C) further below the LWML with a regression of $\delta D = 5.778\ O^{18}\delta - 63.32$ ($r^2 = 0.652$). Both regressions showed statistical correlation with r-values above 0.65. These results would suggest that ice wedge IW1 was formed from precipitation as it was close to the LMWL, while ice wedge IW6 could potentially have been a mixture of precipitation and water refreezing that would drop the slope below the LMWL. On the other hand, regressions for ice wedges IW3 and IW8 plotted well below the LWML (Figure 33D and Figure 34D), with the regression for ice wedge IW8 generating a negative slope. However these regressions showed little or no statistical correlation ($r^2 < 0.3$), and therefore the regressions are not representation of the data. As a result, it is not possible to determine the source of water

for the formation of these ice wedges, however, they were likely either filled by precipitation or re-freezing of meltwater.

4.2.3. Pleistocene Ice Wedges

As mentioned earlier, $\delta^{18}O$ values of Pleistocene aged ice wedges were 2-6‰ lower than those of Holocene age. Ice wedge IW2 produced the most depleted $\delta^{18}O$ values seen in all of the ice wedges, with values between -31 to -26.2‰ (Figure 35A), showing significant variability and no trend in $\delta^{18}O$ across the horizontal extent of the ice wedge. These values are similar to those obtained by Kotler & Burn (2000) from nearby Mayo, where ice-rich loess deposits from the Late Wisconsinan indicative of full-glacial conditions returned $\delta^{18}O$ values between -32 to -29‰. $\delta^{18}O$ values in ice wedge IW2 were on average more depleted than those seen in the surrounding Ice/Till layer, with values up to -4‰ more depleted in $\delta^{18}O$. The second ice wedge of Pleistocene age, ice wedge IW7 (Figure 35B), displayed $\delta^{18}O$ values that were 2‰ more enriched than those seen ice wedge IW2 with an average $\delta^{18}O$ of -26.4‰, but still depleted relative to $\delta^{18}O$ values seen Holocene ice wedges. On a δD vs. $\delta^{18}O$ plot, ice wedge IW2 produced a regression well below the LMWL (Figure 35C) suggestive of the refreezing of meltwater, while ice wedge IW7 was slightly below the LMWL (Figure 35D) potentially on a mixture of precipitation and refreezing of meltwater.

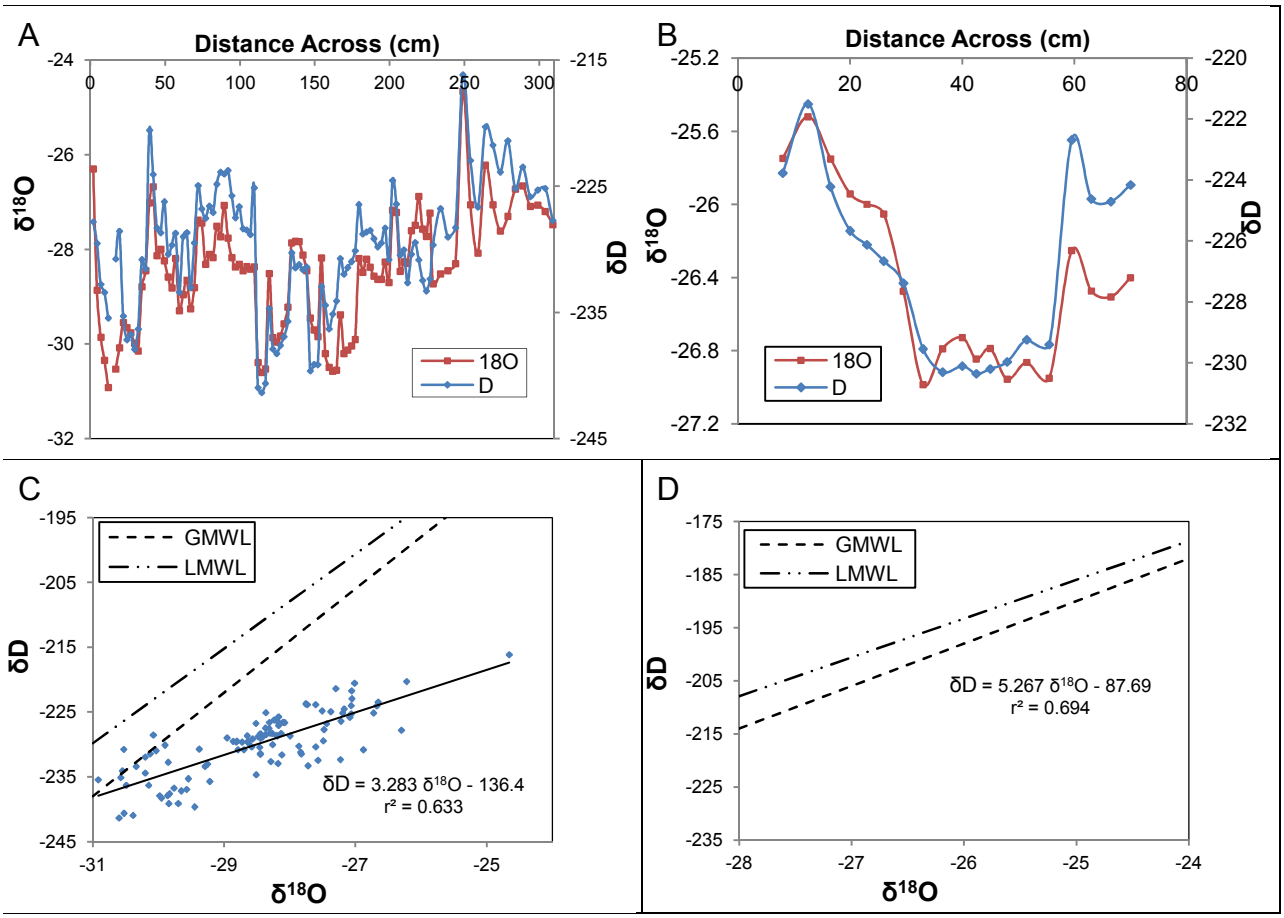

Figure 35. Horizontal stable O-H isotope profile for A) Ice Wedge #2 (IW2, N=108); and B) Ice Wedge #7 (IW7, N=19). δD vs. $\delta^{18}O$ plot for C) IW1; and D) IW2. GMWL represents the Global Meteoric Water Line (δD= 8 $\delta^{18}O$+10), and LMWL represents Inuvik's Local Meteoric Water Line (δD= 7.3 $\delta^{18}O$-3.5).

4.3. Radiocarbon (^{14}C)

Radiocarbon analysis on ice wedges using Dissolved Inorganic Carbon (DIC) and Dissolved Organic Carbon (DOC) as the carbon source is a recent method, with conventional methods often using allochthonous particulate organic carbon (POC) material as the carbon source. However, using POC trapped within ice as the dating material can be problematic. In periglacial processes, carbon is often recycled through cryogenic processes by which carbon that was previously trapped within ice is released (during melting) and can be refrozen in to newly formed ice. As such, this 'old' carbon acts essentially as recycled carbon, and in doing so, can result in older ages of the formation of the ice being determined than what is actually the case. Using DIC and DOC reduces the potential of contamination by "old" carbon, and has been shown to produce younger ages that may be more representative of the age of formation (Lachniet et al., 2012). Furthermore, upon visual inspection and melting of ice from the ice

wedges at Two Moose Lake, there did not appear to be any visible POC in the form of branches, twigs or roots available for radiocarbon dating, thus it was decided that radiocarbon dating by DIC and DOC would be appropriate. The use of DIC and DOC offers a unique opportunity to compare ages obtained in this study to ages in other studies that have used POC as the dating material.

In this paper, it was decided to focus on DOC as the radiocarbon material instead of DIC, although 8 samples using DIC as the radiocarbon material were analyzed for comparison. The main reason for using DOC as opposed to DIC was that, while DIC may become trapped in the ice, there is the possibility of exchange/absorption of CO_2 with DIC into the ice/water years after the formation of the ice, and therefore may represent more modern carbon than at the time of formation producing a radiocarbon age younger than the actual ice wedge. However, Lachniet et al. (2012) suggested it may be used to place an age constraint on the ice wedge, giving the youngest possible age (DIC) relative to the oldest possible age (DOC). Secondly, there is the possibility for the production of secondary DIC due to decomposition and respiration, thus potentially altering the composition of the DIC to give an ice that is not represented of the age of the formation of ice. Lastly, the possibility for exchange with current atmospheric CO_2 during melting, albeit minimal, can alter the age of the DIC if it the carbon that is found within the ice is much older.

In total 7 ice wedges were sampled for radiocarbon dating (Table 7). In some cases, only a single sample was extracted for radiocarbon analysis to determine a single point-source age (Ice wedges IW1 and IW4), while others had two or more extracted in order to attempt to determine the chronology of the formation of the ice wedge (i.e. maximum and minimum age of formation).

Upon analysis of radiocarbon results, two periods of ice wedge formation at Two Moose Lake took place, most recently during the middle to late Holocene and a previous period of activity during the late Pleistocene. Thus it was based on the ages from radiocarbon analysis that the ice wedges were differentiated in to the two types of ice wedges: Holocene and Pleistocene ice wedges. The most recent period of ice wedge growth during the Holocene, from which a total of 4 were analyzed for radiocarbon dating, ranged in age from as old as 6,361 years cal BP, to as young as 893 years cal BP (Table 7). The largest of the ice wedges, ice wedge IW8, was found to be the oldest of the Holocene ice wedges, producing DOC-^{14}C ages of 6,361 and 6,295 years cal

BP (DIC-^{14}C age of 5,629 years cal BP), and a minimum age of 2,481 years cal BP. Overlapping the period of growth of ice wedge IW8, ice wedge IW3 returned a maximum DOC-^{14}C age of 3,985 years cal BP, an intermediate age of 2,753 years cal BP, and a minimum ages of 1,631 and 1,530 years cal BP. While only a single DIC-^{14}C value of 1,658 cal years BP was obtained for ice wedge IW1, based on suggestions from Lachniet et al. (2012), it is likely that ice wedge IW1 was initiated prior to this date as using DIC as the dating material has been shown to produce a younger radiocarbon age of formation of the ice than what would be obtained using DOC-^{14}C. The youngest and smallest (in width) of the ice wedges, ice wedge IW6, has a relative recent age of formation, with a maximum age of 1,720 years cal BP and a most recent date of 893 years cal BP. As such, and expected by ice wedge size, ice wedge IW8 experienced the longest period of formation, spanning just under 5000 years, followed by ice wedge IW3 at 2500 years and ice wedge IW6 at just under 1000 years. While there is no continuous age record (there is often a 1,000 years of more between radiocarbon dates for each ice wedge), the fact that ice and ice veins occur between the sampling points would suggest that favourable conditions for ice wedge growth would have occurred between these dates.

The oldest period of ice wedge formation at Two Moose Lake occurred during the Late Pleistocene. These ice wedges were found in the I/T layer (lower extent of the outcrop), where they had grown in to after its (I/T layer) deposition, and were later truncated by an erosional event and covered by a Silt layer. Ice wedges from this period of formation (3 ice wedges were sampled) ranged from as young as 12,990 years cal BP, to as old as 31,400 years cal BP (Table 7). The oldest of the exposed ice wedges, IW7 produced maximum ^{14}C-DOC ages of 31,608 and 31,192 years cal BP (duplicate from the same sample) and a minimum ^{14}C-DOC age of 13,686 years cal BP. ^{14}C-DIC ages of 22,560 and 13,501 years cal BP respectively were also determined for ice wedge IW7. The oldest of the ice wedge IW7 samples were also analyzed using a glass filter as opposed to a nitrocellulose filter, whereby a ^{14}C-DOC age of 29,617 years cal BP and a ^{14}C-DIC age of 24,134 years cal BP were obtained when a glass filter was used. The ^{14}C-DOC from the glass filter produced a younger age than the nitrocellulose filter while the ^{14}C-DIC that was obtained was younger. A single radiocarbon sample from IW4 returned ^{14}C-DOC and ^{14}C-DIC ages of 22,368 and 21,636 years cal BP respectively. The youngest of the Pleistocene ice wedges, IW2, returned a ^{14}C-DOC age of 12,990 years cal BP and a Holocene age for the ^{14}C-

DIC (7,889 years cal BP), however, the certainty of these values, specifically the ^{14}C-DIC value, is somewhat problematic as they were analyzed over a year after extraction and melting and there is the possibility of atmospheric and bacterial contamination.

Table 7. Summary of Radiocarbon results completed on DIC and DOC samples from various ice wedges.

Sample ID	Carbon Source	Lab ID[a]	Orientation in Ice Wedge[b]	Filter Type[c]	Uncalibrated ^{14}C age (yr BP)[a]	Calibrated ^{14}C age (yr cal BP)[d] Oldest Age	Youngest Age	Median Age	Epoch
Ice Wedge #1									
13-MG-IW1-2	DIC	UOC-0137	Middle	C	1749	1715	1604	1658	Holocene
Ice Wedge #2									
13-MG-IW2-1	DOC	UOC-0141	Left Side	G	11137	13104	12826	12990	Pleistocene
13-MG-IW2-3	DIC	UOC-0143	Center	C	7047	7950	7831	7889	Holocene
Ice Wedge #3									
14-MG-C-10	DOC	UOC-0129	Left Side	C	3656	4090	3868	3985	Holocene
14-MG-C-11-1/2	DIC	UOC-0130	Middle	C	4777	5588	5471	5520	Holocene
14-MG-C-11-1	DOC	UOC-0131	Middle	C	2623	2845	2713	2753	Holocene
14-MG-C-12	DOC	UOC-0133	Right Side	C	1640	1619	1413	1530	Holocene
14-MG-C-12-Dup	DOC	UOC-0121	Right Side	C	1707	1694	1557	1613	Holocene
Ice Wedge #4									
14-MG-C-13	DOC	UOC-0134	Center	C	18498	22572	22134	22368	Pleistocene
14-MG-C-13	DIC	UOC-0144	Center	C	17852	21825	21444	21636	Pleistocene
Ice Wedge #6									
14-MG-C-4	DOC	UOC-0118	Left Side	C	1793	1813	1628	1720	Holocene
14-MG-C-5	DOC	UOC-0119	Middle	C	1236	1263	1074	1179	Holocene
14-MG-C-6	DOC	UOC-0120	Center	C	983	936	800	893	Holocene
Ice Wedge #7									
14-MG-C-8	DOC	UOC-0122	Left Side	C	27914	31938	31316	31608	Pleistocene
14-MG-C-8	DIC	UOC-0123	Left Side	C	18692	22785	22377	22560	Pleistocene
14-MG-C-8-Dup	DOC	UOC-0124	Left Side	C	27285	31392	30997	31192	Pleistocene
14-MG-C-8-3-G	DIC	UOC-0125	Left Side	G	20069	24334	23932	24134	Pleistocene
14-MG-C-8-3-G	DOC	UOC-0126	Left Side	G	25506	30041	29255	29617	Pleistocene
14-MG-C-9-1	DIC	UOC-0127	Right Side	C	11668	13570	13434	13501	Pleistocene
14-MG-C-9-1/2	DOC	UOC-0128	Right Side	C	11882	13819	13553	13686	Pleistocene
Ice Wedge #8									
14-MG-C-1	DOC	UOC-0114	Right Side	C	2410	2700	2347	2481	Holocene
14-MG-C-3	DOC	UOC-0116	Center	C	5579	6437	6295	6361	Holocene
14-MG-C-3-Dup	DOC	UOC-0117	Center	C	5496	6390	6217	6295	Holocene

[a]Sample ID and results obtained from the the Andre E. Lalonde Radiocarbon Laboratory, University of Ottawa, Canada.
[b]Horizontal location in which the sample was removed from the Ice wedge. Middle refers to the sample between the exterior and center samples.
[c]Filter type. "C" denotes 0.45um nitrocellulose filters that were pre-washed as per the methods. "G" denotes 0.7um glass filters treated as per the methods.
[d]Ages were calibrated using OxCal 4.2 and IntCal13 (Bronk Ramsey, 2013; Reimer et al., 2013) to calendar years Before Present (Present=AD 1950) and reported as median ages with two sigma uncertainty and age ranges (Youngest and Oldest) to a 95.4% confidence interval.

5. Discussion

5.1. Cyrostratigraphy and Sedimentary History

At Two Moose lake four distinct layers were exposed in the outcrop along with two distinct sets of ice wedges. The timing and sequence of the various layers and ice wedges play an important role in the understanding of the sedimentation history and formation of the outcrop. This sequence is also fundamental in reconstructing the paleoclimate and sedimentary history of the region. As radiocarbon samples were only obtained for ice wedges, the sedimentary and ice wedge formation history is based on a age constraints of ice wedges and structural characteristics to infer the sequence of events at Two Moose Lake.

The lowest exposed layer (Unit 4) in the outcrop, the I/T layer, was the first to form at Two Moose Lake. Deposition of this layer, composed of ice-rich sediment with a heterogeneous mixture in grain sizes, occurred prior to 31.6ka cal BP and prior to the formation of the Pleistocene ice wedges within the layer as well as the Holocene ice wedges that extend from the surface and cross-cut through it. Multiple lines of evidence support this notion including GWC, stable isotopes and structure. The Gravimetric Water Content (GWC) of the I/T layer was between 17.43 to 66.10%, ca. 40 times lower than values obtained for ice wedges. Stable isotope values ($\delta^{18}O$ and $\delta^{2}H$) for the I/T layer were also different than those of the ice wedges. $\delta^{18}O$ values within the I/T layer became less enriched with a decrease depth from -27‰ at the base to -22‰ at the top. Meanwhile, $\delta^{18}O$ values in the Pleistocene ice wedges were much more depleted, with average $\delta^{18}O$ values of -26.42‰ in ice wedge IW7 and -28.51‰ in ice wedge IW2. Regressions generated from a δD vs. $\delta^{18}O$ plot were also different between the I/T layer and the ice wedges suggesting a different origin of formation. The water line generated for the I/T layer, $\delta D = 7.351\ O^{18}\delta - 16.37$, was nearly identical to the LMWL ($\delta D = 7.3\ O^{18}\delta - 3.5$), suggesting the I/T layer was likely formed from precipitation. On the other hand, the water lines for the ice wedges plotted much lower, suggesting they formed for the melting and re-freezing of water. Similarly, the d-excess, had the ice wedges and I/T formed at the same time, would have generated similar values. This is not the case, as D-excess values for the I/T layer varied around 0±3‰, while those of the ice wedges ranged between -12 to -17‰, suggesting different conditions and sources of water. Evidence suggesting the deposition of the I/T layer prior to the formation of the ice wedges is supported by the tilting of the ice in the I/T layer in contact with

the ice wedges (Figure 36) that would only have occurred had the ice been in place prior to the growth of the ice wedge (epigenetic formation). These lines of evidence suggest that 1) the I/T layer and ice wedges formed at different times and; 2) the I/T layer formed prior to ice wedge growth, and therefore can be assumed to have formed prior to 31.4ka cal BP (max age obtained from the Pleistocene ice wedges).

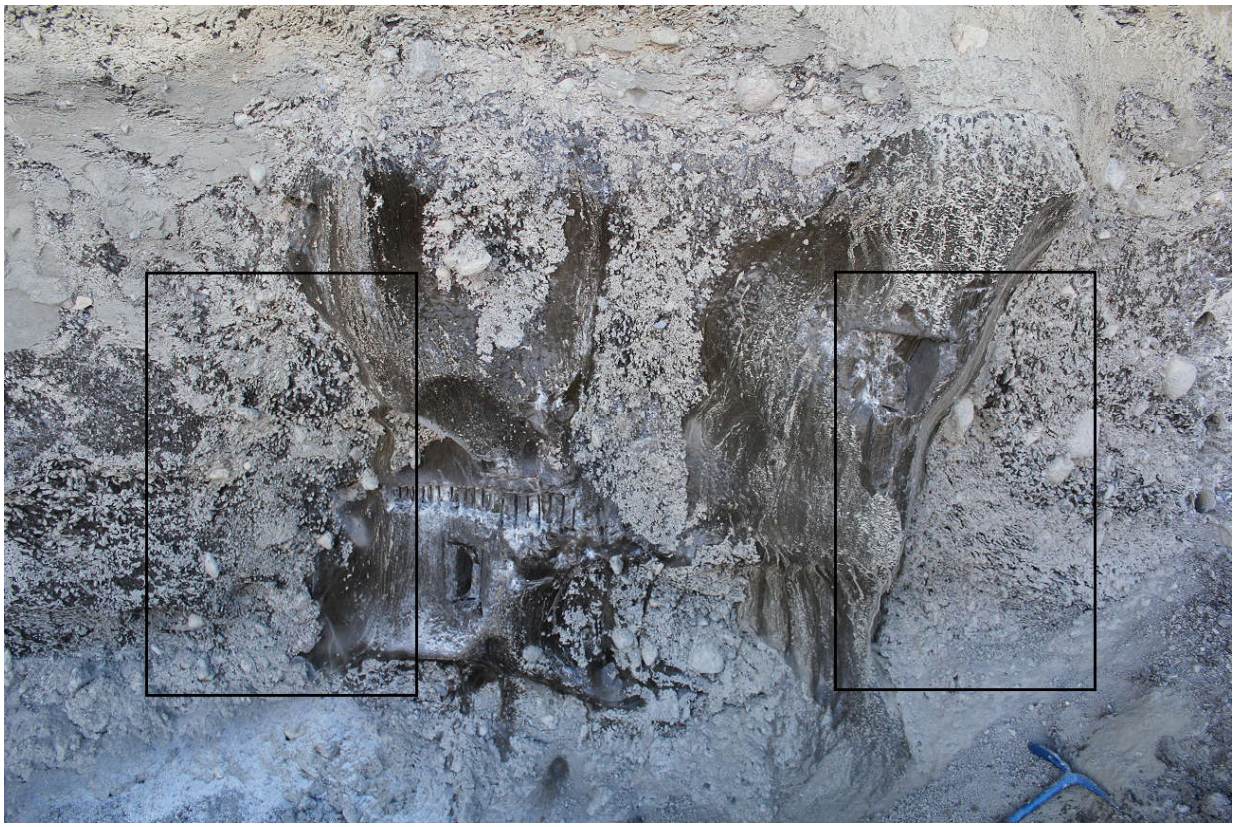

Figure 36. Tilting of ice and sediments in the I/T layer in contact with Pleistocene ice wedge IW7. The tilting of the sediments and ice is highlighted within the black boxes. Tilting angles of up to 45° were visually calculated.

Following the deposition of the I/T layer, it is possible there was a period of accumulation of sediment on top of the I/T layer, however no evidence of this material remains as an unconformity exists between the I/T layer and the silt layer (Unit 3) found above. The only evidence of activity that exists prior to the deposition of the silt layer occurs through the presence of ice wedges. Ice wedge initiation and growth (ice wedges IW2, IW4 and IW7) was shown to have occurred at Two Moose Lake over a period of ca. 20ka years from 31.6ka to 13ka cal BP, as determined by multiple radiocarbon dates obtained from the 3 Pleistocene ice wedges. Formation of these ice wedges occurred prior to the deposition of the silt layer as the tops of ice wedges were truncated at the same height as the unconformity seen for I/T layer, and therefore

were likely subject to the same erosional event. The erosional process leading to this unconformity at Two Moose Lake was not evident, however it is unlikely to have been caused by a glacier as the youngest date obtained from the Pleistocene ice wedges (ca. 13ka cal BP) coincides with the beginning of the Holocene Thermal Maximum (HTM) (Clark et al., 2004, Kaufman et al., 2004, McBean et al., 2005, Viau et al., 2008) during which major recession of the glaciers occurred. As such, it is likely that this erosional surface could have been caused by the expansion of the Blackstone river, presently located ca. 200m east of Two Moose Lake, due to an increase in meltwater from the melting of glaciers (montane and ice sheets) surrounding the region.

Following the erosional event at Two Moose Lake, the deposition of the upper three layers (Units 3, 2 & 1) took place (<13ka cal BP), although the accumulation of some of the Active Layer (Unit 1) likely still occurs. The first in the sequence to occur was the deposition of the silt layer (Unit 3). The deposition of the silt layer after Pleistocene ice wedge growth and deposition of the I/T layer is supported by the erosional contact. Stable isotope data indicates a sudden depletion in $\delta^{18}O$ from -22‰ at the upper portion of the I/T layer to -24‰ at the bottom of the silt layer. Furthermore, stable isotope values for the Pleistocene ice wedges were significantly more depleted, by up to 2-5‰ relative to the silt layer. This is as to be expected as the silt layer was likely deposited during the HTM, when temperatures were up to 5°C warmer today, and supported by the increasing enrichment of the $\delta^{18}O$ of the silt layer from -24‰ at the lower contact to -22‰ at the upper contact. Kotler & Burn (2000) also determined from studies at nearby Mayo, that the end of the McConnel Glaciation (~12ka BP) was a period of intense geomorphic activity with the removal of silt, sand and organic matter from valley sides by glacial meltwater, and their eventual deposition in valleys.

The transition from the deposition of silt to silt with organics and silty loam (Unit 2) likely occurred continuously, where the only reasoning for the separation of the two units was based on the visual appearance of organic matters within unit 2 that was otherwise not seen in the silt. Organic matter within the silt layer comprised less than 3% weight, slowly increasing through the silt loam w/ organics layer from 5% to 12%. The increase in organic matter over deposition indicates a change in climate whereby conditions favourable to the growth of vegetation were present. The amelioration of climate conditions along with the continuous

deposition of units 2 and 3 can be seen in the stable isotope profile as $\delta^{18}O$ increases in a smooth and consistent manor from -24‰ at the bottom of the silt layer to -20.5‰ at the top of the silt with organics layer. The deposition of these 3 layers was likely to have occurred prior to the formation of the Holocene ice wedges, from 13.6ka to ca. 6.3ka cal BP when the oldest age was obtained from Ice wedge IW8.

The second to last features to form at Two Moose Lake were the Holocene ice wedges. Holocene ice wedge activity occurred from 6.3ka cal BP to 0.89 ka cal BP. While all of the Holocene ice wedges penetrated down to I/T layer from the surface, their initiation and growth was likely to have occurred after the deposition of all of the units at Two Moose Lake starting at 6.3ka BP. The grain size distribution was similar amongst the various ice wedges and the upper 3 sedimentary units, however, stable isotope values and the physical characteristics of the ice wedges and surrounding sediments suggest deposition after the upper 3 sedimentary units. Holocene ice wedges were on average, 2 to 3‰ more depleted in $\delta^{18}O$ than values obtained from the upper 3 sedimentary units, and had the ice wedges formed con-currently with the sediments, stable isotope values should have seen similar values. Furthermore, the sediments in contact with the sides of the Holocene ice wedges were tilted upwards (relative to their original position in the layer) by as much as much as 45°, similar to what was seen in the I/T layer by the Pleistocene ice wedges (Figure 36). Tilting of the layers occurs as a result of the horizontal expansion of the ice wedge during freezing of melt water in the crack, and would only occur if sediments/layers had already been in place prior to ice wedge expansion. Although the last obtained radiocarbon date from an ice wedge was 0.89ka BP, it is possible that ice wedge activity continued after this date.

The last event to occur was the exposure of this outcrop at Two Moose Lake that made this study possible. The outcrop was exposed as a result of a thaw slump along the edge of the lake. The frequency of thaw slumps has been increasing across the arctic with increasing temperatures, and as temperatures continue to rise, the number of these ice-rich outcrops is likely to increase (Lacelle et al., 2010). However, as of May 2015, the recession of the headwall appears to have stabilized and vegetation re-growth has begun on slumped material. In summary, the sequence and timing of the formation of the outcrop at Two Moose Lake is as follows:

Order	Time (yr cal BP)	Event
1.	> 31,608	Deposition of I/T Layer.
2.	31,608 to 12,990	Formation and Growth of Pleistocene aged ice wedges
3.	Between 2 &4	Erosional event.
4.	<12,990 to 6,298	Deposition of Units 3, 2 and 1.
5.	6,298 to 893	Formation and Growth of Holocene aged ice wedges.
6.	<893	Potential ice wedge growth/activity and Active layer accumulation.
7.	>2007 AD	Exposure of outcrop through thaw slumping.

5.2. Radiocarbon dates

5.2.1. Implications for Glaciation

Climate conditions during the late Pleistocene, beginning with the initiation of the Wisconsinan glaciation (ca. 107ka BP) until the onset of the McConnell Glaciation (MIS-2, ca. 29ka BP), were such that much of North America was covered in ice sheets over 1000m thick, while at the same time, parts of Yukon and Alaska remained unglaciated. Furthermore, temperatures in the central Yukon were as much as 5°C lower, along with drier conditions than present (Lacelle et al., 2009). At Two Moose Lake, multiple ice wedges of various ages were exposed. The presence of these ice wedges suggests of a MAAT below -4°C, as well as extreme cold temperatures (<-20°C) during the winter for the initiation of ground/ice wedge cracking to occur. Furthermore, the formation of ice wedges requires exposed ground, and thus can be used as an indication of ice-free conditions.

At Two Moose Lake multiple ice wedges were exposed at various depths, suggestive of multiple periods of ice wedge formation as well as changes in sedimention and climate. The presence of these ice wedges would indicate that the surrounding region was ice-free in order for them to form. These ice wedges were dated using radiocarbon dating. In some cases, only a single radiocarbon sample was obtained from an ice wedge, while other ice wedges had multiple radiocarbon samples that were extracted horizontally across an ice wedge to study the

age of formation and duration of the ice wedges. It should be noted that these ages, being the oldest (minimum) and youngest (maximum) ages obtained across a horizontal extent of an ice wedge, may not necessarily represent the initiation and termination of ice wedge growth, however, they can be used as age constraints to indicate ice wedge activity and therefore climate conditions favourable for ice wedges (i.e. MAAT <-4°C, ice-free). Furthermore, in some cases there are large gaps in age/time between the oldest and youngest radiocarbon ages. The time between these DOC-^{14}C ages within an ice wedge does not necessarily indicate that the ice wedge was inactive, or conversely, active, or that the area remained ice-free during that period as re-initiation of an ice wedge is possible.

The oldest of the ice wedges, IW7, produced a ^{14}C-DOC radiocarbon dated age of 31.4ka cal BP (±300 years) from the lower left portion of the ice wedge (Table 8, Figure 37). The formation of ice wedge IW7 at Two Moose Lake could only have occurred had the ground surface been exposed in order for conditions for cracking to have occured, and `as such, it's presence would indicate that the region around Two Moose Lake was unglaciated at this time. An additional sample from ice IW7 produced a ^{14}C-DOC age of 29.6ka cal BP. The last age produced by ice wedge IW7, located in the middle of the ice wedge, returned a ^{14}C-DOC age of 13.7ka cal BP. ^{14}C-DIC ages were also obtained for the same samples used for ^{14}C-DOC from ice wedge IW7, with respective ages of 22.6ka and 13.5ka years BP. Both DIC ages were younger than their corresponding DOC ages, but can be used as minimum age constraints. The possibility for the continued growth of ice wedge IW7 between 29.6ka cal BP and 13.7ka cal BP is supported by a ^{14}C-DOC age of 22.4ka cal BP returned from a single sample from Ice Wedge IW4. Additional ^{14}C-DOC and ^{14}C-DIC ages were obtained from ice wedge IW2, with ages of 12.9ka and 7.9ka cal BP respectively. The validity of these results are in question however, as other samples from the ice wedge produced ages younger than the Holocene ice wedges despite occurring below them, as well as being buried below ca. 2m of sediment. With these results in mind, there appears to be a period of ice wedge activity (supported by 3 different ice wedges) beginning ca. 31.4ka cal BP and terminating ca. 13ka cal BP (Figure 37). While the activity may not have been continuous, the presence and activity of these ice wedges would indicate that during this period of this time, the region surrounding Two Moose Lake would have been ice-free in order for ice wedge formation to occur. Furthermore, the extremely negative d-excess values of ca. -10‰, and as low as -18‰, would suggest that conditions at

time of formation of the ice wedges were cold and dry, approaching those seen in modern day coastal Antarctica (Raffi & Steffi, 2011). Such dry and cold and dry conditions would not have been conducive to the formation of glaciers.

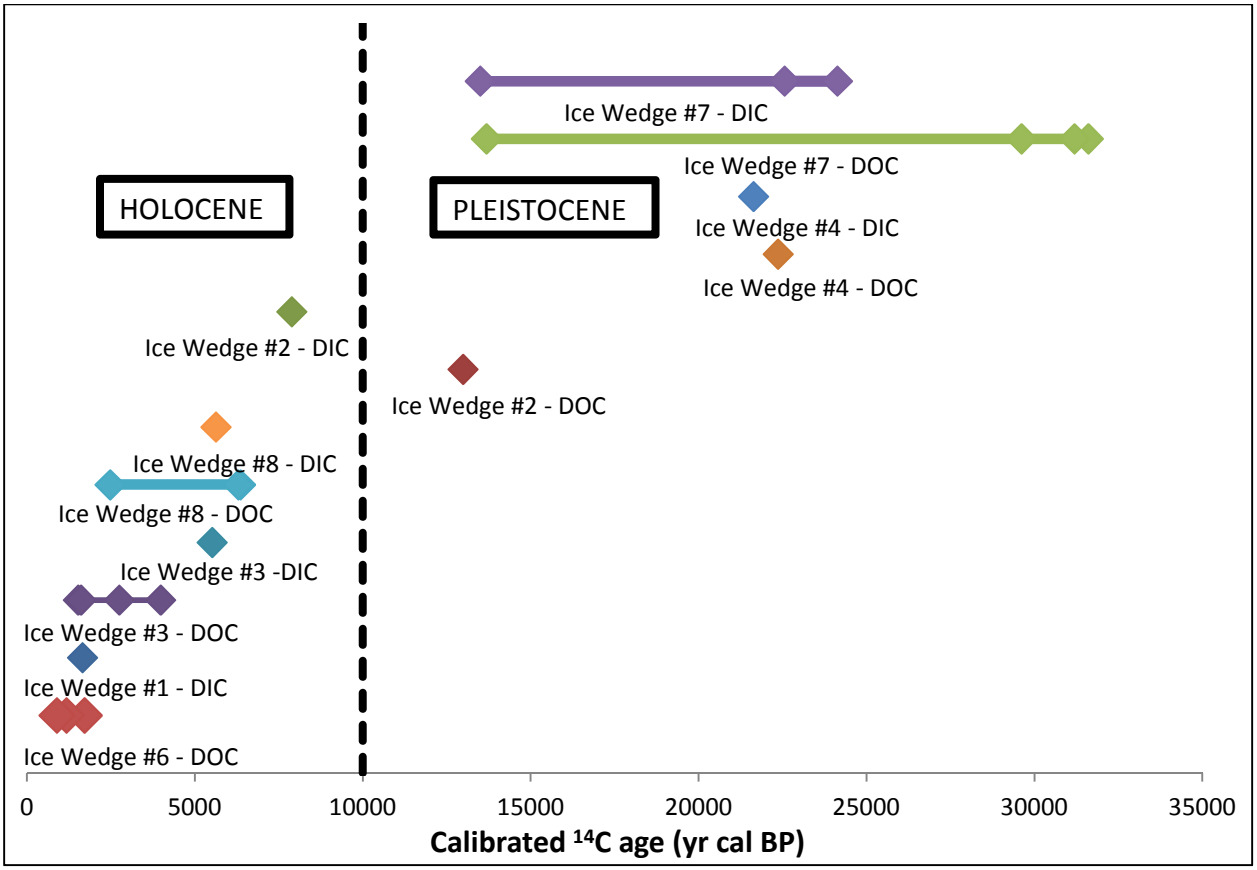

Figure 37. Comparison of calibrated ^{14}C ages (yr cal BP) obtained for the various Ice wedges found at Two Moose Lake, Yukon, Canada. Radiocarbon ages obtained from samples are indicated by points, while lines connecting points indicate possible time periods of activity/existence of an Ice Wedge. Dissolved Organic Carbon (DOC) and Dissolved Inorganic Carbon (DIC) were separated for each of the ice wedges as indicated by the labels in the figure. A vertical line (hashed) was used to indicate the separation between the Pleistocene and Holocene at 10,000 years BP.

Table 8. ^{14}C-DOC and ^{14}C-DIC dates for various Ice Wedges at Two Moose Lake, Yukon.

			0.45um Nitro-cellulose Filter						0.70um Glass Filter	
			DOC			DIC			DOC	DIC
	δD	$\delta^{18}O$	Age[a]	Max	Min	Age[a]	Max	Min	Age[a]	Age
IW1	-193.53	-22.72	—	—	—	1658	—	—	—	—
IW2	-230.01	-28.51	12990	—	—	7889	—	—	12990	—
IW3	-201.55	-23.82	—	3985	1572	5520	—	—	—	—
IW4	-228.20	-28.34	22368	—	—	21636	—	—	—	—
IW6	-195.91	-23.12	—	1720	893	—	—	—	—	—
IW7	-226.87	-26.42	—	31400	13686	18031	22560	13501	29617	24134
IW8	-201.01	-25.57	—	6328	2481	5629	—	—	—	—

[a]Age was used when a single radiocarbon sample was taken and analyzed.
[b]Max and min ages reflect the oldest and youngest ages obtained for an Ice Wedge. NOTE: In some cases additional samples were taken with ages between the max and min age displayed.

5.2.2. Post-Glaciation Implications: Conditions favourable for Ice Wedge activity

Between ca. 13ka cal BP (Ice wedge IW2) until ca. 6.3ka cal BP there is no record of ice wedge activity in the outcrop at Two Moose Lake. An unconformity exists between the I/T layer and Silt layer above, however any ice wedge activity is highly unlikely to have occurred as this period, known as the Holocene Thermal Maximum, experienced temperatures up to 7°C warmer than present. Ice wedge activity at Two Moose Lake re-initiated at least ca. 6.3ka cal BP with a ^{14}C-DOC date obtained from the edge of Ice wedge IW8 (Table 8, Figure 38). An additional ^{14}C-DOC age of 2.5ka cal BP was obtained for the middle of the ice wedge. While no age was obtained between the two dates, it is likely ice-wedge activity occurred, at least sporadically, between 6.3ka and 2.5ka cal BP as there was ca. 0.7m of ice between the two samples, and therefore conditions for ice wedge growth were likely present. The suggestion that conditions were present for ice wedge activity were present between the two dates obtained for ice wedge IW8 is supported by a ^{14}C-DOC age of 3.99ka cal BP obtained for Ice wedge IW3, occurring between the dates obtained for ice wedge IW8. Further ^{14}C-DOC dates of 2.75ka and 1.57ka cal BP were obtained moving across the extent of ice wedge IW3. Similar to ice wedge IW8, there was ~0.5m of ice between samples, and therefore conditions favourable for ice wedge growth. The youngest (and smallest) of the ice wedges, ice wedge IW6 produced ^{14}C-DOC ages of 1.72ka, 1.18ka and 0.89ka (from outside to center) cal BP. With these overlapping dates of multiple different ice wedges in mind, it can be shown that ice wedge activity at Two Moose Lake has been consistently occurring from 6.3ka to 0.89ka cal BP (Figure 38), and may still be continuing to present. The continued activity of these ice wedges during this period would suggest that on average, conditions were such that the climate was present in order to support ice wedges (i.e. MAAT <-4°) as well as for the continued growth of ice wedges (i.e. extreme winter conditions <-20°C).

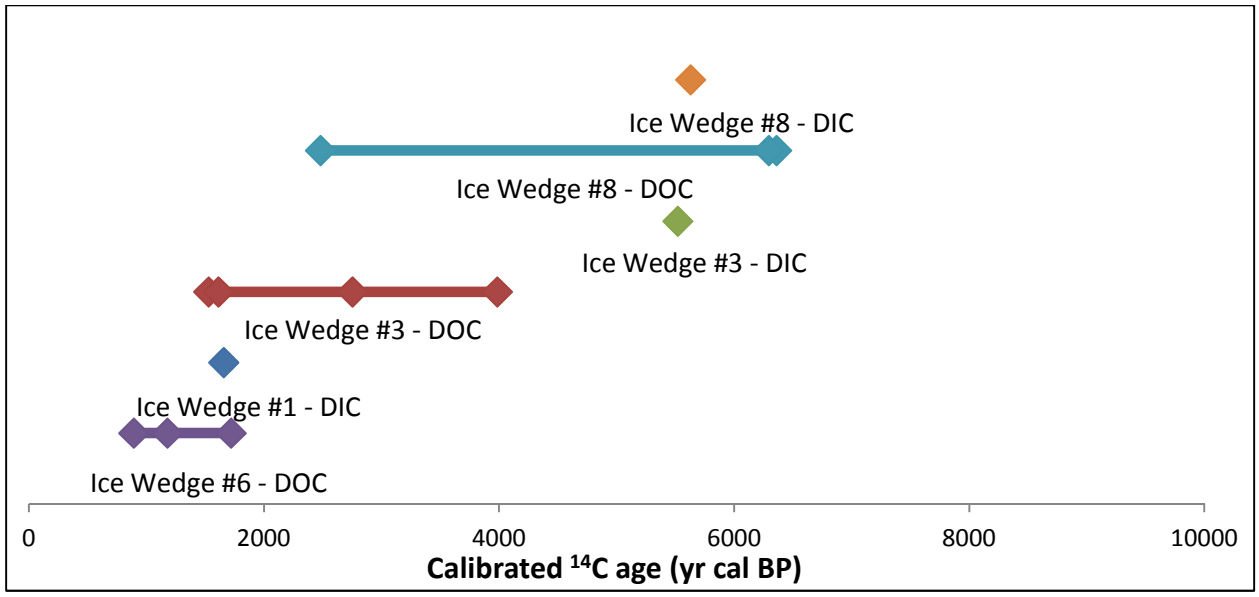

Figure 38. Comparison of calibrated ^{14}C ages (yr cal BP) of Holocene age obtained for the various Ice wedges found at Two Moose Lake, Yukon, Canada. Radiocarbon ages obtained from samples are indicated by points, while lines connecting points indicate possible time periods of activity/existence of an Ice Wedge. Dissolved Organic Carbon (DOC) and Dissolved Inorganic Carbon (DIC) were separated for each of the ice wedges as indicated by the labels in the figure.

5.3. Stable Isotopes: Paleotemperatures and Ice Wedge Infilling

Stable isotopes of ice and wedge ice can provide many clues about the method of formation, source of water, as well as the winter temperatures at the time of formation. In general, it has been commonly accepted in North America that the $\delta^{18}O$ seen in ice wedges is often a reflection of the winter precipitation, which is often depleted in $\delta^{18}O$ compared to the average annual $\delta^{18}O$ for precipitation. Furthermore, during snowmelt in the spring, the meltwater that infiltrates the ice wedge crack is enriched in $\delta^{18}O$ relative to the remaining snowpack.

While the $\delta^{18}O$ of ice and wedge ice is often suggestive of winter temperatures, and thus can be used as an indicator of the climate at the time of formation, the values alone with no dates make it difficult to associate the climate and temperatures with a particular time period. In the case where no dates are available, it is possible to correlate the $\delta^{18}O$ values obtained from ice or an ice wedge from one site to $\delta^{18}O$ values obtained from nearby sites with known ages. This method can be used to approximate ages, however, numerous factors can influence trends in isotopic values and may not always be possible to correlate between two sites. Furthermore,

where dates are available, it can be used as a method to compare $\delta^{18}O$ values obtained from similar times periods, or to add on to a time scale with missing $\delta^{18}O$ values.

This study of the ice and ice wedges from Two Moose Lake offered a unique situation where, along with medium-resolution sampling of $\delta^{18}O$ from which winter temperatures could be determined, 23 radiocarbon samples were obtained directly from the same sampling transects as the $\delta^{18}O$ samples. This in turned provided a situation where specific $\delta^{18}O$ values obtained from the ice wedges could be linked to a defined age. Furthermore, as multiple radiocarbon samples were taken along a sampling transect, it allowed for a relative timescale to be developed for the transect, and thus an attempt at creating a continuous $\delta^{18}O$ and temperature record with age associations.

As previously determined, there was a clear distinction between the $\delta^{18}O$ of Holocene (N=4) age ice wedges in comparison to Pleistocene (N=2) age ice wedges, as Pleistocene ice wedges are more depleted in $\delta^{18}O$ (Table 9). $\delta^{18}O$ values in the Holocene ice wedges ranged between -22.29‰ to -26.33‰, with younger (ca. 3000 years and under) ice having $\delta^{18}O$ values between -22‰ to -24‰ (Figure 39, IW1, IW3-left side & IW6) and older ice (3000 to 6300 years) with $\delta^{18}O$ value between -25‰ to -26.5‰ (Figure 39, IW3-right side & IW8). Variations in $\delta^{18}O$ values are linearly related to the temperature, and thus using the equation derived by Dansgaard (1964), the approximate average winter temperature during the formation of the ice wedge can be calculated:

$$\delta 18O = 0.695T \quad 13.6‰ \qquad (11)$$

Table 9. Summary of Isotope Data for the Outcrop and Ice wedges.

		δ18O (‰)			δD (‰)		
Ice Wedge #	Age[c]	Average	Max	Min	Average	Max	Min
IW1[b]	Holocene	-22.72	-22.29	-22.99	-193.53	-190.08	-196.92
IW8[b]	Holocene	-25.59	-25.15	-26.33	-200.99	-197.55	-204.79
IW3[b]	Holocene	-23.94	-22.64	-26.50	-201.54	-196.92	-208.04
IW6[b]	Holocene	-23.12	-22.52	-23.40	-195.91	-191.21	-198.14
IW2[a]	Pleistocene	-28.51	-24.66	-30.92	-230.01	-216.16	-241.34
IW7[b]	Pleistocene	-26.42	-25.52	-26.98	-226.87	-221.50	-230.35

[a]Samples obtained in August 2013.
[b]Samples obtained in April 2014.
[c]Age based on radiocarbon results from this study.

The corresponding winter temperatures transect for the various Holocene ice wedges were calculated using $\delta^{18}O$ values and the formula developed by Dansgaard (1964). Winter temperatures for the various Holocene ice wedges ranged between -12.51°C to -18.56°C (Figure 39). Similar to the $\delta^{18}O$ values, the younger ice wedges returned warmer temperatures, ranging from -12.51°C to -15.24°C (IW1, IW3-left side & IW6), while the older ice wedges experienced temperatures between -16.62°C to -18.53°C (Figure 40, IW3-right side & IW8), a difference between 2 to 3°C. When compared to values from Winter Precipitation and Mayo (Figure 40, horizontal hashed lines), all of the ice wedges produced lower temperatures than current precipitation at Mayo (-12.55°C). On the other hand, Ice wedges IW3-right side and IW8 were the only ice wedges to produce temperatures lower than calculated for Winter Temperatures (-15.06°C).

Based on recent climate data from Dawson in central Yukon, snowfall in the region typically begins by October and over by the beginning of May, with minor overlaps of rainfall in October and April. With this in mind, snow cover can be made up of a mixture of snowfall from the various 'winter' months (October to May), during which temperatures will drop as much as 20°C from the beginning of snowfall (October: MMT of -4.7°C) to midwinter (January: MMT of -26°C), then returning to above freezing temperatures in April, giving an overall average temperature during this period of snowfall of -15.06°C. If the average temperature (-15.06°C) during the period of snowfall is converted to $\delta^{18}O$, an average $\delta^{18}O$ value of -24.07‰ is obtained for this period. This $\delta^{18}O$ value is lower than that of modern precipitation collected from nearby Mayo (-22.32±3.06‰; IAEA/WMO, 2015) however, this is likely due to the data from Mayo being composed of all precipitation, not just snowfall. Modern precipitation at Mayo returned an annual temperature value of -12.55°C.

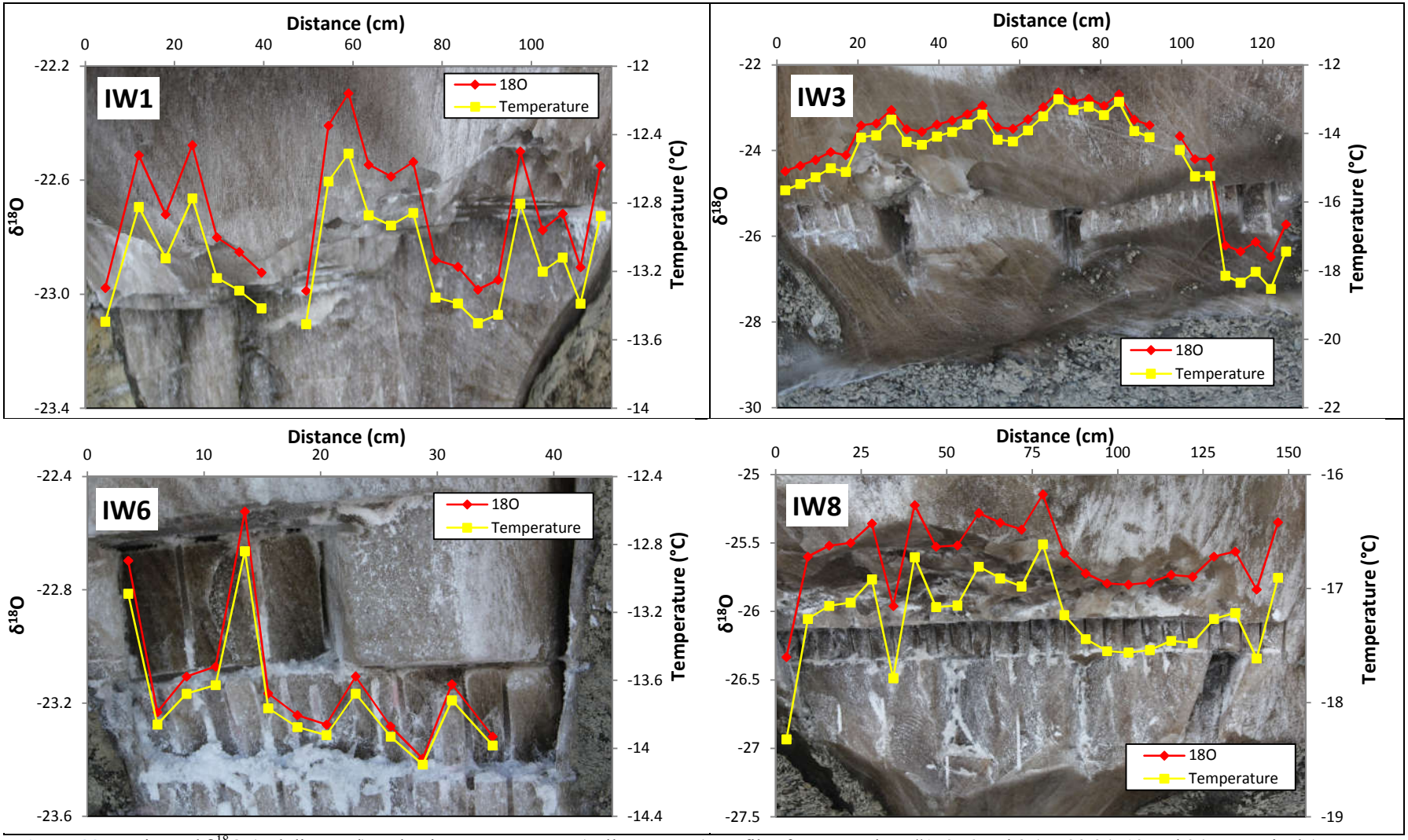

Figure 39. Horizontal $\delta^{18}O$ (red diamond) and Winter temperature (yellow square) profiles for Ice wedges #1, 3, 6 and 8 (N=23,34, 13 and 24 respectively). Winter temperatures were calculated as per the formula described by (Dansgaard, 1964).

The commonly accepted process of ice wedge infilling in North America has been through snow meltwater (Mackay, 1975; Mackay, 1992; Lauriol et al., 1995; Plug and Werner, 2002; Murton, 2013), although some have suggested hoar frost or precipitation as the method of infill (Shumski, 1964; Mackay, 1992; French and Guglielmin, 2000). As many of the ice wedges returned warmer temperatures that what was calculated from current Winter Temperatures at Mayo, this would suggest that perhaps the conclusion that $\delta^{18}O$ values from ice wedges are a reflection of winter temperatures may not be the case, but rather a mix of various sources of precipitation. This case was specifically shown with the younger ice wedges as it has been proposed that the time period from 4.2ka to 2ka BP was up to 1.5°C cooler than present (Kurek et al., 2009; Bunbury and Gajewski, 2008) and therefore, had ice wedge infilling been solely from winter precipitation meltwater, the ice wedges should have returned temperatures much lower than that calculated for current Winter Temperatures for Mayo. Furthermore, the notion of a mixture of various sources (snow meltwater and various forms of precipitation) for the infilling of the ice wedge can be supported by the temperatures obtained for the younger ice wedges falling between those obtained from modern precipitation and calculated winter temperatures for Mayo. $\delta^{18}O$ and δD plots have also been used to infer origin of infilling as well as source of water. Ice wedges IW1($\delta D = 6.64\ \delta^{18}O - 42.1$, $r^2=0.699$) and IW6 produced regressions close to the LMWL of Inuvik ($\delta D = 7.3\ \delta^{18}O - 3.5$) with some statistical correlation, suggesting origin of formation through precipitation, either as snow or rain. On the other hand, ice wedges IW3 ($\delta D = 2.37\ \delta^{18}O - 146.5$, $r^2=0.215$) and IW8 ($\delta D = -2.83\ \delta^{18}O - 273.5$, $r^2=0.129$) produced much lower regressions than that of the LMWL, suggesting an origin of formation from the re-freezing of meltwater. However, the minimal statistical correlation of the regressions for ice wedges IW3 and IW8 would indicate that, despite the lower regression, the source of infill cannot be attributed to re-freezing of meltwater with certainty, and may possibly be a mixture of various sources of infilling. With this in mind, it has been shown that the process and source of infilling is in fact highly variable as indicated by the differences between $\delta^{18}O$/calculated Winter temperature from Mayo and values obtained from the various the ice wedges, along with the various methods of ice wedge infilling indicated by varying regressions with highly variable statistical correlation.

Despite questions regarding the method and source of ice wedge infilling and whether or not $\delta^{18}O$ values are a true reflection of winter temperatures, $\delta^{18}O$ values from ice wedges can

nevertheless still be used in the determination of paleotemperatures. Because this study sampled horizontal transects of $\delta^{18}O$ across multiple ice wedges along with multiple radiocarbon ages across a transect, it was possible to re-create $\delta^{18}O$ and temperature profiles from 6,328 yr cal BP to 893 yr cal BP, a span of ca. 5,500 years (Figure 40). This study appears to be the first attempt to be able to create continuous $\delta^{18}O$ and temperature profiles using multiple radiocarbon dates directly from the sampling transect. The purpose of the creation of these profiles was to attempt to compare $\delta^{18}O$ and radiocarbon ages in literature to those obtained in this study to see if in fact the trends line up.

In each $\delta^{18}O$ sampling transect, between 2 to 3 radiocarbon samples were collected in two fashions, across the entire transect of the ice wedge (ice wedge IW3) and from the edge of the ice wedge to the center (ice wedges IW6 and IW8). Because there were spaces between each of the radiocarbon samples taken, a continuous age profile was created/extrapolated by dividing the difference in age between the two radiocarbon samples by the number of $\delta^{18}O$ samples, and therefore assigning each $\delta^{18}O$ sample a relative age. The creation of these time profiles do take in to account several assumptions:

1) The continuous expansion of the ice wedge at a constant cracking interval (i.e. cracking frequency between radiocarbon samples occurs as the same intervals)

2) The ages obtained are not contaminated by old or new carbon

3) Cracking of the ice wedge occurs at the same location year after year (i.e. cracking does not stray from the middle of the ice wedge)

With these assumptions in mind, along with no age inversions across any transects, an attempt was made to create a continuous time profile of $\delta^{18}O$ and temperatures (Figure 40). The results from the continuous age profiles returned interesting and somewhat consistent results. The region of overlapping age between ice wedges IW3 and IW6 from 1720 to 1613 yr BP returned nearly identical $\delta^{18}O$ values (ca. -23.2°) and temperatures (ca. -13.6°C). This is as should be expected since the ice wedges are within 20m of each other, and therefore would be subject to same climate, receiving the exact same $\delta^{18}O$ values from precipitation and likely infilling in similar manors. A single radiocarbon sample from ice wedge IW1 from 1658 yr BP also returned a similar $\delta^{18}O$ value (-23‰) as seen for the same time period for ice wedges IW3 and IW6. On the other hand, the time period overlapping between ice wedges IW3 and IW8 did not return

similar results. Between ca. 3400 to 2500 yr cal BP ice wedge IW8, the older of the ice wedges, had $\delta^{18}O$ values around -26‰ and temperatures around -17°C, both 3‰ and 3°C lower than those for ice wedge IW3. However, on the right side of ice wedge IW3, from 3985 to ca. 3500 yr BP, $\delta^{18}O$ values (26‰) and temperatures were slightly lower, but similar to those from ice wedge IW8. This difference between the $\delta^{18}O$ of ice wedges IW3 and IW8 could be explained by ice wedge IW3 becoming dormant after its initial period of growth during which values were similar to ice wedge IW8, but re-activating later on during warmer conditions. This period of dormancy would also explain the rapid increase in $\delta^{18}O$ for ice wedge IW3 from -26.2‰ to -24.2‰ between samples. However, the period of this dormancy likely ended prior to 2753 yr cal BP as a radiocarbon age from the middle of the ice wedge was obtained. When considering a possible period of dormancy for ice wedge IW3, the overlap of difference in $\delta^{18}O$ values between ice wedges IW3 and IW8 potentially occurs over a shorter period of time.

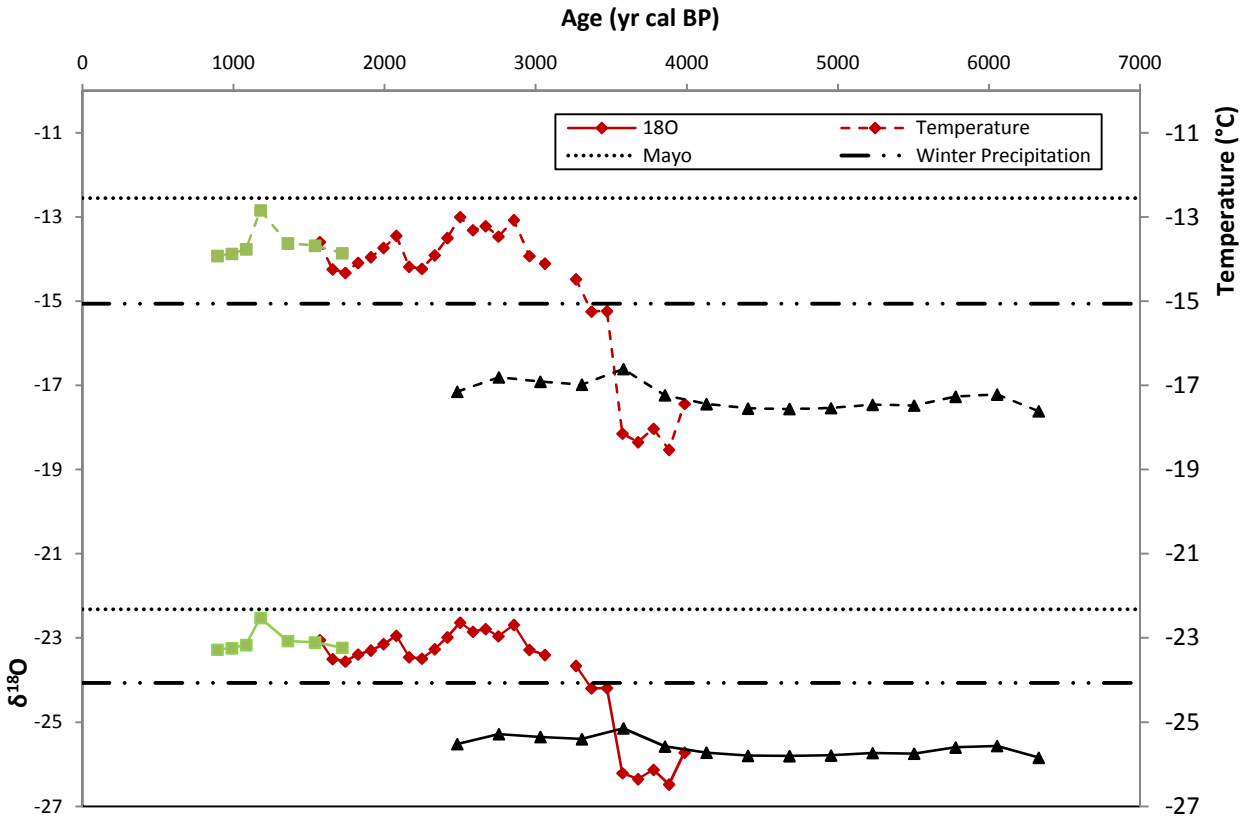

Figure 40. $\delta^{18}O$ (solid line) and Winter temperature (hashed line) Radiocarbon (^{14}C) age profiles for Ice wedges #3 (red diamond), 6 (green square) and 8 (black triangle) (N= 26, 7, 15 respectively). $\delta^{18}O$ and Temperatures calculated for Winter Precipitation and from Mayo are shown. Note: Not all $\delta^{18}O$ and Winter temperature values for each ice wedge were displayed as they fell out of the range between youngest and oldest age obtained for each specific ice wedge.

With these considerations in mind, the $\delta^{18}O$ and temperature time profiles (Figure 40) suggest that cooler conditions than present persisted starting from 6,328 yr cal BP, with winter (or annual) temperatures hovering around -17°C±0.5. These temperatures continued to persist until 3,985 yr cal BP with the formation of ice wedge IW3, and continued for at least another 500 years. However, the length of which these cooler temperatures (ca. -17°C) persisted is not clear as there is an overlap of ca. 300 years between 2,753 to 2,481 yr cal BP where temperatures of ca. -17°C and -13.5°C respectively, were calculated from two different ice wedges. However, at some point during this period, there was a sharp amelioration in climate conditions, with temperatures rising to -13.5°C by no later than 2,481 yr cal BP. From this date on, temperatures oscillated between -13°C to - 14°C until the last obtained date of 893 yr cal BP.

5.4. Paleoclimate Reconstruction

In order to re-create the paleoclimatic history at Two Moose Lake over the past >40ka, information from the previous sections (cryostratigraphy, sedimention, glaciation and post-glaciation history, ice wedge initiation and growth, stable isotopes (paleotemperatures) and continuous T and $\delta^{18}O$ age profiles) from this study were used to complete an in-depth analysis. Furthermore, results and dates from nearby studies were also accounted for in order to ensure consistency and to validate the paleoclimatic history. This paleoclimatic reconstruction will attempt to associate temperatures and climate to specific periods in time using radiocarbon information obtained.

Paleoclimate reconstruction of Two Moose Lake begins prior to the first available radiocarbon date from Pleistocene ice wedge IW7 of 31,608 yr cal BP with the deposition of the I/T layer. It was established, based on various lines of evidence, that the I/T layer was in place prior to the formation of ice wedge IW7, and therefore would have been deposited prior to 31,608 yr cal BP during the Boutellier nonglacial interval, although the exact date is unknown. Ice at this base of this layer returned $\delta^{18}O$ values around -27‰, increasing to -23‰ at the top of the layer. This layer contained a randomly oriented mixture of till, ranging from conglomerates of clay up to pebbles (4-64mm) and cobbles (6.4-25.6cm) suspended within a body of ice. It has been hypothesized that this layer is of buried basal glacial or snowback origin. The lower $\delta^{18}O$ values within this layer suggest that the body of ice/till was not derived from modern precipitation, nor of the extreme cold temperatures seen during the late Pleistocene by Kotler and

Burn (2000) of -31.9 to -29.3‰, but nevertheless during colder (glacial) conditions than present. At a nearby site in Klondike gold fields near Dawson, Yukon (Kotler and Burn, 2000) collected pore and ice wedges samples from a layer that was dated to pre-McConnell glaciation (>40ka BP) of between -28.3 to -26.3‰, similar to those seen in the I/T layer. Furthermore, $\delta^{18}O$ values between -25.8 and -25.0‰ were obtained from massive ice located only 10km north of Two Moose Lake at Chapman lake, Yukon (Lacelle et al., 2007), similar to those obtained from the I/T layer. Lacelle et al. (2007) hypothesized this massive ice to be of glacial origin and of MIS 4 age (<71ka BP) as the $\delta^{18}O$ values were slightly enriched over other MIS age (late Wisconsin) relict massive ground ice located in the northwestern Canadian Arctic, during which conditions were warmer than during the late Wisconsin full glacial period (Harris, 2005). Further evidence suggesting the I/T layer as glacial origin comes from a stable isotope co-plot, where a regression of $\delta D_{I/T}=7.351\ \delta^{18}O-16.37$ ($r^2=0.985$) similar to that of the LMWL would suggest origination from precipitation. Due to the random orientation and suspension of larger sized sediments (>10cm) it is unlikely that the I/T layer is a buried snowback similar to that seen by Lacelle et al., (2009) dated to ca. 30ka BP, nor of segregated intrusive ice origin as instantaneous freezing would be required to maintain the large sediments in suspension.

Following the deposition of the I/T layer prior, the first of the ice wedges, IW7, was initiated at Two Moose Lake 31,608 yr cal BP. $\delta^{18}O$ values from ice wedge IW7 ranged between -25.5 to -27‰. These $\delta^{18}O$ values were on average 2-3‰ enriched relative to those seen by Lacelle et al. (2009) in a massive ice body (-30.2 to -27‰) north of Two Moose lake at Red Creek, Yukon, dated to 30,720 yr cal BP. The depletion in $\delta^{18}O$ of 2-3‰ of ice wedge IW7 relative to the massive ice at Red Creek can be explained by the transition from the MIS 3 interstadial (56,000 to 30,000 yr BP) into full glacial conditions with the commencement of the McConnell glaciation at 29,600 yr BP (Matthews et al., 1990) that were likely represented in the buried massive ice seen by Lacelle et al. (2007). Furthermore, due to the problem of recycling of 'old-carbon' in the permafrost, specifically when using POC as the dating source (Lachniet et al., 2012), it is possible that the age obtained for the body of buried ice at Red Creek may have been over-estimated, and as such, may actually reflect temperatures closer to the full on-set of the McConnell glaciation. Nevertheless, $\delta^{18}O$ values obtained from ice wedge IW7 indicate that temperatures were between 3-4°C cooler than present temperatures experienced at nearby Mayo. Most notably however, the presence of ice wedge IW7 would indicate that the region

surrounding Two Moose Lake remained unglaciated at 31,608 yr cal BP, as it did during much of the Pleistocene (Bostock, 1966; Duk-Rodkin, 1996, Hopkins, 1982). This falls in line with multiple observations made by Fraser and Burn (1997) from an outcrop in the Klondike region. Willow pieces and their enclosing sediments obtained from an outcrop in the Klondike area were suggestive of a proglacial environment between 36 to 30ka BP. Fraser and Burn (1997) also noted the high non arboreal pollen percentages , presence of tundra beetles and the absence of spruce macrofossils and bark beetle fossils are a clear indication that the lowlands in the Mayo area of central Yukon were dominated by a type of tundra environment and remained ice free. Supporting the growth of ice wedges during this period of time, Kotler and Burn also noticed a high abundance of epigenetic ice wedges within a layer dated to >40ka BP, and possibly to a similar time period as ice wedge IW7.

Following the initiation of ice wedge IW7 at Two Moose Lake, much of North of America was launched into a full-scale glacial period, during which much of North America was covered in various ice sheets (Coordilleran, Innuitian, Greenland, and Laurentide). In the Yukon, this period of glaciation began with the onset of the McConnell glaciation during the late Wisconsinan (MIS-2, 27-29ka BP) (Fraser and Burn, 1997, Zazula et al., 2006) as well as the opening of the Beringia Land Bridge (Zazula et al., 2006; Froese et al., 2009). However, it does not appear the McConnell glaciation reached Two Moose Lake with the presence of ice wedge IW4 dated to 22,368 yr cal BP. This time period coincides with results from several studies indicating a maximum expansion of glacial sheets (Last Glacial Maximum - LGM) that occurred between 24 to 21ka BP (Matthews et al., 1990; Clark and Mix, 2000; Beierle, 2002; Zazula et al., 2006; Froese et al., 2009), with insolution reaching a minimum at 21ka BP (Dyke et al., 2002). Had Two Moose Lake been covered by the McConnell glaciation during its maximum expansion, conditions for the formation of an ice wedge would not be present, and therefore would not have been possible for ice wedge IW4 to form. Furthermore, if ice wedge IW7 were to follow a similar trend to that seen in the Holocene ice wedges whereby, under the assumption that ice wedge IW7 is an epigenetic ice wedge (as shown by the tilting of the I/T layer in contact with the ice wedge), there were no age inversions across the growth of the ice wedge and cracking continued in the same location, an additional age of 13, 686 yr cal BP obtained from the ice wedge at almost 1m to the right of the older date would suggest that growth, at least intermittently, occurred between 31,608 yr cal BP and 13,686 yr cal BP. The presence of ice

wedge IW4 would support the possibility of the continued growth of ice wedge IW7, however, as no ages were obtained between the two dates, continued growth still remains inconclusive. The $\delta^{18}O$ values (IW7: -27‰, 31,608 yr cal BP, IW4: -29.34‰, 22,368 yr cal BP and IW7: -27.88‰, 13,686 yr cal BP) obtained from the three ice wedges also returned similar values to those from ice of similar ages. $\delta^{18}O$ values from a layer in the Klondike "muck" deposits (Kotler and Burn, 2000) dated to between 27.15 ± 0.66 ka BP and 22.30 ± 0.19 ka BP were between -31.9 to -29.3‰. The difference in $\delta^{18}O$ values (2-3‰) can be attributed to the Klondike "muck" site being closer in proximity to the ice margin than Two Moose Lake. While dated to 30,720 yr cal BP, when the age of the buried snowbank at Red Creek, Yukon (Lacelle et al., 2009) is shifted closer to the age of the Dawson tephra directly overlying the snowbank (25,300 yr cal BP, Froese et al., (2006)), $\delta^{18}O$ values within the snowbank (-30.2 to -27‰) are nearly identical to those in ice wedges IW7 and IW4. The extreme negative values seen at the edge of ice wedge IW2 (between -29 to -30.92‰), inferring an older date than the date of 12,990 yr cal BP from the middle of the ice wedge, may be a reflection of the extreme temperatures seen during the LGM, however, as no date was obtained from that section it is not possible to conclude if that portion of the ice wedge formed during this period. Nevertheless, $\delta^{18}O$ values from all three sites suggest formation of ice under full-glacial conditions, with temperatures at Two Moose Lake ranging between -19 to -22.65°C, up to 4-6°C cooler than present. These temperatures are in line with results from plant macrofossil assemblages from Red Creek (Lacelle et al., 2009), lack of spruce or other three macrofossils and paleoecological data (pollen assemblages) for Eastern Beringia during MIS-2 (Zazula et al., 2006) suggestive of a regional vegetation dominated by open herb-tundra or steppe-tundra type habitats indicative of temperatures 3.6 to 6.6°C colder than present and much drier (Matthews et al., 1990; Zazula et al., 2006; Viau et al., 2008; Lacelle et al., 2009). Dry conditions during this period are supported by the extreme negative d-excess values between -12.6 to -18.2 for ice wedges IW4 and IW7, indicating enhanced evaporation loss has occurred and thus dry conditions.

Extreme cold conditions persisted past the LGM (21ka BP)(Kurek et al., 2009) until at least 12,990 yr cal BP with a radiocarbon date obtained from the youngest of the Pleistocene ice wedges, ice wedge IW2. This period coincides with the end of the McConnell glaciation dated to ca. 13,000 ka BP (Hopkins, 1982). $\delta^{18}O$ values from the ice wedge ranged between -24.66 to -30.92‰, with an $\delta^{18}O$ value of -28.3‰ obtained from the location of the radiocarbon sample.

Similar values were also obtained from ice wedge IW7, where a radiocarbon age of 13,686 yr cal BP returned an $\delta^{18}O$ value of -27.88‰. Based on $\delta^{18}O$ values, temperatures during the formation of ice wedge IW2 ranged between -15.9 to -24.9°, while a temperature of -21.15°C was obtained for the sample dated to 12,990 yr cal BP (ice wedge IW2) and -20.55°C for 13,686 yr cal BP. These temperatures are slightly lower than those seen ca. 10ka prior, however, temperatures at Two Moose Lake were still 6-8°C cooler than present. The time period between 14.5ka BP and 12ka BP appears to be a time of conflicting dates in literature associated to warming and cooling events. Several studies have associated the beginning of a "warm" interval known as the Bølling–Allerød interstadial to 12,200 ^{14}C BP, a period during which temperatures reached modern values (Kotler and Burn, 2002), followed by sudden plunge into a sudden cold event known as the Younger Dryas at 10,000 ^{14}C BP. On the other hand, GISP2 ice core from Greenland indicate the Bølling–Allerød interstadial commenced ca. 14.5ka BP (McBean et al., 2005), lasting less than 2,000 years before plunging upwards of 2°C in to a short-lived colder period during the Younger Dryas as a result of the re-advance of the Laurentide ice sheet (McBean et al., 2005; Kurek et al., 2009). The latter set of dates for the warming and cooling events are supported by studies in northern (Kurek et al., 2009) and southern Yukon (Vermaire and Cwynar, 2010) where lake sediments indicate an increase in Chironomid richness suggestive of temperatures similar to present around 15ka BP, with coldest temperatures being experienced around 13ka BP. These dates are in agreement with the extreme cold temperatures experienced at Two Moose Lake around 13ka BP as suggested by the low $\delta^{18}O$ values, however, there is no reflection of the Bølling–Allerød interstadial in the ice wedges. The lack of Bølling–Allerød interstadial signal in the ice wedges can either be a reflection of the region not experiencing the warmer conditions, or ice wedge activity ceasing during this warm period. Furthermore, the persistence of colder conditions at the end of the Pleistocene are supported by an $\delta^{18}O$ value of -29.1‰ obtained by Kotler and Burn (2000) from the Klondike gold fields dated to a similar date of 11.62 ± 0.09 ka BP.

Following the Younger Dryas event at ca. 13ka BP, the next major change in climate in the central Yukon began approximately 11.3 ka BP during the transition between the late Pleistocene and Early Holocene, lasting until ca. 8.2ka BP. This transition, known as the Holocene Thermal Maximum (HTM), brought an end to the glacial period and subsequent cold temperatures experienced during the late Pleistocene, transitioning to a warmer period where

temperatures reached as high as 5°C above present (Clark et al., 2004, Kaufman et al., 2004, McBean et al., 2005, Viau et al., 2008). Direct evidence of the HTM warm period was not present at Two Moose Lake, however, the unconformity between the I/T layer and silt layer along with the truncation of the Pleistocene age ice wedges may be a reflection and remnant of this period. At a nearby site in Mayo, Burn et al. (1986) discovered a thaw unconformity ca. 2m below the surface extending across an 80m headwall and was believed to be stratigraphic evidence of the climatic optimum. Furthermore, multiple ice wedges across the outcrop were truncated at the same level as the thaw unconformity. Organic material found in the drill core at 212cm below the surface was dated to 8870±200 yr BP, suggesting the unconformity occurred during the HTM during a period of greatest thermokarst development and is representative of the maximum active-layer development in the region. While the thaw unconformity seen in Mayo may not have occurred at the same time as that at Two Moose Lake, it does however indicate that mechanisms and climate was such that the creation of an unconformity is possible. While deeper (3.15m) than the thaw unconformity in Mayo, the similar circumstance of truncated ice wedges would suggest that it is likely possible the truncation of the ice wedges occured during the HTM. Furthermore, it is likely this unconformity was to have occurred between at least 12,990 yr cal BP, the oldest possible age of the unconformity as seen by truncated ice wedge IW2, and 6,328 yr cal BP, the youngest possible age as indicated by epigenetic ice wedge IW8. However, it is likely the unconformity occurred thousands of years prior 6,328 yr cal BP as more than 3m of sediment over lays the I/T layer.

Following the creation of the unconformity, over 3m of sediment (3 units outlined above) was deposited prior to the initiation of ice wedge IW8 at 6,328 yr cal BP. In the central Yukon, Vernon and Hughes (1966) noted the extensive deposits of silty clay found in valley bottoms suggesting their deposition in proglacial lakes during the retreat of the ice sheets. While the sediments deposited at Two Moose Lake were more of a sandy silt nature (19.04% sand, 76.65% silt and 4.31% clay), it is possible these sediments were laid down during the possible expansion of the Blackstone river located 200m to the east of Two Moose Lake. $\delta^{18}O$ values of the overlaying sediments may also indicate deposition during the HTM. $\delta^{18}O$ values increased from -24.53‰ at the base (Unit 3), ca. 2‰ below current precipitation at Mayo, to -19.91‰ 1m below the current active layer (Unit 2), ca. 2-3‰ above current precipitation at Mayo. Similar $\delta^{18}O$ values between -27 to -25‰ were obtained from a layer in the Klondike (Kotler and Burn, 2000)

region dated to 10.12 ± 0.38 ka BP and 10.18 ± 0.20 ka BP. As the $\delta^{18}O$ value obtained from the bottom of the sediments was slightly more enriched than those seen at Mayo, it is likely deposition of the layer occurred shortly after ca. 10ka BP. This trend in $\delta^{18}O$, from colder than present to warmer than present, was also a seen in central Yukon and indicative of post-glaciation warming seen during the HTM, where temperatures reached as high as 7° above present by 8.2ka BP (Kaufman et al., 2004, Clark et al., 2004, Viau et al., 2008). The $\delta^{18}O$ value of -19.91‰ located 1m below the surface suggests temperatures between 6-7°C above present, and thus it is possible the deposition up to 1m below the surface occurred between 12,990 yr cal BP and 8.2ka BP. After the -19.91‰ $\delta^{18}O$ value, a sudden drop in $\delta^{18}O$ to -22.48‰ occurs, signifying a sudden drop in temperatures in a short period, followed by an immediate return to near pre-event $\delta^{18}O$ value of -20.46‰. This pattern falls in line with Pollen, chironomid, and ostracode records from southwest Yukon (Bunbury and Gajewski, 2008) and Mt Logan Holocene–late Wisconsinan isotope records (Fisher et al., 2008) representative of warming temperatures to greater than present until 8.2ka BP, a severe cold and dry event lasting less than a century, followed by a rapid increase in temperatures to pre-event temperatures.

Following the deposition of at least stratigraphic Units 3 and 2 at Two Moose Lake, a period of ice wedge activity took place between 6,328 yr cal BP right up to 893 yr cal BP (Figure 40). $\delta^{18}O$ values from the first ice wedge to appear, IW8, ranged between -25.15 to -26.33‰, reflective of temperatures ca. 2-3°C below the current temperature at Mayo. Temperatures of ice wedge IW8 remained relative stable during its growth to a youngest obtained age of 2,481 yr cal BP. However, this is in contrast to pollen data from the Yukon (Viau et al., 2008) that indicated temperatures cooled from 5°C above present at 8.2ka BP to near-present temperatures by 4.2ka BP. Around this time, the formation of ice wedge IW3 began (3,985 yr cal BP) with initial low $\delta^{18}O$ values of ca. -26.5‰. This low $\delta^{18}O$ value, along with those from ice wedge IW3, are consistent with the most significant cooling event of the Holocene coinciding with neoglacial and wet conditions beginning at 4.2ka BP (Menounos et al., 2009). The rapid decrease in temperature was reflected in from southern Yukon indicating a temperature drop of up to 2°C below present (Bunbury & Gajewski, 2008; Kurek et al., 2009). While the temperatures obtained from the ice wedge were much lower than those reported, the larger decrease in temperature at Two Moose Lake can be attributed to being further in proximity to a body of water, and thus a more continental climate with more extreme variations in temperatures and less precipitation.

By 2,753 yr cal BP, $\delta^{18}O$ values at Two Moose Lake began to rise to ca. -23‰, and remaining as such until the last obtained radiocarbon date of 893 yr cal BP. Temperatures during this period varied between 0.5 to 1.5°C below present, consistent from pollen records from across the Arctic (Viau et al., 2012). A summary of the paleoclimatic events at Two Moose Lake can be found below (Table 10):

Table 10. A summary of the major events from the paleoclimatic reconstruction of Two Moose Lake, central Yukon. The reconstruction spans >30ka yr, from ca. 40,000 yr BP to 893 yr cal BP. Dates highlighted correspond to calibrated ^{14}C-DOC obtained from this study.

Date[a] (yr BP)	Event	Diagnostic Unit in Outcrop	$\delta^{18}O$ (‰)	Temperature difference[b]		Dating Source[c]	Features
				Mayo Precipitation (°C)	Constructed Winter (°C)		
>31,608 (40,000?)	Boutellier Interglacial	I/T layer	-27 to -23	-6.7 to -0.98	-4.2 to 1.5	Relative Dating	Glacial origin
31,608	Pre-McConnel Glaciation	Ice wedge IW7	-27 to -25	-6.7 to -3.9	-4.2 to -1.3	^{14}C-DOC	Ice-free
22,368	McConnel Glaciation	Ice wedge IW4	-29.3	-10.1	-7.6	^{14}C-DOC	Ice-free, full-glacial conditions
13,686	McConnell Glaciation	Ice wedge IW7	-27.9	-8	-5.5	^{14}C-DOC	Full-glacial conditions
12,990	Younger Dryas	Ice wedge IW2	-28.3	-8.6	-6.1	^{14}C-DOC	Re-advance of Ice Sheets
<12,990 to ~10,000	HTM	Unconformity	N/A	~5° (Literature)		Relative Dating	Truncated Pleistocene age ice wedges
<10,000 to >8,200	HTM	Unit 3 and 2	-24.5 to -19.9	-3.2 to 3.5	-0.7 to 6.0	Relative Dating	Deposition of Silt and Silt w/ organics
~8.2	Cooling Event	Unit 2	-22.5	-0.2	2.3	Relative Dating	Rapid drop in temperatures for <100yr
<8.2 to >6,328	Warming Event	Unit 2	-20.5	2.7	5.2	Relative Dating	Return to pre-cooling event temperatures
6,328 to 4.2	Ice wedge growth	Ice wedge IW8	-26.3 to -25.2	-5.8 to -4.1	-3.3 to -1.6	^{14}C-DOC	Initiation of ice wedge growth
3,985 to >2,753	Cooling Event	Ice wedge IW3	-26.5 to -25.7	-6 to -4.9	-3.4 to -2.4	^{14}C-DOC	Neoglacial conditions
2,752 to **893**	Warming Event	Ice wedge IW1,3,6	-23.5 to -22.5	-1.6 to 0.3	0.9 to 2.2	^{14}C-DOC	Warming to near present temperatures

[a]Dates were generated based on calibtrated ^{14}C-DOC dates from this study and correlative/relative dating to dates from other studies.
[b]Temperature differences were determined by comparing temperatures calculated from $\delta^{18}O$ from the diagnostic unit to 1) temperatures calculated from current $\delta^{18}O$ precipitation values from Mayo, and 2) calculated current Winter temperatures from Mayo (October-March).
[c]Refers to the dating source used to determine the timing of the specific event.

6. Conclusion

The purpose of this thesis was to develop and use radiocarbon in Dissolved Organic Carbon (DOC) and Dissolved Inorganic Carbon (DIC) from ice wedges as a dating method for use in the reconstruction of the paleoclimate at Two Moose Lake, central Yukon. Due to the rich glaciation history of the region, Two Moose Lake has experienced a wide range of climates over its history. Using field observations, granulometry, stable isotopes and ^{14}C-DOC/^{14}C-DIC radiocarbon dates from sediment-rich ice of glacial origin, ice wedges, and the enclosing sediments, this thesis was able to 1) reconstruct the sedimentation and cryostratigraphy history of the outcrop; 2) demonstrate that Two Moose Lake remained ice-free during the McConnell glaciation; 3) examine the water source of ice wedge infilling; 4) develop continuous δ^{18}O and temperature age profiles from 6,328 yr cal to 893 yr cal BP using ice wedges; and 5) create a continuous paleoclimate reconstruction from >40ka BP to 893 yr cal BP. These five principal conclusions from Two Moose Lake are summarized below.

1. The permafrost section found to outcrop at Two Moose Lake has four principal units which have been divided into 7 discrete events:

   Units:

   1. Active & Peat (paleo-active) Layer (0-0.5m)
   2. Silt Loam with Organics Layer (0.5-1.75m)
   3. Silt Layer (1.75-3.15m)
   4. Ice/Till layer (3.15-4.35m)

   Events:

   1. *> 31,608 yr cal BP*: Deposition of the sediment-rich layer (Unit 4, I/T layer).
   2. *31,608 to 12,990 yr cal BP*: Formation and growth of Pleistocene age ice wedges.
   3. *Between events 2 and 4*: Thawing/Erosional event causing the unconformity seen between Unit 4 and Unit 3.
   4. *<12,900 to >6,298 yr cal BP*: Deposition of Units 3,2 and potentially 1.
   5. *6,298 to 893 yr cal BP*: Formation and growth of Holocene aged ice wedges.
   6. *<893 yr cal BP*: Potential ice wedge activity and Active layer accumulation.
   7. *>2007 AD*: Exposure of the outrcop at Two Moose Lake through thaw slumping.

2. Ice wedge formation requires a MAAT below -4°C, extreme cold temperatures (<-20°C) during the winter for the initiation of ground/ice cracking and an exposed surface in order for a rapid decrease in temperature to occur (i.e. little to no insulating snow or vegetation). ^{14}C-DOC ages of 31.4, 29.6 and 13.7ka cal BP from ice wedge IW7, 22.4ka cal BP from ice wedge IW4 and 12.9ka cal BP from ice wedge IW2 were obtained from the I/T layer at Two Moose Lake. The presence of these ice wedges suggest a MAAT below -4°C as well as ice-free conditions, contradicting previous research indicating that much of central Yukon, including Two Moose Lake, was glaciated throughout the McConnell glaciation (29.6ka to 13ka BP).

3. The commonly accepted method of ice wedge infilling through spring (snow) meltwater, with δ^{18}O values of the ice reflecting winter precipitation/temperatures,may not be the rule, but rather the exception. Many of the Holocene ice wedges, specifically younger ice wedges (<3ka BP), saw enriched δ^{18}O (-22‰ to -24‰) values relative to those calculated for constructed winter temperatures (-24.07‰) despite reports of temperatures being 1-2°C cooler than present during this period. Since δ^{18}O values for the ice wedges fall between those of the constructed winter temperatures and current precipitation at Mayo (-22.32‰), it was concluded that δ^{18}O values may not solely be a representation of winter precipitation as suggested, but potentially year-round. Supporting this notion, δ^{18}O and δD plots from the ice wedges showed high variability between ice wedges, with some plotting close to the LMWL, originating from precipitation while others plotted much lower, suggesting re-freezing of meltwater. Furthermore, the low statistical correlation of some of the plots may indicate a multitude of different sources of moisture forming the ice.

4. Due to the unique nature of this study sampling horizontal transects from epigenetic ice wedges at a medium-scale resolution (2-5cm) with multiple ^{14}C-DOC samples directly from the transect, it was possible to create a continuous δ^{18}O and Temperature age profile across multiple ice wedges from the Holocene from 6,328 yr cal BP to 893 yr cal BP. This was also possible as no age inversions occurred. The δ^{18}O and Temperature age profiles from ice wedges IW8, IW3 and IW6 showed a surprising consistency of δ^{18}O values and temperature during overlapping ages with only a few inconsistencies. This appears to be the first continuous δ^{18}O and Temperature age profiles obtained solely from an ice wedge without the

use of ages from carbon (allochthonous) material suspended within the ice wedge or the surrounding sediments.

5. A comprehensive re-creation of the paleoclimatic history at Two Moose Lake from 40ka BP to modern time was completed using ^{14}C-DOC dates and δ^{18}O values from this study along with correlative and relative dating from other studies. This re-creation was unique in that it provided a history of many of the events during the late Pleistocene and Holocene in one outcrop, as well as from the central Yukon. This study appears to be the first study from central Yukon to provide a record of many of the warming and cooling events seen throughout the Holocene in southwestern Yukon. This study also appears to be the first to confirm an unglaciated terrain using ice wedges during the McConnell glaciation. Key findings are summarized below:

Time (ka BP)	Event	δ^{18}O Temperatures	Features during event
31.6	Boutellier Interstadial	-19.3 to -13.5	Deposition of I/T layer (glacial origin)
31.6 to 14.5	McConnel Glaciation	-22.6 to -16.4	Ice-free (unglaciated)
14.5 to 12.9	Younger Dryas	-21.15	Re-expansion of Glaciers
<12.9 to >8.2	Holocene thermal maximum	-15.7 to -9.1	Deposition of Silt and Silt w/ organics layer
~8.2	Cooling Event	-12.8	Rapid drop in temperatures for <100 years
<8.2 to >6.3	Warming Event	-9.9	Return to pre-cooling event temperatures
6.3 to 4.2	Ice wedge growth	-18.3 to -16.6	Initiation of Holocene ice wedge growth
4 to >2.8	Cooling Event	-18.5 to -17.4	Neoglacial conditions
2.8 to 0.9	Warming Event	-14.2 to -12.8	Warming to near present temperatures

Overall, the findings from this study have contributed to the popular belief of an unglaciated central Yukon during the McConnell glaciation. δ^{18}O values along with ^{14}C-DOC dates enabled a detailed reconstruction and record of the climate at Two Moose Lake over the past 40,000 that have been consistent with findings from other studies. The use of DOC as the radiocarbon source has proved to be a powerful tool. It has allowed for the direct dating of an ice wedge using the ice from the ice wedge as opposed to allocthonous organic material suspended within the ice wedge or found within sediments surrounding the ice wedge that are often subject to age inversions due to cryoturbation. This also offers the possibility for a reduced chance of contamination by 'old' or recycled carbon that has been show to be a problem with dating in the Arctic, and will likely only become a larger issue with projected future warming releasing 'old' carbon back in to the system. Considering studies have indicated the relatively high

concentration of DOC in ice wedges, this may prove to be a powerful tool moving forward in the use of ice wedges as dating tools for paleoclimate reconstruction at future sites.

6.1. Future Work

While ^{14}C-DOC has proved to be a powerful dating tool, further research and understanding is required to develop its full potential. Despite no age inversions being found in this study, higher density sampling of ^{14}C-DOC will help to determine if the possibility for age inversions can occur using ^{14}C-DOC. Considering the study by Lachniet et al. (2012) was the first study to use DOC as the dating material in ice and showed ^{14}C-DOC ages were younger than those of particulate organic matter (POC), further studies are required in order to determine if this the rule, or if it's the exception before too much weight is placed on the power of DOC as a dating material. A detailed analysis of the components of the DOC within the ice, as well as from region melt water may be useful in the development of an error model to be able to quantify and potential contamination by 'old' carbon. Lastly, with regards to the specific sedimentary and paleoclimate history at Two Moose Lake, additional 14C-DOC samples obtained directly from the sediments and I/T layer could be useful in the confirmation of the chronology developed within this study.

References

Abbott, M.B. and Stafford, T.W. 1996. Radiocarbon geochemistry of modern and ancient Arctic lake systems, Baffin Island, Canada. Quaternary Research, 45: 300–311.

Allard, M. and Kasper, J. 1998. Temperature conditions for ice wedge cracking: field measurements from Salluit, northern Quebec, In Proceedings of the 7th International Permafrost Conference, Yellowknife, N.W.T., June 1998.

Arctic Climate Impact Assessment (ACIA). 2004. Impact of A Warming Climate, Overview Report. Cambridge University Press, Cambridge, United Kingdom, 139 pp.

Barrow, E., Maxwell, B. and Gachon, P., (Eds). 2004. Climate Variability and Change in Canada: Past, Present and Future, ACSD Science Assessment Series No. 2, Meteorological Service of Canada, Environment Canada, Toronto, Ontario, 114p.

Beirle, B.D. 2002. Late Quaternary glaciation in the Northern Ogilvie Mountains: revised correlations and implications for the stratigraphic record. Canadian Journal of Earth Sciences, 39: 1709–1717.

Berger, A. and Loutre, M.F. 1991. Insolation values for the climate of the last 10 million years. Quaternary Science Reviews, 10: 297-317.

Berger, G.W., Pewe, T.L., Westgate, J.A. and Preece, S.J. 1996. Age of Sheep Creek tephra (Pleistocene) in central Alaska from hermoluminescence dating of bracketing loess. Quaternary Research, 45: 263–270.

Berman, E.S.F , Levin, N.E., Landais, A., Li, S. and Owano,T. 2013. Measurement of δ 18O, δ17O, and 17O-excess in Water by Off-AxisIntegrated Cavity Output Spectroscopy and I sotope Ratio MassSpectrometry. Analytical Chemistry, 85: 10392 10398.

Black, R. F. 1976. Periglacial features indicative of permafrost: ice and soil wedges. Quaternary Research, 6: 3–26.

Bostock, H.S. 1966. Notes on glaciation in central Yukon Territory. Geological Survey of Canada, Paper 65-36.

Bourgeois, J.C., Koerner, R,M., Gajewski, K. and Fisher, D.A. 2000. A Holocene ice-core pollen record from Ellesmere Island, Nunavut, Canada. Quaternary Research, 54: 275–283.

Bradley, R.S. 1990. Holocene paleoclimatology of the Queen Elizabeth Islands, Canadian high Arctic. Quaternary Science Reviews, 9: 365–384.

Bray, M.T., French, H.M. and Shur, Y. 2006. FurtherCryostratigraphic Observations in the CRREL Permafrost Tunnel, Fox, Alaska. Permafrost and Periglacial Processes, 17: 233-243.

Briner, J.P., Kaufman, D.S., Manley, W.F., Finkel, R.C. and Caffee, M.W. 2005. Cosmogenic exposure dating of late Pleistocene moraine stabilization in Alaska. Geological Society of America Bulletin, 117: 1108–1120.

Bronk Ramsey, C. 2009. Bayesian analysis of radiocarbon dates. Radiocarbon, 51: 337–60.

Bunbury, J. and Gajewski, K. 2008. Postglacial climates inferred from a lake at treeline, southwest Yukon Territory, Canada. Quaternary Science Reviews, 28: 354-369.

Burn, C.R. 1990. Implications for Paleoenvironmental Reconstruction of Recent Ice-wedge Development at Mayo, Yukon Territory.Permafrost and Periglacial Processes, 1: 2-14.

Burn, C.R. 1994. Permafrost, tectonics and past and future regional climate change, Yukon and adjacent Northwest Territories. Canadian Journal of Earth Sciences, 31: 182– 191.

Burn, C. R. 1997. Cryostratigraphy, paleography, and climate change during the early Holocene warm interval, western Arctic coast, Canada. Canadian Journal of Earth Sciences, 34: 912-925.

Burn, C.R. 1998. The Active Layer: Two Contrasting Definitions. Permafrost and Periglacial Processes, 9: 411-416.

Burn, C.R., Michel, F.A. and Smith, M.W. 1986. Stratigraphic, isotopic, and mineralogical evidence for an early Holocene thaw unconformity at Mayo, Yukon Territory. Canadian Journal of Earth Sciences, 23: 794–803.

Burn, C.R. and Kokelj, S.V. 2009. The Environment and Permafrost of the Mackenzie Delta Area. Permafrost and Periglacial Processes, 20: 83–105.

Calmels, F., Gagnon, O. and Allard, M. 2005. A portable earth-drill system for permafrost studies. Permafrost and Periglacial Processes, 16: 311-315.

Christiansen, H.H. 2005. Thermal Regime of Ice-wedge Cracking in Adventdalen, Svalbard. Permafrost and Periglacial Processes, 16: 87-98.

Clark, I. and Fritz, P. 1997. Environmental Isotopes in Hydrogeology. Lewis Publishing, New York. 342p.

Clark, I.D., Lauriol, B., Marshner, M., Sabourin, N., Chauret, Y. and Desrochers, A. 2004. Endostromatolites from permafrost karst, Yukon, Canada: paleoclimatic proxies for the Holocene hypsithermal. Canadian Journal of Earth Sciences, 41: 387–399.

Clark, P.U. and Mix, A.C. 2000. Global change: Ice sheets by volume. Nature, 406: 689–690.

Collins, M., Knutti, R., Arblaster, J., Dufresne, J-L., Fichefet, T., Friedlingstein, P., Gao, X., Gutowski, W.J., Johns, T., Krinner, G., Shongwe, M., Tebaldi, C., Weaver, A.J. and Wehner, M. 2013: Long-term Climate Change: Projections, Commitments and Irreversibility. In: Climate Change 2013: The Physical Science Basis. Contribution of Working Group I to the

Fifth Assessment Report of the Intergovernmental Panel on Climate Change [Stocker, T.F., D. Qin, G.-K. Plattner, M. Tignor, S.K. Allen, J. Boschung, A. Nauels, Y. Xia, V. Bex and P.M. Midgley (eds.)]. Cambridge University Press, Cambridge, United Kingdom and New York, NY, USA.

Craig, H. 1961. Isotopic variations in meteoric waters. Science, 133: 1702–1703.

Dansgaard, W. 1964. Stable isotopes in precipitation. Tellus, 16: 436–468.

Demuro, M., Roberts, R.G., Froese, D.G., Arnold, L.J., Brock, F. and Bronk Ramsey, C. 2008. Optically stimulated luminescence dating of single and multiple grains of quartz from perennially frozen loess in western Yukon Territory, Canada: comparison with radiocarbon chronologies for the late Pleistocene Dawson tephra. Quaternary Geochronology, 3: 346–364.

Demuro, M., Froese, D.G., Arnold, L.J. and Roberts, R.G. 2012. Single-grain OSL dating of glaciofluvial quartz constrains Reid glaciation in NW Canada to MIS 6. Quaternary Research, 77: 305-316.

Douglas, T. A., Fortier, D., Shur, Y. L., Kanevskiy, M. Z., Guo, L. D., Cai, Y. H. and Bray, M. T., 2011, Biogeochemical and Geocryological Characteristics of Wedge and Thermokarst-Cave Ice in the CRREL Permafrost Tunnel, Alaska: Permafrost and Periglacial Processes, 22(2); 120-128.

Duk-Rodkin, A. 1996. Surficial Geology, Dawson, Yukon Territory, 1:250,000. Geological Survey of Canada. Open file 3288.

Duk-Rodkin, A., Barendregt, R.W., Tarnocai, C. and Phillips, F.M. 1996. Late Tertiary to late Quaternary record in the Mackenzie Mountains, Northwest Territories, Canada; stratigraphy, paleosols, paleomagnetism and chlorine-36. Canadian Journal of Earth Sciences, 33: 875–895.

Duk-Rodkin, A., Barendregt, R.W., Froese, D.G., Weber, F., Enkin, R., Smith, I.R., Zazula, G.D., Waters, P. and Klassen, R. 2004. Timing and extent of Plio-Pleistocene glaciations in north-western and east-central Alaska. In: Ehlers, J., Gibbard, P.L. (Eds.), Quaternary Glaciations—Extent and Chronology, Part II: North America. Elsevier, The Netherland, pp. 313–345.

Dyke, A.S., Andrews, J.T., Clark, P.U., England, J.H., Miller, G.H., Shaw, J. and Veillette, J., 2002. The Laurentide and Innuitian ice sheets during the last glacial maximum. Quaternary Science Reviews, 21: 9–31.

Edwards, M.E., Mock, C.J., Finney, B.P., Barber, V.A. and Bartlein, P.J. 2001. Potential analogues for palaeoclimatic variations in eastern interior Alaska during the past 14,000 yr: Atmospheric circulation controls of regional temperature and moisture responses. Quaternary Science Reviews, 20: 189–202.

Environment Canada, Meteorological Service of Canada, Climate Research Branch, 2008, Climate Trends and Variations Bulletin for Canada, Annual 2007.

Environment Canada, 2015. Canadian Climate Normals 1981– 2010: Dawson. Canada Atmospheric Environment Service, Minister of Supply and Services Canada, Ottawa, ON, Canada.

Environment Canada, 2015. Canadian Climate Normals 1981– 2010: Mayo. Canada Atmospheric Environment Service, Minister of Supply and Services Canada, Ottawa, ON, Canada.

Fisher, D., Osterberg, E., Dyke, A., Dahl-Jensen, D., Demuth, M., Zdanowicz, C., Bourgeois, J., et al. 2008. The Mt Logan Holocene–late Wisconsinan isotope record: Tropical Pacific – Yukon connections. The Holocene, 18: 667 –677.

Fortier, D. and Allard, M. 2005. Frost-cracking conditions, Bylot Island, Canadian Arctic Archipelago. Permafrost and Periglacial Processes, 16: 145–161.

Fraser, T.A. and Burn, C.R. 1997. On the nature and origin of "muck" deposits in the Klondike area, Yukon Territory. Canadian Journal of Earth Sciences, 34: 1333-1344.

French, H.M. 2007. The Periglacial Environment, third edition. Addison Wesley Longman Limited, John Wiley and Sons: Chichester, England; Hoboken, NJ. 478 pp.

French, H.M. and Pollard, W.H. 1986. Ground-ice investigations, Klondike District, Yukon Territory. Canadian Journal of Earth Sciences, 23(4): 550–560.

French, H.M. and Slaymaker, O. 1997. Canada's Cold Environment. McGill-Queens University Press, Canada. 368p.

French, H.M. and Guglielmin, M. 2000. Frozen ground phenomena in the vicinity of Terra Nova Bay, Northern Victoria Land, Antarctica: A preliminary report. Geografiska Annaler, 82(4): 513–526.

French, H. and Shur, Y. 2010. The principles of cryostratigraphy: Earth-Science Reviews, 101(3-4): 190-206.

Fritz, M., Wetterich, S., Meyer, H., Schirrmeister, L., Lantuit, H. and Pollard, W.H. 2011. Origin and Characteristics of Massive Ground Ice on Herschel Island (Western Canadian Arctic) as revealed by Stable Water Isotope and Hydrochemical Signatures. Permafrost and Periglacial Processes, 22: 26-38.

Fritz, M., Wetterich, S., Schirrmeister, L., Meyer, H., Lantuit, H., Preusser, F. and Pollard, W.H. 2012. EasternBeringia and beyond: Late Wisconsinan and Holocene landscape dynamics along the Yukon Coastal Plain, Canada. Palaeogeography, Palaeoclimatology, Palaeoecology, 319–320: 28–45.

Fritz, M., Opel, T., Tanski, G., Herzschuh, U., Meyer, H., Eulenburg, A. and Lantuit, H. 2015. Dissolved organic carbon (DOC) in Arctic ground ice. The Cryosphere, 9: 737–752.

Froese, D.G., Barendregt, R.W., Enkin, R.J. and Baker, J. 2000. Paleomagnetic evidence for multiple late Pliocene – early Pleistocene glaciations in the Klondike area, Yukon Territory. Canadian Journal of Earth Sciences, 37: 863–877.

Froese, D.G., Zazula, G.D. and Reyes, A.V. 2006. Seasonality of the late Pleistocene Dawson tephra and exceptional preservation of a buried riparian surface in central Yukon Territory, Canada. Quaternary Science Reviews, 25: 1542–1551.

Froese, D.G., Zazula, G.D., Westgate, J.A., Preece, S.J., Sanborn, P.T., Reyes, A.V. and Pearce, N.J.G 2009. . The Klondike goldfields and Pleistocene environments of Beringia. GSA Today, 19 (8): 4-10

Geological Survey of Canada, Surveys and Mapping Branch, 1965. Surficial Geology of Dawson Yukon Territory. Map 1170A. Scale 1:253,440.

Geological Survey of Canada, Surveys and Mapping Branch, 1972. Geology of Dawson Yukon Territory. Map 1284A. Scale 1:250,000.

Green, L.H. 1972. Geology of Nash Creek, Larsen Creek, and Dawson area maps. Geological Survey of Canada, Memoir 364, 157 p.

Griffing, C. 2011. Pleistocene climate in Alaska from stable isotopes in an ice wedge: University of Nevada, Las Vegas, 65 p.

Guo, L., Ping, C.-L., and Macdonald, R. W. 2007. Mobilization pathways of organic carbon from permafrost to arctic rivers in a changing climate. Geophysical Ressearch Letters, 34: L13603.

Hamilton, T. D., Craig, J. L. and Sellmann, P. V. 1988. The Fox Permafrost Tunnel - A Late Quaternary geologic record in Central Alaska: Geological Society of America Bulletin, 100(6): 948-969.

Harris, S.A. 2005. Thermal history of the Arctic Ocean environs adjacent to North America during the last 3.5 Ma and a possible mechanism for the cause of the cold events (major glaciations and permafrost events). Progress in Physical Geography, 29: 218–237.

Harry, D. G., and Gozdzik, J. S. 1988. Ice wedges: Growth, thaw transformation, and palaeoenvironmental significance. Journal of Quaternary Science, 3: 39–55.

Hartmann, D.L., Klein Tank, A.N.G, Rusticucci, M., Alexander, L.V., Brönnimann, S., Charabi, Y., Dentener, F.J., Dlugokencky, E.J., Easterling, D.R., Kaplan, A., Soden, B.J., Thorne, P.W., Wild, M. and Zhai, P.M. 2013: Observations: Atmosphere and Surface. In: Climate Change 2013: The Physical Science Basis. Contribution of Working Group I to the Fifth Assessment Report of the Intergovernmental Panel on Climate Change [Stocker, T.F., D. Qin,G.-K. Plattner, M. Tignor, S.K. Allen, J. Boschung, A. Nauels, Y. Xia, V. Bex and P.M. Midgley (eds.)]. Cambridge University Press, Cambridge, United Kingdom and New York, NY, USA.

Heginbottom, J.A. and Radburn, L.K. 1992. Permafrost and Ground Ice Conditions of Northwestern Canada; Geological Survey of Canada Map 1619A. Scale 1:1,000,000.

Heginbottom, J.A., Dubreil, M.A. and Harker, P.T. 1995. Canada Permafrost Map,1:5,000,000, scale. National Atlas of Canada, 5th edition, Government of Canada, Ottawa.

Heiri, O., Lotter, A.F. and Lemcke, G. 2001. Loss on ignition as a method for estimating organic and carbonate content in sediments: reproducibility and comparability of results. Journal of Paleolimnology, 25: 101–110.

Hengeveld, H., Whitewood, B. and Fergusson, A. 2005. An Introduction to Climate Change: A Canadian Perspective. Environment Canada, 53 pp.

Hoefs, J. 1997. Stable Isotope Geochemistry. Springer-Verlag Berlin Heidelberg. New York. 286.

Hopkins, D.M. 1982. Aspects of the paleogeography of Beringia during the Late Pleistocene. In Paleoecology of Beringia. Academic Press, New York. pp. 3–28.

Hughes, O.L., Harington, C.R., Schweger, C. and Matthews Jr., J.V. 1987. Stop 15: Ash Bend Section. In: Morison, S.R., Smith, C.A.S. (Eds.), Guidebook for field excursion A20, Quaternary research in Yukon. 12th International Quaternary Congress (INQUA), National Research Council of Canada, Ottawa, pp. 50–53.

Huscroft, C.A., Ward, B.C., Barendregt, R.W., Jackson Jr., L.E. and Opdyke, N.D. 2004. Pleistocene volcanic damming of Yukon River and the maximum age of the Reid Glaciation, west-central Yukon. Canadian Journal of Earth Sciences, 41: 151–164.

Jackson Jr., L.E., Ward, B., Duk-Rokin, A. and Hughes, O.L. 1991. The last Cordilleran Ice Sheet in southern Yukon Territory. Géographie Physique et Quaternaire, 45: 341–354.

Jouzel, J. and Souchez, R.A. 1982. Melting-refreezing at the glacier sole and isotopic composition of the ice. Journal of Glaciology, 28(98): 35–41.

IAEA/WMO. 2015. Global Network of Isotopes in Precipitation. The GNIP Database. http://www.iaea.org/water

Karanfil, T., Erdogan, I. and Schlautman, M.A. 2003.Selecting Filter Members for measuring DOC and UV_{245}. American Water Works Association, Vol. 95, 3: 86-100.

Kaufman, D.S., Ager, T.A., Anderson, N.J., Anderson, P.M., Andrews, J.T., Bartlein, P.J., Brubaker, L.B., Coats, L.L., Cwynar, L.C., Duvall, M.L., Dyke, A.S., Edwards, M.E., Eisner, W.R., Gajewski, K., Geirsdo ´ttir, A., Hu, F.S., Jennings, A.E., Kaplan, M.R., Kerwin, M.W., Lozhkin, A.V., MacDonald, G.M., Miller, G.H., Mock, C.J., Oswald, W.W., Otto-Bliesner, B.L., Porinchu, D.F., Ru ¨ hland, K., Smol, J.P., Steig, E.J. and Wolfe, B.B. 2004. Holocene thermal maximum in the western Arctic (0–180W). Quaternary Science Reviews, 23: 529–560.

Kennedy, K.E., Froese, D.G., Zazula, G.D. and Lauriol, B. 2010. Last glacial maximum age for the northwest Laurentide Ice Sheet maximum from the Eagle River spillway and delta complex, northern Yukon, Quaternary Science Review, 29: 1288–1300.

Khan, E. and Subramania-Pillai, S. 2007. Interferences contributed by leaching from filters on measurements of collective organic constituents. Water Research, 41: 1841-1850.

Kirtman, B., Power, S.B., Adedoyin, J.A., Boer, G.J., Bojariu, R., Camilloni, I., Doblas-Reyes, F.J., Fiore, A.M., Kimoto, M., Meehl, G.M., Prather, M., Sarr, A., Schär, C., Sutton, R., van Oldenborgh, G.J., Vecchi, G., and Wang, H.J. 2013: Near-term Climate Change: Projections and Predictability. In: Climate Change 2013: The Physical Science Basis. Contribution of Working Group I to the Fifth Assessment Report of the Intergovernmental Panel on Climate Change [Stocker, T.F., D. Qin, G.-K. Plattner, M. Tignor, S.K. Allen, J. Boschung, A. Nauels, Y. Xia, V. Bex and P.M. Midgley (eds.)]. Cambridge University Press, Cambridge, United Kingdom and New York, NY, USA.

Kojima, S. 1996. Ecosystem Types of Boreal Forest in the North Klondike River Valley, Yukon Territory, Canada, and their Productivity Potentials. Environmental Monitoring and Assessment, 39: 265-281.

Kokelj, S.V., Tunnicliffe, J., Lacelle, D., Lantz, T.C., Chin, K.S. and Fraser, R. 2015. Increased precipitation drives mega slump development and destabilization of ice-rich permafrost terrain, northwestern Canada. Global and Planetary Change, 129: 56-68.

Kotler, E. and Burn, C.R. 2000. Cryostratigraphy of the Klondike "muck" deposits, west- central Yukon Territory. Canadian Journal of Earth Sciences, 37: 849-861.

Kurek, J., Cwynar, L.C. and Vermaire, J.C. 2009. A late Quaternary paleotemperature record from Hanging Lake, northern Yukon Territory, eastern Beringia. Quaternary Research, 72: 246-257.

Lacelle, D. 2011. On the d18O, dD and D-excess relations in meteoric precipitation and during equilibrium freezing: theoretical approach and field examples. Permafrost and Periglacial Processes, 22: 13-25.

Lacelle, D., Bjornson, J., Lauriol, B., Clark, I.D. and Troutet, Y. 2004. Segregated-intrusive ice of subglacial meltwater origin in retrogressive thaw flow headwalls, Richardson Mountains, NWT, Canada. Quaternary Science Reviews, 23(5–6): 681–696.

Lacelle, D., Lauriol, B., Clark, I.D., Cardyn, R. and Zdanowicz, C. 2007. Nature and origin of a Pleistocene-age massive ground ice body exposed in the Chapman Lake moraine complex, central Yukon Territory, Canada. Quaternary Research, 68(2): 249–260.

Lacelle, D., Lauriol, B. and Clark, I.D. 2009. Formation of seasonal ice bodies and associated cryogenic carbonates in Caverne de l'Ours, Quebec, Canada: Kinetic isotope effects and pseudobiogenic crystal structures. Journal of Cave and Karst Studies, 71: 48–62.

Lacelle, D., St-Jean, M., Lauriol, B., Clark, I.D., Lewkowicz, A., Froese, D.G., Kuehn, S.C. and Zazula, G. 2009. Burial and preservation of a 30,000 year old perennial snowbank in Red Creek valley, Ogilvie Mountains, central Yukon, Canada. Quaternary Science Reviews, 28: 3401–3413.

Lacelle, D., Bjornson, J. and Lauriol, B. 2010. Climatic and Geomorphic Factors Affecting Contemporary (1950–2004) Activity of Retrogressive Thaw Slumps on the Aklavik Plateau, Richardson Mountains, NWT, Canada. Permafrost and Periglacial Processes 21(1): 1 - 15.

Lacelle, D**.,** Lauriol, B., Zazula, G., Ghaled, B., Utting, N. and Clark, I.D. 2013. Timing of advance and basal conditions of the Laurentide Ice Sheet during the last glacial maximum in the Richardson Mountains, NWT. Quaternary Research, 80: 274-283.

Lacelle, D., Fontaine, M., Forest, A. and Kokelj, S. 2014. High-resolution stable water isotopes as tracers of thaw unconformities in permafrost: A case study from western Arctic Canada. Chemical Geology, 368: 85–96.

Lacelle, D., Brooker, A., Fraser, R.H. and Kokelj, S.V. 2015. Distribution and growth of thaw slumps in the Richardson Mountains–Peel Plateau region, northwestern Canada. Geomorphology, 235: 40-51.

Lachenbruch, A. H. 1966. Contraction theory of ice-wedge polygons: a qualitative discussion. In Permafrost International Conference, Proceedings, Lafayette, Indiana, November 1963, pp. 63–71.

Lachniet, M.S., Lawson, D.E. and Sloat, A.R. 2012. Revised ^{14}C dating of ice wedge growth in interior Alaska (USA) to MIS 2 reveals cold paleoclimate and carbon recycling in ancient permafrost terrain. Quaternary Research, 78: 217–225.

Lauriol, B., Duchesne, C. and Clark, I.D. 1995. Systematique du remplissage en eau des fentes de gel: les resultats d'une etude oxygene-18 et deuterium. Permafrost and Periglacial Processes, 6: 47–55.

Lauriol, B., Grimm, W., Cabana, Y., Cinq-Mars, J. and Geurtz, M.A. 2002. Cliff-top eolian deposits as indicators of Late Pleistocene and Holocene in Beringia. Quaternary International, 87: 59–79.

Lee, J., Feng, X., Faiia, A. M., Posmentier, E. S., Kirchner, J. W., Osterhuber, R. and Taylor, S. 2010. Isotopic evolution of a seasonal snowcover and its melt by isotopic exchange between liquid water and ice: Chemical Geology, 270: 126-134.

Leonard, A., Castle, S., Burr, G.S., Lange, T. and Thomas, J. 2013.A wet oxidation method for AMS radiocarbon analysis of dissolved organic carbon in water. Radiocarbon, 55: 545–552.

Lewkowicz, A. G. 1994. Ice-wedge rejuvenation, Fosheim Peninsula, Ellesmere Island, Canada. Permafrost and Periglacial Processes, 5: 251- 268.

Lis, G., Wassenaar, L.I. and Hendry,M.J. 2008. High-Precision Laser Spectroscopy D/H and $^{18}O/^{16}O$Measurements of Microliter Natural Water Samples. Analytical Chemistry,80:287-293.

Mackay, J. R. 1975. The closing of ice-wedge cracks in permafrost, Garry Island, Northwest Territories. Canadian Journal of Earth Sciences, 12: 1668–1674.

Mackay, J.R. 1983. Oxygen isotope variations in permafrost. Geological Survey of Canada, Paper 83-1B, 67–74.

Mackay, J. R. 1992. The frequency of ice-wedge cracking (1967–1987) at Garry Island, western Arctic coast, Canada. Canadian Journal of Earth Sciences, 29: 236–248.

Mackay, J. R. 2000. Thermally induced movements in ice-wedge polygons, western arctic coast: a long-term study. Geographie Physique et Quaternaire, 54: 41–68.

Mackay, J. R., and Burn, C. R. 2002. The first 20 years (1978– 1979 to 1998–1999) of ice-wedge growth at the Illisarvik experimental drained lake site, western Arctic coast, Canada. Canadian Journal of Earth Sciences, 39: 95–111.

Matthews, J.V., Schweger, C.E. and Hughes, O.L. 1990. Plant and insect fossils from the Mayo Indian Village Section (central Yukon): new data on middle Wisconsinan environments and glaciations. Géographie physique et Quaternaire, 44: 15–26.

McBean, G., Alekseev, G., Chen, D., Førland, E., Fyfe, J., Groisman, P.Y., King, R., Melling, H., Vose, R. and Whitfield, P.H. 2005. Arctic climate: past and present. Arctic Climate Impacts Assessment (ACIA), C. Symon, L. Arris and B. Heal, Eds., Cambridge University Press, Cambridge, 21-60.

Menounos, B., Osborn, G., Clague, J.J. and Luckman, B.h. 2009. Latest Pleistocene and Holocene glacier fluctuations in western Canada, Quaternary Science Reviews, 28: 2049–2074.

Meyer, H., Dereviagin, A., Siegert, C., Schirrmeister, L. and Hubberten, H.W. 2002. Palaeoclimate Reconstruction on Big Lyakhovsky Island, North Siberia – Hydrogen and Oxygen Isotopes in Ice Wedges. Permafrost and Periglacial Processes, 13: 91–105.

Meyer, H., Schirrmeister, L., Andreev, A., Wagner, D., Hubberten, H.-W., Yoshikawa, K., Bobrov, A., Wetterich, S., Opel, T., Kandiano, E., and Brown, J. 2010. Lateglacial and Holocene isotopic and environmental history of northern coastal Alaska - Results from a buried ice-wedge system at Barrow: Quaternary Science Reviews, 29(27-28): 3720-3735.

Murton, J. 2013. Encyclopedia of Quaternary science: Ice wedges and Ice-wedge casts. Elsevier,Boston. Pg. 436–451.

Murton, J.B. and French, H.M. 1994. Cryostructures in permafrost, Tuktoyaktuk coastlands, western arctic Canada. Canadian Journal of Earth Sciences, 31: 737–747.

Nelson, R.E., Carter, L.D. and Robinson, S.W. 1988. Anomalous radiocarbon ages from a Holocene detrital organic lens in Alaska and their implications for radiocarbon dating and paleoenvironmental reconstructions in the Arctic. Quaternary Research, 29: 66–71.

Opel, T., Dereviagin, A. Y., Meyer, H., Schirrmeister, L. and Wetterich, S. 2011. Palaeoclimatic Information from Stable Water Isotopes of Holocene Ice Wedges on the Dmitrii Laptev Strait, Northeast Siberia, Russia: Permafrost and Periglacial Processes, 22(1): 84-100.

Orlanski, I. 2005. A new look at the Pacific storm track variability: Sensitivity to tropical SSTs and to upstream seeding. Journal of Atmospheric Sciences, 62: 1367 –1390.

Plug, L.J. and Werner, B. 2002. Nonlinear dynamics of icewedge networks and resultant sensitivity to severe cooling events. Nature, 417: 929-933.

Plug, L.J. and Werner, B.T. 2008. Permafrost and Periglacial Processes, 19: 63-69.

Pollard, W.H. and French, H.M. 1980. A first approximation of the volume of ground ice, Richards Island, Pleistocene Mackenzie Delta, Northwest Territories, Canada. Canadian Geotechnical Journal, 17: 509-516.

Preece, S.J., Westgate, J.A., Froese, D.G., Pearce, N.J.G. and Perkins, W.T. 2011. A Catalogue of late Cenozoic tephra beds in the Klondike goldfields and adjacent areas, Yukon Territory. Canadian Journal of Earth Sciences, 48: 1386-1418.

Raffi, R., and Stenni, B. 2011. Isotopic Composition and Thermal Regime of Ice wedges in Northern Victoria Land, East Antarctica: Permafrost and Periglacial Processes, 22(1):65-83.

Reimer, P.J., Bard, E., Bayliss, A., Beck, J.W., Blackwell, P.G., Bronk Ramsey, C., Buck, C.E., Cheng, H., Edwards, R.L., Friedrich, M., Grootes, P.M., Guilderson, T.P., Haflidason, H., Hajdas, I., Hatté, C., Heaton, T.J., Hoffmann, D.L., Hogg, A.G., Hughen, K.A., Kaiser, K.F., Kromer, B., Manning, S.W., Niu, M., Reimer, R.W., Richards, D.A., Scott, E.M., Southon, J.R., Staff, R.A., Turney, C.S.M., van der Plicht, J. 2013. IntCal13 and Marine13 radiocarbon age calibration curves 0–50,000 years cal BP. *Radiocarbon,* 55(4):1869–1887.

Ritchie, J.C., Cwynar, L.C. and Spear, R.W. 1983. Evidence from northwest Canada for an early milankovitch thermal maximum. Nature, 305: 126–128.

Schuur, E. A. G., Bockheim, J., Canadell, J. G., Euskirchen, E., Field, C. B., Goryachkin, S. V., Hagemann, S., Kuhry, P., Lafleur, P. M., Lee, H., Mazhitova, G., Nelson, F. E., Rinke, A., Romanovsky, V. E., Shiklomanov, N., Tarnocai, C., Venevsky, S., Vogel, J. G., and Zimov, S. A. 2008. Vulnerability of permafrost carbon to climate change: Implications for the global carbon cycle: Bioscience, 58(8): 701-714.

Schuur, E.A.G., Vogel, J.G., Crummer, K.G., Lee, H., Sickman, J.O. and Osterkamp, T.E. 2009. The effect of permafrost thaw on old carbon release and net carbon exchange from tundra. Nature, 459: 556–559.

Shumsky, P.A. (1964). Principles of structural glaciology. Translated from the Russian by D. Kraus. Dover Publications Inc., New York. 497p.

Shur, Y., French, H.M., Bray, M.T. and Anderson, D.A. 2004.Syngenetic Permafrost Growth: Cryostratigraphic Observations from the CRREL Tunnel near Fairbanks, Alaska. Permafrost and Periglacial Processes, 15: 339-347.

Shur, Y., Hinkel, K.M. and Nelson, F.E. 2005.The Transient Layer: Implications for Geocryology and Climate-Change Science. Permafrost and Periglacial Processes, 16: 5–17.

Sloat, A. 2014. Modern to Late Pleistocene Stable Isotope Climatology of AlaskaUniversity of Nevada, Las Vegas, 195 p.

Smith, S.L. and, Burgess, M.M. 2000. Ground temperature database for northern Canada. Geological Survey of Canada, Open File report 3954.

Smith, S.L., Romanovsky, V.E., Lewkowicz, A.G., Burn, C.R., Allard, M., Clow, G.D., Yoshikawa, K. and Throop, J. 2010. Thermal State of Permafrost in North America: A Contribution to the International Polar Year. Permafrost and Periglacial Processes, 21: 117-135.

St-Jean, M., Lauriol, B., Clark, I.D., Lacelle, D. and Zdanowicz, C. 2011.Investigation of Ice-Wedge Infilling Processes using Stable Oxygen and Hydrogen Isotopes, Crystallography and Occluded Gases (O_2, N_2, Ar). Permafrost and Periglacial Processes, 22: 49–64.

Stanley, J-D. 2001. Dating modern deltas: progress, problems, and prognostics, Annual Review in Earth and Planetary Science, 29: 257–294.

Turner, D.G., Ward, B.C., Bond, J.D., Jensen, B .J.L., Froese, D.G., Telka, A.M., Zazula, G.D. and Bigelow, N.H. 2013. Middle to Late Pleistocene ice extents, tephrochronology and paleoenvironments of the White River area, southwest Yukon, Quaternary Science Reviews,75: 59-77.

USEPA, 1999.Enhanced Coagulation and Enhanced Precipitative Softening Guidance Manual, EPA 815-R-99-012.Office of Water, Cincinnati, OH.

Walker, 2005. Quaternary Dating Methods. Wiley, England. 304p.

Ward, B.C., Bond, J.D. and Gosse, J.C. 2007. Evidence for a 55–50 ka (early Wisconsin) glaciation of the Cordilleran ice sheet, Yukon Territory, Canada, Quaternary Research, 68: 141–150.

Ward, B.C., Bond, J.D., Froese, D.G. and Jensen, B. 2008. Old Crow tephra (140 10 ka) constrains penultimate Reid glaciation in central Yukon Territory. Quaternary Science Reviews, 27: 1909–1915.

Wentworth, C.K. 1922, A scale of grade and class terms for clastic sediments. Journal of Geology, 30: 377-392.

Westgate, J.A., Preece, S.J., Froese, D.G., Pearce, N.J.G., Roberts, N.G., Demuro, D., Hart, W.K. and Perkins, W. 2008. Changing ideas on the identity and stratigraphic significance of the Sheep Creek tephra beds in Alaska and the Yukon. Quaternary International.

Vasil'chuk, Y. 2013. Monograph Synopsis - Syngenetic Ice Wedges: Cyclical Formation, Radiocarbon Age and Stable Isotope Records. Permafrost and Periglacial Processes, 24: 82–93.

Vasil'chuk, Y. K. 2013. Syngenetic ice wedges: cyclical formation, radiocarbon age and stable-isotope records, Permafrost and Periglacial Processes, 24: 82–93.

Vasil'chuk, Y.K, Kim, J-C. and Vasil'chuk, A.C. 2004. AMS ^{14}C dating and stable isotope plots of Late Pleistocene ice-wedge ice. Nuclear Instruments and Methods in Physics Research, 223–224: 650–654.

Vasil'chuk, Y.K. and Vasil'chuk, A.C. 2014. Strategy of valid ^{14}C dates choice in syngenetic permafrost. The Cryosphere, 8: 5589-5621.

Vermaire, J.C. and Cwynar, L.C. 2010. A revised late-Quaternary vegetation history of the unglaciatedsouthwestern Yukon Territory, Canada, from Antifreeze and Eikland ponds. Canadian Journal of Earth Sciences, 47: 75-88.

Vernon, P. and Hughes, O.L. 1966. Surficial geology, Dawson, Larsen Creekand Nash Creek map-areas. Geological Survey of Canada, Bulletin 136,25 pp.

Viau, A.E., Ladd, M. and Gajewski, K. 2012. The climate of North America during the past 2000 years reconstructed from pollen data. Global and Planetary Change, 84-85: 75-83.

Viau, A.E., Gajewski, K., Sawada, M.C. and Bunbury, J. 2008. Low- and high-frequency climate variability in eastern Beringia during the past 25 000 years. Canadian Journal of Earth Sciences, 14: 1435-1453.

Vonk, J.E., Mann, P.J., Davydov, S., Davydova, A., Spencer, R.G.M., Schade, J., Sobczak, W.V., Zimov, N. Zimov, S., Bulygina, E., Eglinton, T.I. and Holmes, R.M. 2013. High biolability of ancient permafrost carbon upon thaw. Geophysical Research Letters, 40: 2689–2693.

Zazula, G.D., Telka, A.M., Harington, C.R., Schweger, C.E. and Mathewes, R.W. 2006. New spruce (Picea spp.) macrofossils from Yukon Territory: implications for Late Pleistocene refugia in Eastern Beringia. Arctic, 59: 391–400.

Zazula, G.D., Froese, D.G., Elias, S.A., Kuzmina, S. and Mathewes, R.W. 2007. Arctic ground squirrels of the mammoth-steppe: paleoecology of late Pleistocene middens (w24,000–29,450 ^{14}C yr BP), Yukon Territory, Canada. Quaternary Science Reviews, 26: 979–1003.

Zdanowicz, C., Fisher, D., Bourgeois, J., Demuth, M., Zheng, J., Mayewski, P., Kreutz, P., Osterberg, E., Yalcin, K., Wake, C., Steig, E.J., Froese, D. and Goto-Azuma, K. 2014. Ice Cores from the St. Elias Mountains, Yukon, Canada: Their Significance for Climate, Atmospheric Composition and Volcanism in the North Pacific Region. Arctic, 67: 35-57.

Zimov, S. A., Schuur, E.A.G. and Chapin, F.S. 2006. Permafrost and the global carbon budget. Science, 312: 1612–1613.